



Norwegian University of
Science and Technology

Synthesis and Characterisation of Co- based Fischer-Tropsch Catalysts and Supports, using hydrothermal and chemical attrition Method

The magnesium moderation Effect

Aina Elin Karlsen

Chemical Engineering and Biotechnology

Submission date: June 2011

Supervisor: Anders Holmen, IKP

Co-supervisor: Erling Rytter, Statoil



Declaration

I declare that this is an independent work according to the exam regulations at the Norwegian University of Science and Technology, NTNU.

Trondheim, June 13th 2011

Aina-E. Karlsen

Aina-Elin Karlsen



Preface

Five wonderful student years at the Norwegian University of Science and Technology (NTNU), leading to the degree of *sivilingeniør* (MSc) is finalized with the completion of this thesis.

The work that forms the basis for this thesis was conducted during the spring semester of 2011. The project was initiated by my supervisors Prof. Anders Holmen at NTNU and Prof. Erling Rytter at Statoil and received financial support from Statoil ASA.

Support and catalyst preparation and characterization were performed at the Statoil Research Centre at Rotvoll. I would like to dedicate special thanks to all the great people at Rotvoll for being exceptionally obliging and co-operative. Sigrid Eri; thank you for your insight and advice both experimentally and theoretically. Torild Hulsund Skagseth; without your guidance and support I would remain confused and helpless in the laboratory. Øyvind Borg; thank you for writing a solid PhD thesis. Without it I wouldn't know where to begin this work. Thank you also for your experimental and theoretical assistance. Nikolaos Tsakoumis; thank you for teaching me how to perform XRD analyses.

The Fischer-Tropsch synthesis analyses were conducted in a fixed-bed unit operated by Andreas Helland Lillebø at the Department of Chemical Engineering at NTNU. I would like to thank Andreas, without whom FT-experiments would have been impossible. Thank you for your patience and for teaching me how to run the rig. Thanks are also dedicated to Georg Voss for lending me his office.

Special thanks are dedicated to my supervisors Prof. Anders Holmen and Prof. Erling Rytter. Thank you for your ideas, informative discussions and for pointing me in the right direction when I was lost.



Summary

Magnesium modification at different calcination temperatures of γ -alumina supports for cobalt Fischer-Tropsch catalysts was investigated. Support modification and catalyst preparation were performed by applying the incipient wetness impregnation method and resulted in supports containing 7,5 wt. % Mg and catalysts containing 12 wt. % Co and 0,5 wt. % Re. Selected support samples have in addition been promoted with 2 wt. % Al post magnesium modification, while others have been treated hydrothermally with water at 300 °C and 30 bar. The modified supports and the corresponding catalysts have been characterized by N₂ adsorption, H₂ chemisorption, X-ray diffraction and Fischer-Tropsch synthesis analysis in a dual isotherm fixed-bed unit at 20 bar, 210 ± 0,5 °C and H₂/CO = 2,1.

It was established that high temperature calcination of magnesium modified γ -alumina leads to a support material consisting of crystalline α -alumina and MgAl₂O₄ spinel. α -alumina formation was intensified by the addition of extra aluminium post magnesium impregnation. For the low temperature calcined magnesium modified γ -alumina supports only γ -alumina was detected, and for the medium temperature calcined supports only MgAl₂O₄ spinel was detected. Hydrothermal treatment with water appeared to induce boehmite formation in the magnesium modified support material.

High temperature calcination led to low surface areas, small pore volumes and large pore diameters and magnesium modification does not have the ability to counteract this effect. High to medium temperature calcination resulted in larger surface areas, indicating that the collapse of pore structure to a certain degree is counteracted by introducing a 2-valent metal in the support material. A small decrease in surface area was observed upon addition of extra aluminium due to the initiating effect of extra aluminium addition to form α -alumina.

Both the low temperature and the high temperature calcined magnesium modified alumina supported cobalt/rhenium catalyst were essentially inactive for the Fischer-Tropsch synthesis. The medium temperature calcined samples displayed relatively low activity as well.



Increased C_{5+} selectivity was observed accompanying an increase in CO conversion and an increase in C_{5+} selectivity was observed upon magnesium modification of the γ -alumina support compared to the standard when $MgAl_2O_4$ spinel and/or α -alumina were present. The effect of increased surface acidity was an increase in C_{5+} selectivity at the expense of C_4 . It appears that magnesium moderation does not cause any changes in methane selectivity.



Table of contents

DECLARATION	I
PREFACE	II
SUMMARY	III
TABLE OF CONTENTS	V
1 INTRODUCTION	1
2 LITERATURE REVIEW	2
2.1 SUPPORTED COBALT CATALYSTS FOR THE SLURRY PHASE BUBBLE COLUMN FISCHER-TROPSCH SYNTHESIS.....	2
2.2 THE EFFECT OF HYDROTHERMAL TREATMENT.....	4
2.3 MAGNESIUM MODERATION EFFECT.....	5
2.4 THE EFFECT OF FISCHER-TROPSCH SYNTHESIS CONDITIONS.....	7
2.5 SCOPE OF THIS STUDY.....	7
3 THEORY	9
3.1 FISCHER-TROPSCH SYNTHESIS.....	9
3.1.1 <i>History</i>	9
3.1.2 <i>Principles</i>	10
3.1.3 <i>Gas chromatography</i>	14
3.2 ADSORPTION.....	16
3.3 CATALYST AND SUPPORT CHARACTERIZATION.....	18
3.3.1 <i>Hydrogen (H₂) chemisorption</i>	18
3.3.2 <i>Cobalt particle size</i>	19
3.3.3 <i>X-ray diffraction</i>	20
3.3.4 <i>Nitrogen (N₂) adsorption/desorption and the BET-method</i>	22
4 EXPERIMENTAL	24
4.1 SUPPORT AND CATALYST PREPARATION.....	24
4.1.1 <i>Metal loading</i>	24
4.1.2 <i>Hydrothermal treatment in an Autoclave Parr CSTR</i>	28
4.2 SUPPORT AND CATALYST CHARACTERISATION.....	29
4.2.1 <i>X-ray diffraction</i>	29
4.2.3 <i>Hydrogen (H₂) chemisorption</i>	29
4.2.4 <i>Nitrogen adsorption/desorption</i>	30
4.3 FISCHER-TROPSCH SYNTHESIS.....	31
4.3.1 <i>Procedure</i>	31



4.3.2	Data ANALYSES	34
5	RESULTS AND DISCUSSION	40
5.1	SUPPORT AND CATALYST PREPARATION	40
5.2	SUPPORT AND CATALYST CHARACTERISATION	42
5.2.1	X-ray diffraction	42
5.2.2	Nitrogen (N_2) adsorption/desorption	46
5.2.3	Hydrogen (H_2) chemisorption	51
5.3	FISHER-TROPSCH SYNTHESIS	54
6	FURTHER WORK	62
7	CONCLUSIONS	64
	LIST OF SYMBOLS	66
	LIST OF ABBREVIATIONS	68
	REFERENCES	69
	APPENDICES	I
A	DERIVATIONS AND CALCULATIONS	II
A.1	SUPPORT AND CATALYST PREPARATION	II
A.1.1	Water absorptivity	ii
A.1.2	Metal nitrate X hydrate needed for impregnation	ii
A.1.3	Perrhenic acid needed for impregnation	iii
A.2	COBALT METAL PARTICLE SIZE FROM HYDROGEN CHEMISORPTION DATA	IV
A.3	GAMMA ALUMINA PARTICLE SIZE FROM X-RAY DIFFRACTION DATA	V
B	ADDITIONS TO THE PROCEDURE	VIII
B.1	HYDROTHERMAL TREATMENT IN THE AUTOCLAVE PARR CSTR	VIII
B.1.1	MOUNTING THE AUTOCLAVE PARR REACTOR	VIII
B.1.2	Applying temperature and rate of rotation	viii
B.2	MASS FLOW CONTROLLER CALIBRATION	VIII
B.3	FISCHER-TROPSCH SYNTHESIS	XI
B.3.1	Pressure testing	xi
B.3.2	GC CALIBRATION	XI
C	X-RAY DIFFRACTION STANDARDS	XIV
D	TABLES AND DATA	XV
D.1	CD-ROM CONTENTS	XV
E	RISK ASSESSMENT	XVII



1 Introduction

The world's population is expected to reach between 7,5 and 10,5 billion by the year 2050. Most of those people will be born in Asia and Africa where today poverty is most widespread. The average Chinese for example, uses about one tenth of the average Norwegian energy consumption per day. Living standards are on the rise in these areas together with the rest of the world. Fossil fuels accounts for an overwhelmingly large portion of the world's energy supply and will become even more important as the world's population keeps growing and becoming wealthier.

On the other hand, if we keep burning fossil fuels like we do today, the planet will appose and make itself unendurable to us. The oil supply is currently being drained, however gas production is on the rise and reservoirs of natural gas represent a huge energy resource. Large reservoirs of remote natural gas could help sustain energy demand growth. The Fischer-Tropsch (FT) synthesis attracts great attention in gas-to-liquids conversion (GTL) as a tool to produce high quality products like transportation fuels and chemicals, essentially contaminant free, from natural gas, cheap coal or biomass. In this respect the FT synthesis could in the future play an important role.

The FT synthesis is a catalytic process and the main features of a Fischer-Tropsch catalyst are its activity, selectivity and stability. Preparation costs and raw material expenses must also be taken into account. Supported cobalt is considered to be the most favourable catalyst for the synthesis of long-chain hydrocarbons from natural gas based synthesis gas. Cobalt based catalysts exhibit high activity, high selectivity for long, linear paraffins, low water-gas shift activity and relatively low price compared to noble metals [1].

The FT reactions are highly exothermic and thus the Fischer-Tropsch synthesis part of the GTL process is preferably performed in a slurry phase bubble column reactor. This is a system favouring cobalt based catalysts due to its gradient less nature. The three-phase bubble column reactor is a churning environment for the catalyst. It exerts significant mechanical and chemical stress on the suspended particles. This means that high chemical and mechanical attrition resistance is important for the Fischer-Tropsch catalysts. [2]



2 Literature review

This chapter presents some of the available literature relevant for this study. A full literature review is far beyond the scope of this work. The main focus of this thesis is of experimental nature, but this section will provide the reader with an overview of and an insight into the most important factors and variables that have been and should be addressed. A large body of information may be found in the given references. In section 2.1 information about supported cobalt catalysts are presented. Section 2.2 describes previously reported effects of hydrothermal treatments of alumina supports. The effects of magnesium moderation of alumina supported cobalt Fischer-Tropsch catalysts are presented in section 2.3. The impact of Fischer-Tropsch synthesis conditions on analysis results are summarized in section 2.4. Finally the scope of this study is presented in section 2.5.

2.1 SUPPORTED COBALT CATALYSTS FOR THE SLURRY PHASE BUBBLE COLUMN FISCHER-TROPSCH SYNTHESIS

The main features of a Fischer-Tropsch catalyst are its activity, selectivity and stability. Preparation costs and raw material expenses must also be taken into account. In this context the focus, with respect to selectivity, is the formation of wax (C_{5+}) and subsequent potential for diesel production by cracking.

The most active metals for the hydrogenation of carbon monoxide to hydrocarbons are ruthenium, iron, nickel and cobalt. Supported cobalt is considered to be the most favourable catalyst for the synthesis of long-chain hydrocarbons from natural gas based synthesis gas. Cobalt based catalysts exhibit high activity, high selectivity for long, linear paraffins, low water-gas shift activity and relatively low price compared to noble metals [1].

The Fischer-Tropsch synthesis is preferably performed in a slurry phase bubble column reactor. As mentioned in the introduction, the slurry system favours cobalt based catalysts due to its gradient less nature. The three-phase bubble column reactor is a churning environment for the catalyst. It exerts significant mechanical and chemical stress on the suspended particles.



Dissolution of catalyst and support (chemical attrition) leads to loss of catalytic material and contamination of the Fischer-Tropsch products. Dissolution of the support and leaching of cobalt into the slurry environment is not only economically unsound, but pose a potential threat to the environment. In addition, internal filtration is the method used to separate and remove the heavy hydrocarbons produced, in commercial slurry reactor technology. Hence, the ions and fines created by the degradation of the catalyst particles can lead to reduced separation rates and, eventually, partly or complete blocking of filters. This means that high chemical and mechanical attrition resistance is ideal for the Fischer-Tropsch catalysts in a slurry reactor operation. [3]

In order to increase the exposure of cobalt metal to gaseous reactants, cobalt is usually deposited on a high surface area carrier. Alumina, silica and titania are commonly used support materials. Due to favourable mechanical properties, alumina is a particularly attractive support for cobalt based Fischer-Tropsch catalysts. [4]

The support may interact strongly with the active phase. Metal-support interactions could lead to a fraction of the cobalt metal being chemically inactive after reduction. A small amount of a second metal can be introduced into the catalyst system to lower the amount of unreduced cobalt. For such alterations rhenium is a frequent choice. [5]

2.2 THE EFFECT OF HYDROTHERMAL TREATMENT

Alpha alumina (α - Al_2O_3 , corundum) is one of the most widely used ceramic materials due to favourable properties such as high mechanical strength and hardness, good wear resistance, low electric conductivity, low refractoriness and high corrosion resistance in a broad range of chemical environments. [6] Several of these properties are favoured in support materials for the slurry Fischer-Tropsch process. Nanosized α - Al_2O_3 powders are being sought as a thermally stable alternative to widely used transition aluminas, which undergo phase transformations during high temperature use and thus suffer loss of surface area. The hexagonally closest packed α - Al_2O_3 is the only stable oxide in the Al_2O_3 - H_2O system and can be synthesized by several high-temperature methods. When aluminium hydroxides or oxide hydroxides are heated in air at atmospheric pressure, they undergo a series of compositional and structural changes before ultimately being converted to α - Al_2O_3 .

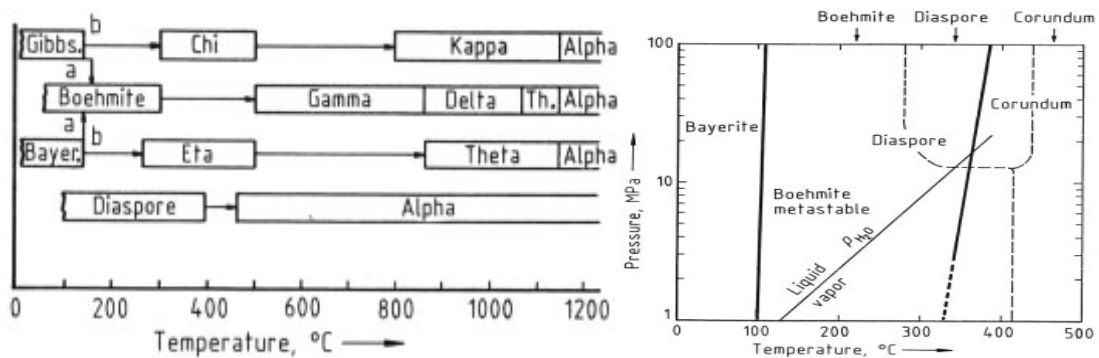


Figure 2.1 Left: Decomposition sequence of aluminium hydroxide. Right: The Al_2O_3 - H_2O system [7].

The high temperature calcination procedures as means to prepare alpha alumina yield support materials with a low specific surface area. Several low-temperature approaches to yield higher surface area corundum exist as well. The simplest being the transformation of diaspore to corundum by calcination at 500 °C. Another is the calcination of gels also at about 500 °C. This approach involves the use of toxic alkoxides and is therefore expensive and not environmentally sound. [8]

Hydrothermal synthesis is an environmentally benign technology that crystallizes materials directly from aqueous media at low temperatures and moderate to high pressures. This process is a promising alternative to the abovementioned α - Al_2O_3 preparation methods, as it has the potential of synthesizing α - Al_2O_3 powders with relatively high surface areas ($\sim 35 \text{ m}^2/\text{g}$) as showed by Suchanek et al. [8].

In addition, hydrothermal treatment of alumina support has the potential of modifying both the physical and the chemical properties of the alumina support materials as reported by Zhang et al. in [9].



2.3 MAGNESIUM MODERATION EFFECT

γ -alumina is the most common catalyst carrier, but as mentioned above they undergo phase transformations during high temperature use and thus suffer loss of surface area. A number of transition phases occur before the thermodynamically stable α -alumina phase is reached. It has been shown by Schanke et al. [10] that high temperature calcination accompanied by changes in pore geometry and partial transformation of γ -alumina to α -alumina gives cobalt FT catalysts with a significant increase in selectivity. Such a treatment drastically reduces the alumina surface area, from typically ~ 180 to ~ 10 m^2/g [11]. Then the dispersion of active cobalt becomes restricted by the low available surface area. Schanke et al. [10] reported that cobalt/rhenium catalysts supported on low surface area alumina resulted in the lowest cobalt dispersion and in reduced activity for secondary hydrogenation of propene. The collapse of pore structure can be counteracted by introducing a 2-valent metal in the support material that forms an aluminate spinel phase during high-temperature treatment. Examples are supports containing a mixture of α -alumina and either Mg-, Zn-, or Ni-spinel. [12]. Enger et al. [13] showed that by adding magnesium before high temperature calcination of the support the C_{5+} selectivity and the turnover frequency (TOF) were reduced whereas the addition of nickel had a positive effect on the rate compared to low surface area α -alumina supported catalysts. In addition the C_{5+} selectivity remained high. XRD analysis revealed the presence of Mg/Ni Al_2O_4 spinel structures.

It has previously been found that by adding nickel as a promoter to a cobalt on alumina support catalyst (post or co-impregnation then calcined at 200 - 600 °C) increases activity, stability and/or selectivity depending on the composition and type of oxide support employed. The intention with this procedure was that nickel would be reduced in subsequent reduction steps and thus play an active role as promoter to the FT-reactions on cobalt. Rytter reported in [14] that cobalt, rhenium and nickel co-impregnation of high surface area (170 m^2/g) γ -alumina yielded a significant increase in activity compared to catalysts without nickel promotion. The C_{5+} selectivity did not decrease, as would be expected due to the hydrogenation abilities to yield CH_4 of nickel. In addition, increased catalyst stability was observed when nickel was present in the cobalt/rhenium impregnation solution.

Nickel as a modifying component for the support, however is able to suppress the solubility of the catalyst support in aqueous acid or neutral solutions when calcined at higher temperatures (800 - 900 °C). Then NiAl_2O_4 spinel is formed, thus giving a more inert support surface. Rytter also reported in [14] that when nickel was present (2 - 5 wt. %) in a low surface area (12 m^2/g) support comprised of nickel spinel and α - Al_2O_3 very stable catalysts were the result.

The promoting divalent metal could also be an alkaline earth metal, for example magnesium. In addition to improved mechanical properties, magnesium has potential to improve the reducibility of alumina supported cobalt catalysts which has proven to have limited reducibility due to strong interactions between support and cobalt oxides [15]. There is a possibility of formation of cobalt aluminate spinel. Modification of the support surface could suppress this interaction.



A number of investigations are reported on magnesium moderation of alumina supported cobalt Fischer-Tropsch catalysts. Studies reported by Chernavskii et al. [16] on the possibility of inhibiting the interaction between the cobalt oxide and the support by adding magnesia to an alumina support have shown that the magnesia modification increased both the reducibility of cobalt oxide and also the catalytic activity in CO hydrogenation. Pankina et al. [17] found that a considerable fraction of superparamagnetic cobalt particles, which increase selectivity for C₅₊ hydrocarbons and decrease the yield of methane in the FT synthesis, was present in magnesium modified ruthenium containing cobalt catalysts. They also reported an increase in activity. The same trends were observed by Zhang et al. [18] which reported that small amounts of magnesia (0, 3 – 0, 8 wt. %) improved cobalt catalyst activity for the FT synthesis, but that large amounts (2 – 12 wt. %) seemed to reduce catalyst reducibility due to MgO-CoO solid solution formation. They also reported that the C₅₊ hydrocarbon selectivity of the magnesia-modified catalysts was slightly lower than that of unmodified cobalt catalysts and that a mild decrease could be observed with increasing magnesia content. In addition, the surface area and the total pore volume decreased with increasing magnesia content, while the average pore diameter increased slightly.

Borg et al. recently reported in [19] that magnesium post impregnation of Ni-aluminate supported cobalt/rhenium catalysts yielded catalysts with lower activity. The activity decrease was ascribed to physical blocking of cobalt sites.

The intrinsic effect of support modification by magnesium on the metal-support interaction, the reducibility, the activity and selectivity of the cobalt catalysts for FT synthesis are however still unclear.



2.4 THE EFFECT OF FISCHER-TROPSCH SYNTHESIS CONDITIONS

Type of reactor, temperature, total pressure, H₂/CO ratio and partial pressures, co-fed inert or water, conversion level and space velocity (or residence time) are all Fischer-Tropsch conditions that can be controlled.

It has previously been reported that Fischer-Tropsch selectivities depends strongly on CO conversion. CO conversion can be controlled by adjusting the residence time [20].

A review of the effect of process conditions in the Fischer-Tropsch synthesis was published by Van Der Lan et al. [21]. The expected response of changes in process conditions is summarized in Table 2.1 [21].

Table 2.1 The effects of process conditions on Fischer-Tropsch selectivity¹

Parameter	Chain length	Chain branching	Olefin selectivity	Alcohol selectivity	Carbon deposition	Methane selectivity
Temp.	↓	↑	*	↓	↑	↑
Pressure	↑	↓	*	↑	*	↓
H ₂ /CO	↓	↑	↓	↓	↓	↑
Conversion	*	*	↓	↓	*	↓
Space velocity	*	*	↑	↑	↑	↑

2.5 SCOPE OF THIS STUDY

Improved selectivity towards higher hydrocarbons and improved attrition resistance have been reported for low surface area α -alumina supported cobalt/rhenium catalysts for the Fischer-Tropsch synthesis. The positive effects of nickel promotion of alumina support have also been repeatedly reported. It has been found that introducing a 2-valent metal (for example magnesium) into the support material that forms an aluminate spinel phase during high-temperature treatment yields mechanically and chemically strong catalysts with improved FT activity. In addition, hydrothermal synthesis of support material has proven to be suitable when high surface area α -alumina is the desired product. It would be interesting to investigate the possibility of fabricating magnesium spinel/ α -alumina supports with relatively high surface areas and high attrition resistance by hydrothermal treatment in an autoclave Parr CSTR

¹ Increases with increasing parameter ↑. Decreases with increasing parameter ↓. Complex relation *.



with elevated temperature and pressure, and to test whether such supports are suited for Fischer-Tropsch synthesis.

A total of 9 different magnesium modified γ -alumina supports have been prepared for this work. The supports are different with respect to the temperature at which they have been calcined, whether or not the samples have been loaded with extra 2 wt. % aluminium post magnesium moderation, and whether or not they have been treated hydrothermally in an autoclave Parr CSTR. The supports have all been subject to X-ray diffraction and nitrogen adsorption/desorption characterization.

Selected supports have in addition been loaded with cobalt (12 wt. %) and rhenium (0,5 wt. %) to yield FT catalysts that have subsequently been characterized by hydrogen chemisorption, nitrogen adsorption/desorption and FT synthesis analysis.



3 Theory

This section provides information about relevant principles encountered in this work. Some elementary concepts of heterogeneous catalysis and Fischer-Tropsch synthesis is presented in sections 3.1 to 3.2. Section 3.3 provides information about the different support and catalyst characterization methods employed in this work.

3.1 FISCHER-TROPSCH SYNTHESIS

The current section provides the reader with an introduction to the Fischer-Tropsch synthesis. Chemical reactions and principles used for determination of conversion levels, selectivity and reaction rates are described.

3.1.1 HISTORY

Catalytic hydrogenation experiments of carbon monoxide were first carried out in the beginning of the 20th century by Sabatier (1854–1941) and Serenderens (1856–1936). Methane was synthesized from a mixture of carbon monoxide (CO) or carbon dioxide (CO₂) and hydrogen (H₂) over a cobalt or nickel catalyst. [22] Two decades later, Franz Fischer (1877-1947) and Hans Tropsch (1889-1935) reported their studies on the production of hydrocarbons from synthesis gas (H₂ and CO) using alkalized iron catalysts. The technology was rapidly commercialized, but the Fischer-Tropsch process has since then passed through a number of periods with varying interest. At the beginning of World War II, a substantial part of German fuel production was carried out through the Fischer-Tropsch synthesis. Germany produced mid-distillates from direct hydrogenation of coal over promoted cobalt catalysts in fixed-bed reactors at low pressures. Later developments showed that promoted iron catalysts in medium pressure fixed-bed reactors were superior to the cobalt catalysts. [23]

The war destroyed many Fischer-Tropsch plants in Germany. And although several countries planned to construct Fischer-Tropsch plants when the war ended, the discovery of large oil reserves in the Middle East yielded the Fischer-Tropsch process economically unattractive in many areas. Lack of oil resources and the desire to reduce their dependence on imported oil, made coal-rich countries like South-Africa pursue coal-based Fischer-Tropsch technology.



The government owned company Sasol managed to get the Sasol I plants on-stream in 1952-1955. These plants produced wax in fixed-bed and moving-bed reactors over iron based catalysts. Sasol managed to keep the production economical, and through the oil price rise during the 70's and 80's Sasol managed to construct additionally two plants based on iron catalyst technology. Currently, the three Sasol plants are the only indirect coal liquefaction plants producing liquid fuels by the Fischer-Tropsch process. [24]

Recently, the Fischer-Tropsch technology has gained interest as means to convert remote natural gas into liquid fuels. The reserves of natural gas are abundant, but are often located in remote areas where transportation to consumer markets is difficult or too expensive. In addition, the market demand for cleaner fuels has risen. Diesel produced from natural gas by the Fischer-Tropsch process offer significant environmental benefits over fuels derived from crude oil. Free from nitrogen, sulphur, aromatics and metals, FT-diesel exhibit superior environmentally friendly properties.

Shell built a FT-plant in Malaysia that converts remote natural gas into middle distillates over a cobalt based catalyst. The Shell Middle Distillates Synthesis (SMDS) plant has been operating since 1994. Today licensors of gas-to-liquids (GTL) technology are many, and the interest in FT is great. [24]

3.1.2 PRINCIPLES

Synthesis gas production, Fischer-Tropsch synthesis and product upgrade are the three main elements of the GTL process. This thesis focuses on the core of the aforementioned process, namely the Fischer-Tropsch synthesis.

Synthesis gas is catalytically converted into paraffinic and olefinic hydrocarbons with varying carbon content. Products range from methane to hard wax, water and a touch of oxygenates. The chemistry of the Fischer-Tropsch synthesis is very complex and probably not fully understood. However, the fundamental aspects can be represented by a few generalized relationships. The main reactions include formation of paraffins and olefins (reaction 3.1 – 3.2) and carbon dioxide formation as a result of the water gas shift reaction (reaction 3.3). [24]



In addition, side reactions like the formation of alcohols and coke (reactions 3.4 and 3.5) are common.



A point worth emphasizing is the high exothermicity accompanied the Fischer-Tropsch reactions. As a consequence, temperature control is essential in the FT-reactor design. Figure 3.1 depicts a schematic of the currently used reactors; the tubular fixed-bed reactor, the fluidized bed reactor and the slurry reactor.

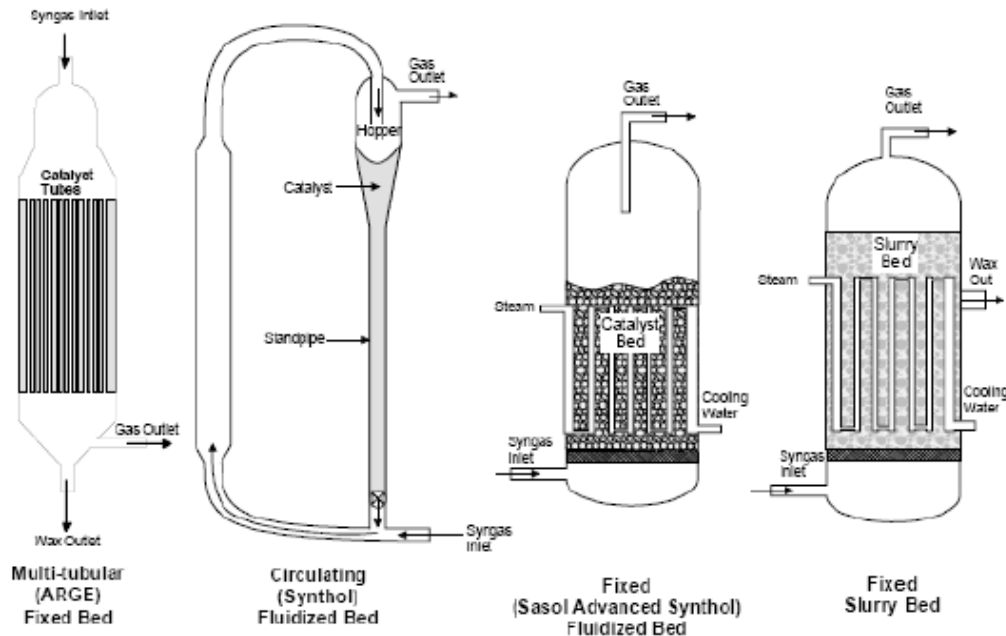
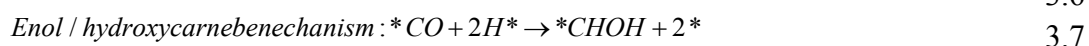
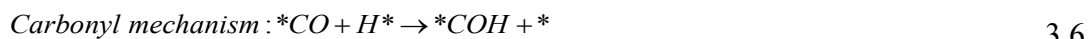


Figure 3.1 Reactor designs used for the Fischer-Tropsch synthesis [25].

All of the abovementioned reactor types are designed for proper heat management. However, temperature control is challenging and complete isothermicity is impossible in a full scale commercial reactor.

Even after significant study several mechanistic details in the Fischer-Tropsch synthesis remain unclear and speculative. The specific CO dissociation pathways to form monomers and their kinetic consequences for chain growth are not yet exclusively determined. Three proposed mechanisms still remain. Fischer and Tropsch suggested the carbide mechanism, in which CO is directly dissociated, resulting in a metal carbide. This carbide is further hydrogenated to the proposed CH_x monomers that initiate growth of hydrocarbon chains [26]. The hydroxycarbene mechanism (the enol mechanism), proposed by Storch et al. suggests that condensation of oxygen-containing intermediates, like hydroxycarbene (HCOH), is responsible for C–C bond formation [23]. Pichler and Schultz proposed the carbonyl mechanism (CO insertion mechanism), in which chemisorbed hydrogen adds to CO at the surface before C–O bond cleavage [27]. In other words, hydrogen assists the activation of CO. The latter explains the rejection of oxygen as H_2O , which is the main oxygenate formed at conditions required for significant chain growth on both Fe-based and Co-based catalysts [28]. Reactions 3.6 to 3.8 describe the three proposals for the Fischer-Tropsch mechanism.





The weakness of the carbide mechanism is the explanation to the formation of oxygenates. Recent studies attempts to find a common mechanism for the production of oxygenates and hydrocarbons. A combination of the carbide mechanism and the carbonyl mechanism has been proposed as an answer [26].

It is reasonable to believe that a dynamic network of possible reaction pathways exist, of which some are more likely to occur than others depending on the prevailing reaction conditions and catalyst properties.

Regardless of what the exact reaction mechanism is, the Fischer-Tropsch synthesis proceeds through successive additions of carbon entities to growing chains on the catalyst surface (polymerization reaction). Figure 3.2 depicts a simplified version of the FT- reactions network.

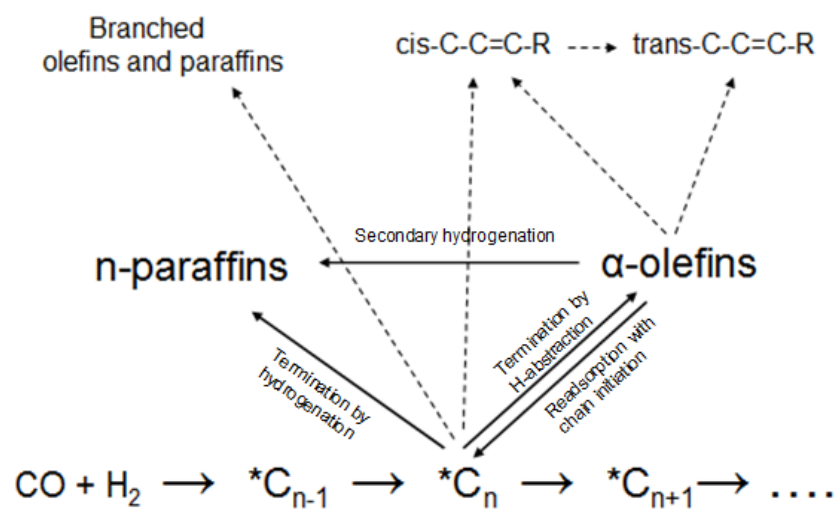


Figure 3.2 The Fischer-Tropsch reaction network [29].

FT-chain propagation and termination have traditionally been explained through the Anderson-Schulz-Flory (ASF) product distribution. When chain-growth and termination rates are independent of chain length, the molecular weight distribution of hydrocarbon products is claimed to follow the ASF chain polymerization kinetic model. The model assumes that the relative probability of chain growth (α) and chain termination ($1-\alpha$) is constant and that the carbon number distribution of products can be presented by the simple statistical model illustrated in Figure 3.3. A Product distribution that follows this model is represented graphically in Figure 3.4.

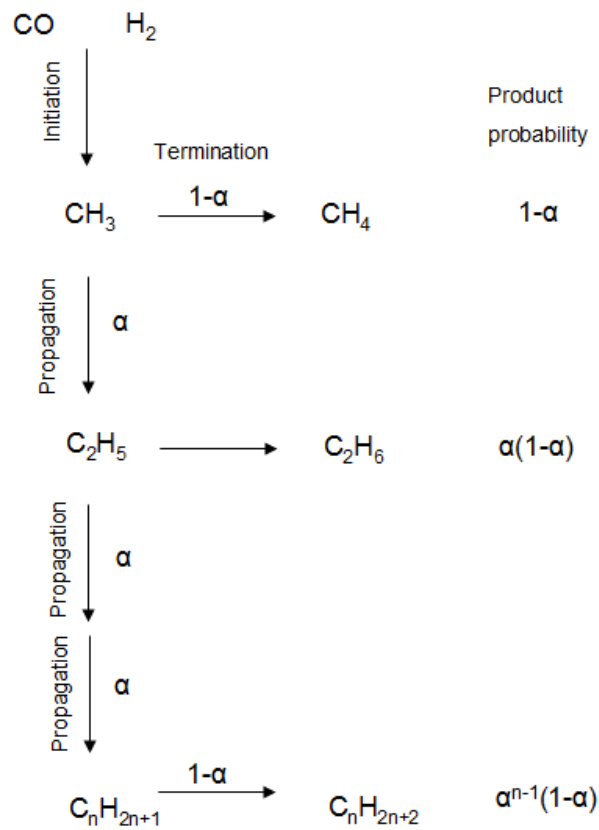


Figure 3.3 Chain-growth mechanism for the FT-synthesis with Anderson-Schulz-Flory kinetic [24].

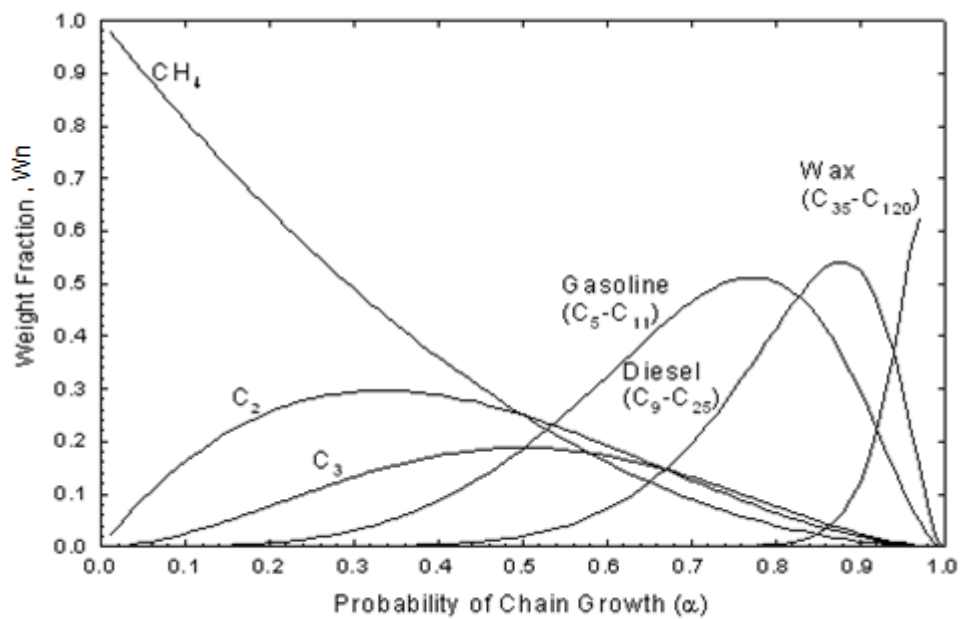


Figure 3.4 An Anderson-Schulz-Flory product distribution.



It is generally acknowledged that α depends on the choice of catalyst and process conditions such as temperature, pressure and feed gas composition. In fact, it is widely accepted that FT-synthesis does not follow the ASF distribution. Synthesis over cobalt catalysts generally yields more methane and C_{5+} and less C_2-C_3 than ASF kinetics would predict.

The kinetics for the FT-synthesis has been the topic of numerous research projects. A general agreement is that Langmuir-Hinshelwood type rate expressions fit FT-kinetics. A general Langmuir-Hinshelwood expression for the FT-synthesis is exemplified in equation 3.1.

$$-r_{CO} = K \cdot \frac{P_{H_2}^a P_{CO}^b}{(1 + kP_{CO}^c)^d} \quad 3.1$$

K represents the temperature dependent rate constant, k is the adsorption constant and a , b , c , and d are constants determining the reaction order. Several different empirical and theoretical rate expressions have been proposed. A general feature is that the activity increases with increasing H_2 pressure and decreases with increasing CO pressure [30].

3.1.3 GAS CHROMATOGRAPHY

The Fischer-tropsch synthesis analysis performed in this work uses gas chromatography to characterize and quantify the product mixture, thus a description of the gas chromatographic method is provided in this section.

In gas chromatography (GC), the mobile phase is a carrier gas. The carrier gas needs to be very pure and inert. The stationary gas phase properties can be compromised by trace amounts of for example oxygen or water. In addition, choice of carrier gas affects the efficiency and the durability of the analysis. Helium and argon are frequently used. [31]

The stationary phase is a microscopic layer of high-boiling liquid on an inert solid support, inside a glass or metal column. The carrier gas function is transportation of the volatile components through the column. [31]

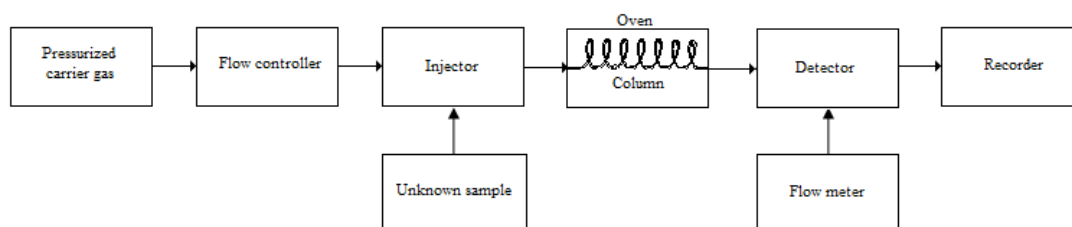


Figure 3.5 A schematic presentation of gas chromatography.



The analysis sequence starts with the carrier gas being passed through a flow controller. This ensures reproducibility and control of the column efficiency. The carrier gas and the unknown sample are then introduced into a preheated injector. The unknown sample is carried with the carrier gas to the head of the separation column. The mixture moves across the column which contains the stationary phase. The gaseous compounds being analyzed interact with the walls of the column, which is coated with different stationary phases. The interaction with both the mobile phase and the stationary phases will influence their velocity through the column and thus cause each compound to elute at different times, known as the retention time of the compound. Components that are very soluble in the mobile phase will move faster than less soluble ones. To achieve separation, a difference in chemical activity of the unknown components in the two phases is essential. The comparison of retention times is what gives GC its analytical usefulness. Identification of components results from comparing retention times with known standards.

After the column the mixture is introduced to a detector. Two different types of detectors exist; concentration sensitive detectors and weight sensitive detectors. The thermal conductivity detector (TCD) and the flame ionization detector (FID) are the two most common ones. The TCD is concentration sensitive and the FID is weight sensitive. The TCD and the FID are described in more detail by Greibrokk et al. [31]. The detector converts amount signals to electrical signals that are amplified to drive a recorder. The recorder displays the separation as chromatograms with characteristic peaks for different components. The chromatogram peak area is proportional to the amount of the specific component in the mixture. The detector response to different components may vary, and peak response factors are needed to get accurate results. The GC needs to be pre-calibrated with response factors and retention times before measurements.

It is difficult to inject samples in the μL range without compromising the reproducibility. To compensate for fluctuations in injected amounts, an internal standard is used as a reference (nitrogen). The internal standard method for quantitative analysis is also described by Greibrokk et al. [31].



3.2 ADSORPTION

The elementary concepts of adsorption are presented in this section. The intention of this section is to provide the reader with information helpful in understanding the adsorption methods used in catalyst and support characterization (section 3.3.1 Hydrogen (H₂) chemisorption and section 3.3.4. Nitrogen (N₂) adsorption/desorption and the BET-method).

The surface phenomenon of adhesion of species of gas, liquid or dissolved solids to a surface is called adsorption. Gas-surface interactions and reactions on surfaces play a crucial role in heterogeneous catalysis. Catalysis is a cycle, which starts with the adsorption of reactants on the surface of the catalyst. Usually at least one of the reactants is dissociated. It is often in the dissociation of strong bonds that the essence of catalytic action lies. [32]

Adsorption on a solid surface and in pores is a complex phenomenon involving mass and energy interaction and phase changes. When an atom or a molecule approaches a surface it feels the potential energy set up by the atoms (usually metal) in the solid. The interaction is divided into two regimes; physical adsorption and chemical adsorption. [32]

Physisorption is weak interactions (van der Waals forces) between adsorbate and surface. No electrons are shared and there is no true chemical bond. The phenomenon is characterized by secondary attractive forces such as dipole-dipole interactions and induced dipoles. [32] The energy effects are comparable to those accompanying physical changes such as liquefaction and are completely reversible (desorption). [33] The process is exothermic, and the heat of adsorption ranges typically from 8 - 40 kJ/mol. Physical adsorption requires no activation energy, and consequently occurs nearly as fast as molecules strike a surface. [34] At low pressures it is plausible to restrict the adsorbed molecules to a monolayer, and at moderate pressures physisorption become multilayered. This forms the basis for the derivation of the BET isotherm and the surface characterisation method called the BET-method. The BET theory begins with the assumption of localized adsorption. The number of layers is not limited, and therefore no saturation of the surface with increasing pressure exists. [33] Section 3.3.4 describes the BET-method in more detail.

Rearrangement of electrons of the adsorbing specie (adsorbate) and the surface (adsorbent), and consequential formation and rupture of chemical bonds is characteristic for chemisorption. This is the type of adsorption that affects the rate of a chemical reaction. Like physisorption, chemisorption is an exothermic process. However, the interactions involved in chemisorption are much stronger, with heats of adsorption in the same order as a chemical reaction, ranging from 80 - 800 kJ/mol. In chemisorption, the bond between the adsorbate and the adsorbent is often very energetic even if the net heat of adsorption is low. The process requires an activation energy, and this explains the low net heat of adsorption at low temperatures and the large net heat of adsorption at high temperatures. Physisorption predominates at low temperatures and chemisorption at elevated temperatures. [35] Chemisorption is



restricted to a monolayer of adsorbed species, but maximum coverage is frequently much less, often a small fraction of a monolayer. In addition, chemisorption may or may not be reversible. [36]

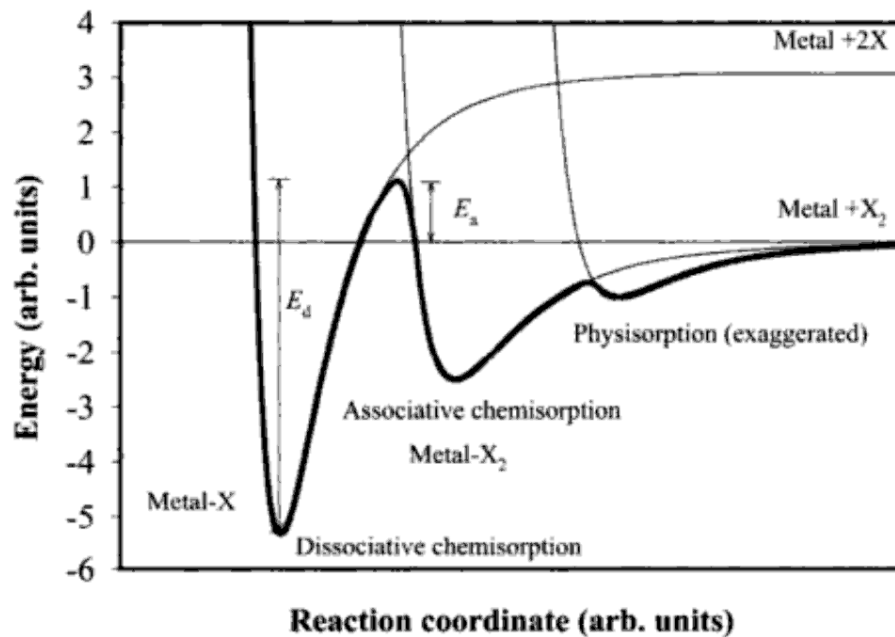


Figure 3.6 Schematic potential energy diagram along the reaction coordinate indicating the energies of chemical and physical adsorption. [32]

Figure 3.6 depicts a schematic potential energy diagram along the reaction coordinate of a molecule X_2 approaching a metal surface. At first the molecule experience weak Van der Waals forces that leads to physisorption. Next, the molecule interacts chemically with the surface, leading to associative chemisorption. If the molecule can overcome the activation barrier E_a it may dissociate into two chemisorbed atoms, X and X. The energy required for the desorption of these atoms again is E_d .

Both physisorption and chemisorption may be used to determine the surface area of solid materials. Physical adsorption of a suitable gas (often nitrogen) can be used to determine the total surface area of a catalyst system (support and active component). Chemisorption can be used to quantify the surface area of the active component alone.

3.3 CATALYST AND SUPPORT CHARACTERIZATION

3.3.1 HYDROGEN (H₂) CHEMISORPTION

The main principles of chemisorption are given in section 3.2. This section provides additional information on the use of volumetric hydrogen chemisorption on supported cobalt catalysts for the determination of catalyst dispersion and cobalt metal particle size.

The principle with the technique of volumetric chemisorption of hydrogen is to measure the amount of adsorbed gas as a function of the equilibrium pressure. This yields an adsorption isotherm like the one depicted in Figure 3.7. The composite isotherm represents the volume adsorbed by both chemisorption and physisorption. In order to differentiate the chemisorption volume from the physisorption contribution, the sample is evacuated after completion of the initial analysis. This procedure removes the reversibly adsorbed gas. The analysis is then repeated with the same conditions as the initial analysis. At this point, the active area of the sample is already saturated with chemisorbed gas. [35]

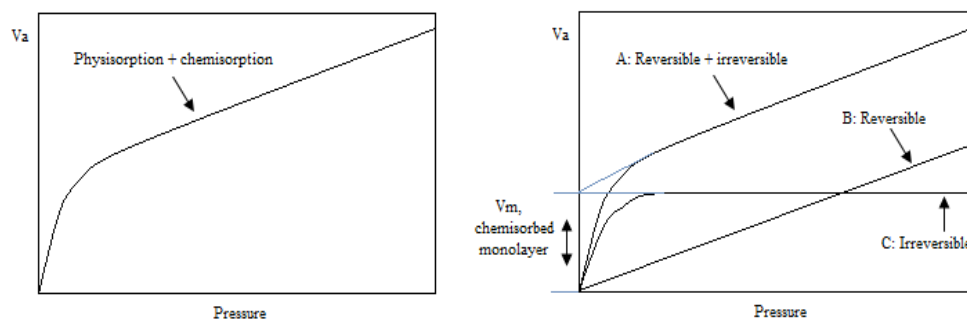


Figure 3.7 Isotherms generated by the volumetric chemisorption technique. Left: A typical composite isotherm. Right: The composite isotherm is divided into one describing reversible physisorption and one describing irreversible chemisorption. [35]

The left side of Figure 3.7 shows the result after the initial analysis. The adsorbed volume V_a represents that by chemisorption plus physisorption. The right side of the figure depicts the same composite isotherm, A, in addition to the result from the repeat analysis where only reversible physisorption occurs, B. Line C is generated by subtracting the adsorbed volume data of isotherm B from that of isotherm A. This procedure yields the quantity of gas irreversibly chemisorbed by the sample. C is typically a Langmuir-type isotherm. A description of the Langmuir-isotherm is described by Webb et al. [35].

The isotherm is obtained by expanding a known amount of gas in a fixed volume containing the sample and recording the pressure decrease for several increments of increasing pressure. The volume of adsorbed gas at monolayer, V_m , can be determined



in two ways; by extrapolating the straight line portion of the composite isotherm to zero pressure, or by subtracting the physisorption isotherm from the combined isotherm as described above, and then extending a line tangent to the plateau of the resulting isotherm to zero pressure.

The dispersion, D , is a measure of the amount of active metal atoms exposed at the catalyst surface. D is defined as the fraction of the total amount of metal atoms, N_t , that exist as surface atoms, N_s . [36]

$$D = \frac{N_s}{N_t} \quad 3.2$$

The dispersion can be calculated from the measured amount of adsorbed gas at monolayer, V_m , obtained by chemisorption from equation 3.3.

$$D = \frac{V_m \cdot M \cdot F}{x} \quad 3.3$$

V_m , is measured in moles per gram catalyst, M is the atomic weight of the adsorbent (metal) given in grams per mole, x is the weight fraction of metal in the catalyst, and F represents the stoichiometry of the adsorption reaction. F is the number of active metal sites occupied by one gaseous adsorbate molecule. In the case of H_2 chemisorption on supported cobalt/rhenium catalysts the value of F is equal to two. This stems from the assumption of dissociative hydrogen adsorption on cobalt. It is also assumed that rhenium does not adsorb any hydrogen.

3.3.2 COBALT PARTICLE SIZE

Cobalt metal particle sizes were estimated from the cobalt dispersion. For monodisperse spherical particles with a site density of $14,6 \text{ atoms/nm}^2$, the relation between cobalt dispersion and cobalt metal particle diameter is given by equation 3.4 [37].

$$d(\text{Co}^0) = \frac{96}{D} \quad 3.4$$

where d is given in nanometres and D in percent.



3.3.3 X-RAY DIFFRACTION

This section will shortly describe the characterisation method of X-ray diffraction (XRD). The reader is advised to study Klug and Alexander [38] for a more thorough treatment of the technique.

X-ray diffraction is a frequently used technique in catalyst characterisation. By means of lattice structural parameters crystalline phases inside the catalyst and/or support can be identified and quantified. For phase determination a XRD analysis requires crystallinity and particles with a diameter of at least 3-4 nm.

XRD is the elastic scattering of X-ray photons by atoms in a periodic lattice (crystal). X-rays have wavelengths in the Å range and are sufficiently energetic to penetrate solids. Monochromatic X-rays are produced by bombarding a X-ray target (such as Cu) with high energy electrons. Some electrons are slowed down by the target and emit a continuous background spectrum. This background spectrum causes the requirement of particle sizes larger than 3 nm. Superimposed on the background spectrum arises characteristic, Cu K α radiation (with an energy of 8.04 eV and a wavelength of 1.54 Å). This radiation arises from primary electrons creating a hole in the K-shell (in the target, Cu). This hole is filled by an electron from the L-shell, and thus emission of an X-ray quantum is emitted (K α radiation). If the hole is filled by an electron from the M-shell, a K β -ray is emitted. K β -rays are normally removed with a filter in the XRD apparatus. [39]

When a sample is bombarded with X-rays, the radiation is scattered by atoms in the ordered lattice. The scattered monochromatic X-rays that are in phase give constructive interference. Bragg's law, equation 3.5 allows us to calculate the lattice spacing.

$$n\lambda = 2d \sin \theta; \quad n = 1, 2, \dots \quad 3.5$$

where

λ	is the X-ray wavelength
d	is the lattice spacing, the distance between to lattice planes
θ	is the angle between the incoming X-rays and the normal to the reflecting lattice plane
n	is the order of the reflection, an integer

The Bragg equation makes it possible to calculate the spacing between the lattice planes from the angles of maximum intensity, and thus allows for phase identification.

The crystallinity is visualized as Gaussian lines in diffractograms measured as a function of 2θ . A stationary X-ray source (Cu K α) and a moveable detector enable the XRD patterns to be created. The detector scans the intensity of the diffracted radiation as a function of the angle between the incoming and the diffracted beams (2θ). [39]



The crystalline materials can be identified by comparing peaks with standards in a database [40].

In addition, XRD patterns can be used to estimate the size of the microcrystallites that may be present in the catalyst and/or support material. The crystal size is given by the Sherrer formula given in equation 3.6.

$$t = \frac{K\lambda}{\beta \cos \theta} \quad 3.6$$

where

λ	is the X-ray wavelength
β	is the full peak width at half maximum of the broadened peak
θ	is the Bragg angle
t	is the thickness of the crystal in a direction perpendicular to the diffracting planes
K	is the particle shape factor

Normally β in the Sherrer equation is calculated by:

$$\beta = \sqrt{B^2 - b^2} \quad 3.7$$

In equation 3.7, B is the experimental width at half the maximum of the relevant peak and b is a correction factor that stems from the instrument contribution to the peak width [41]. b has not been calculated for the Rigaku MiniFlex+ X-ray diffractometer used in this work, but the b -value should be the same for all samples. In this work the value of b is omitted from the calculations, and hence the particle sizes are calculated with the intention of finding relative sizes for the samples tested.

Diffraction peaks for perfect crystals are very narrow (large crystal size). Peak broadening arises from different sources (finite crystals, instrumental effects, and deformation of the atoms from ideal positions/strain). Peaks are broader as crystal size decreases, and for crystallite sizes below 100 nm line broadening can be large due to incomplete destructive interference in scattering directions where the X-rays are out of phase [39]. Amorphous materials show no sharp diffraction peaks, merely broad features. Peak intensity depends on the unit cell contents, point symmetry and phase fractions.

It is important to note that X-ray line broadening not always provides reliable estimates of the particle size, but it can serve as a method for determining relative particle sizes for similar samples.



3.3.4 NITROGEN (N₂) ADSORPTION/DESORPTION AND THE BET-METHOD

For gas reactions catalysed by porous solid materials, the rate of product formation is a function of the available surface area, hence the greater the surface area accessible to reactants the larger the rate of formation of products. [42] Nitrogen adsorption/desorption is a method used for total surface area quantification in porous structures.

Physical adsorption takes place on all surfaces provided temperature and pressure are favourable, and, as mentioned before, physical adsorption frequently leads to multilayer adsorption. Brunauer, Emmett and Teller proposed a model for multilayer physisorption and derived an equation that calculates the monolayer coverage of the adsorbate gas. This equation is called the BET-isotherm and is derived from a model that extends the Langmuir isotherm. It is therefore based on a number of assumptions [36];

1. Each adsorbed molecule in the first layer act as an adsorption site for the second layer, interactions between adsorbed species are ignored.
2. The rate of adsorption on one layer equals the rate of desorption from the layer above.
3. The heat of adsorption for the first layer (ΔH_1^0) is independent of the following layers, and the heat of adsorption for the second layer and all those above it equals the heat of liquefaction (ΔH_i^0) of the adsorbate gas (it is constant).

Measurements of accumulated gas quantity adsorbed vs. gas pressure at one given temperature yields an adsorption isotherm. Classical adsorption theory assumes that gas molecules admitted under increasing pressure to a clean cold surface form a layer that is one molecule deep on the surface before beginning a second layer. The BET technique finds the quantity of gas forming this first layer, and then the area covered is calculated from the number of gas molecules and gas molecule dimensions. [35]

For an infinite number of layers the following BET-equation is obtained, equation 3.8.

$$\frac{p}{V_a(p_0 - p)} = \frac{1}{V_m \cdot C} + \frac{C-1}{V_m \cdot C} \cdot \frac{p}{p_0} \quad 3.8$$

where V_a is the total volume adsorbed (STP) at equilibrium pressure, p , of adsorbed gas, V_m is the volume (STP) adsorbed at monolayer coverage, p_0 is the saturation vapour pressure of the adsorbed gas at the operating temperature, and C is, to a good approximation given by equation 3.9.

$$C = e^{\left(\frac{\Delta H_i^0 - \Delta H_1^0}{RT}\right)} \quad 3.9$$

where R is the gas constant and T is the operating temperature.



If the BET-equation is valid, a plot of $\frac{p}{V_a \cdot (p_0 - p)}$ as a function of $\frac{p}{p_0}$ yields a straight line, $y = ax + b$, where a is the slope and b is intercept. a and b can be used to evaluate the monolayer capacity, V_m .

$$a = \frac{1}{V_m \cdot C} \quad 3.10$$

$$b = \frac{C-1}{V_m \cdot C} \quad 3.11$$

$$V_m = \frac{1}{a+b} \quad 3.12$$

The specific surface area in m^2/g can be calculated from equation 3.13 when the volume of the monolayer is recorded in m^3 .

$$A = \frac{V_m \cdot N_A \cdot \sigma}{V_{ig} \cdot W} \quad 3.13$$

N_A is Avogadro's constant, σ is the area occupied by one adsorbed molecule, V_{ig} is the volume of one mole of ideal gas at STP, and W is the weight of the catalyst. The reader is referred to Tronstad [43] for the complete derivation of the BET-equation.

The Barrett, Joyner, Halenda (BJH) method can be used to calculate pore volumes and pore size distributions. This method assumes desorption data. The BJH method uses the Kelvin equation and a thickness equation (Halsey or Harkins-Jura) and steps off the desorbed volume. The computational algorithm used by this method frequently leads to inconsistencies when carried out to small pore sizes. This results in the calculation of a too large volume of small pores. [35]



4 Experimental

The following chapters give all the information necessary to reproduce the experiments conducted in this work. Additional information is given in Appendix A and B.

4.1 SUPPORT AND CATALYST PREPARATION

4.1.1 METAL LOADING

Catalysts containing 12 wt. % Co and 0,5 wt. % Re on magnesium modified alumina supports were prepared by one-step incipient wetness (co)-impregnation with aqueous solutions of cobalt nitrate hexahydrate, $\text{Co}(\text{NO}_3)_2 \cdot 6\text{H}_2\text{O}$ (Acros Organics, >99 %), and perrhenic acid (Alfa Aesar, 75 - 80 % aq. solution), HReO_4 . The modified supports were first prepared by impregnation of γ -alumina (Sasol Condea Puralox SCCa-45/190 lot 15104) with an aqueous solution of magnesium nitrate hexahydrate, $\text{Mg}(\text{NO}_3)_2 \cdot 6\text{H}_2\text{O}$ (Fisher Scientific). The magnesium loading for all supports was 7,5 wt. % magnesium.

The state of incipient wetness was determined by drop-wise water addition to the supports until filled pores were achieved (full capillary condensation). The point of completely filled pores was perceived to be the point where no free flowing liquid could be detected upon knocking. The water was at this point kept in the support material by surface attractive forces, but could be forced out of the pores by knocking the sample against a solid surface.

After measuring the water absorptivity at the point of incipient wetness (mL/g), the same specific volume of metal precursor(s) was added to the supports. The mixture was then thoroughly homogenized by stirring before it was placed in an ambient air furnace kept at 110 °C. The samples were dried for 3 h and stirred gently every 15 min. the first hour and every 30 min. the last two hours.

The dried magnesium modified supports were calcined in flowing air in a calcination furnace. The different samples underwent a series of calcination steps. The preparation procedure for the different supports is presented in Figure 4.1.

Table 4.1 describes the calcination process for the different calcination temperatures used in this work.

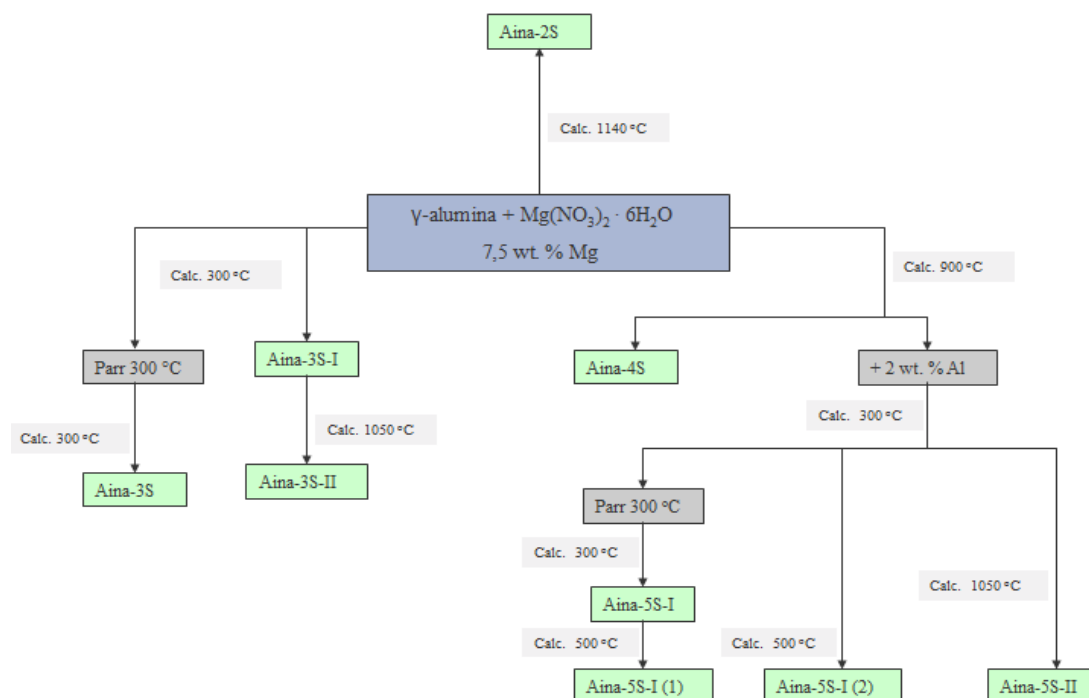


Figure 4.1 Overview of the several preparation steps for the different magnesium modified γ -alumina supports.

Table 4.1 A description of the different calcination processes used in this work.

Calcination temperature [°C]	Heating rate [°C/h]	Dwell time [h]	Cooling rate [°C/h]
300	150	16	150
500	170	10	170
900	190	10	190
1050	300	10	150
1140	300	10	150

Some samples (Aina-5S-I, Aina-5S-I (1), Aina-5S-I (2) and Aina-5S-II) were loaded with extra 2 wt. % aluminium after magnesium loading. Supports containing extra 2 wt. % aluminium were prepared by one step incipient wetness impregnation with aqueous solutions of aluminium nitrate nonahydrate, $\text{Al}(\text{NO}_3)_3 \cdot 9\text{H}_2\text{O}$ (Acros Organics, >99 %) of the magnesium modified alumina supports.

A total of 9 different magnesium modified supports were prepared. The supports are different with respect to the temperature at which they were calcined, whether or not the samples were loaded with extra 2 wt. % aluminium, and whether or not they were



treated hydrothermally in an autoclave Parr-CSTR, see section 4.1.2. All the different support preparation steps are described in Figure 4.1.

A total of 6 different catalysts, all containing 12 wt. % Co and 0,5 wt. % Re, were prepared. Figure 4.2 presents which catalyst corresponds to which support and how the catalysts were prepared.

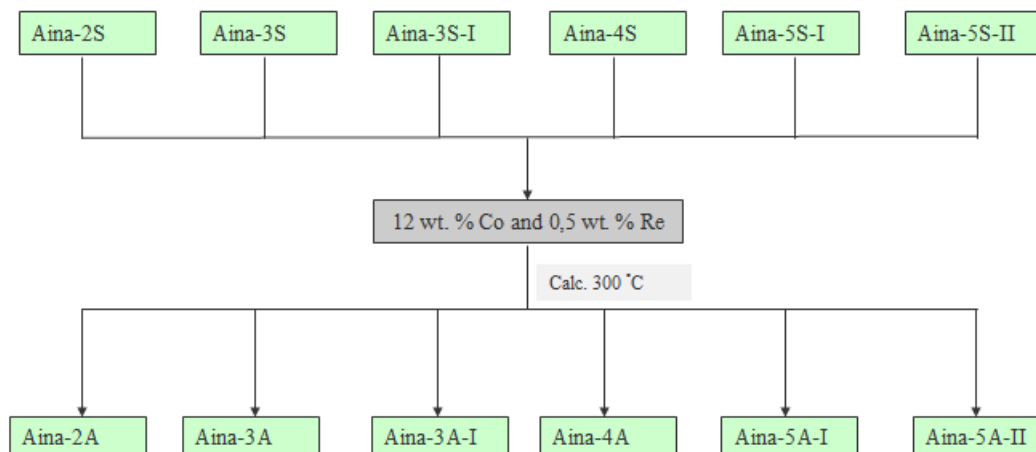


Figure 4.2 Preparation process from support to catalyst.

All samples (supports and catalysts) were sieved after the last calcination step into fractions: $\geq 90 \mu\text{m}$, $53 - 90 \mu\text{m}$, $\leq 53 \mu\text{m}$. The second fraction was used for the Fischer-Tropsch synthesis, the N_2 adsorption/desorption analysis and the H_2 chemisorption analysis. The third fraction (small particles) was used for X-ray diffraction measurements.

To clarify, Table 4.2 describes the preparation process for the different supports and catalysts prepared in this work. Magnesium, aluminium, cobalt and rhenium loadings were all performed through the incipient wetness impregnation method with subsequent drying and calcination. The procedure for calculating the necessary amounts of cobalt nitrate hexahydrate, perrhenic acid, magnesium nitrate hexahydrate, aluminium nitrate nonahydrate and water needed for the impregnation steps, and the necessary amount of water per support mass needed to reach the state of incipient wetness (water absorptivity) are described in appendix A.



Table 4.2 Preparation process for the different supports and catalysts prepared in this work.

Sample	Mg- Al - Co - Re [wt. %]	Hydrothermal support treatment, 300 °C	Support	Support calcination temperature [°C]	Support promoted with 2 wt. % Al	Catalyst calcination temperature [°C]
Aina-2S	7,5-0-0-0	no	γ -alumina	1140	no	-
Aina-3S	7,5-0-0-0	yes	γ -alumina	300,300	no	-
Aina-3S-I	7,5-0-0-0	no	γ -alumina	300	no	-
Aina-3S-II	7,5-0-0-0	no	γ -alumina	300,1050	no	-
Aina-4S	7,5-2-0-0	no	γ -alumina	900	no	-
Aina-5S-I	7,5-2-0-0	yes	γ -alumina	900,300,300	yes	-
Aina-5S-I (1)	7,5-2-0-0	yes	γ -alumina	900,300,300,500	yes	-
Aina-5S-I (2)	7,5-2-0-0	no	γ -alumina	900,300,500	yes	-
Aina-5S-II	7,5-2-0-0	no	γ -alumina	900,300,1050	yes	-
Aina-2A	7,5-0-12-0,5	no	Aina-2S	1140	no	300
Aina-3A	7,5-0-12-0,5	yes	Aina-3S	300,300	no	300
Aina-3A-I	7,5-0-12-0,5	no	Aina-3S-I	300	no	300
Aina-4A	7,5-0-12-0,5	no	Aina-4S	900	no	300
Aina-5A-I	7,5-2-12-0,5	yes	Aina-5A-I	900,300,300	yes	300
Aina-5A-II	7,5-2-12-0,5	no	Aina-5S-II	900,300,1050	yes	300

4.1.2 HYDROTHERMAL TREATMENT IN AN AUTOCLAVE PARR CSTR

Selected supports, (Aina-3S, Aina-5S-I and Aina-5S-I (1)) were treated hydrothermally in an Autoclave Parr CSTR after magnesium and aluminium loading. The Autoclave Parr CSTR is a 500 mL semi-continuous batch reactor that can withstand a temperature of up to 350 °C, a pressure of 70 bar, a rate of rotation of 2000 rpm and a gas flow velocity of 10 NL/min [44]. Rate of rotation, temperature, gas flows (N₂, H₂, air and CO₂) and pressure can be controlled. In addition it is possible to extract samples during an experiment, without shutting down the reactor, by means of a liquid sampling valve. Figure 4.3 depicts the Autoclave Parr-reactor used in this work and a description of the removable head components.

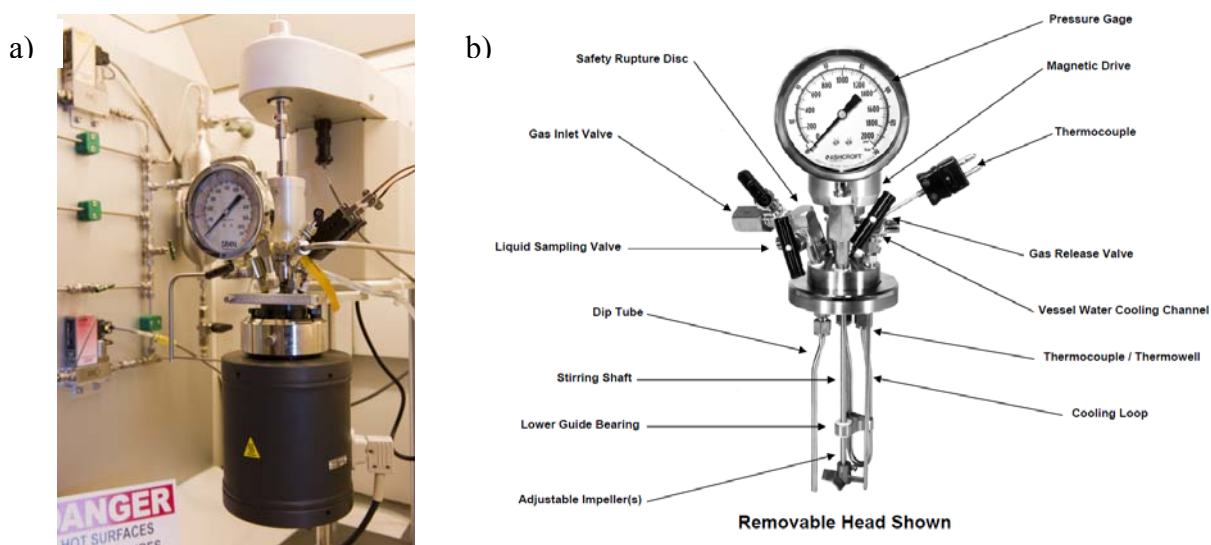


Figure 4.3 a) A picture of the Autoclave Parr-CSTR and b) a description of the components of the removable head.

The reactor was loaded with ~10 g of powder support and 10 g of de-ionized water. A detailed description on how to mount the reactor is given in Appendix B. It was particularly important to check that all valves were closed. [44]

The rate of rotation was carefully adjusted to 500 rpm. This value was kept constant in every experiment. The temperature was adjusted to 300 °C in the control panel. It took about one hour for the system to reach the desired temperature. At 300 °C for the closed system the corresponding water vapour pressure was ~30 bar. The above mentioned conditions were held constant for 1 hour. A detailed description on how to adjust the rate of rotation and temperature is given in Appendix B.

Post treatment in Parr reactor the supports were dried in ambient air in a furnace kept at 110 °C for 1 hour. Subsequently the samples were calcined in a calcination furnace (fitted with a fan to ensure constant air volume exchange) at 300 °C; see Table 4.1 for a description of the calcination process.



4.2 SUPPORT AND CATALYST CHARACTERISATION

This section describes the specific methods used to characterize the supports and catalysts in this work.

4.2.1 X-RAY DIFFRACTION

X-ray diffraction patterns were recorded for all the supports at ambient temperature on a Rigaku MiniFlex+ X-ray diffractometer using CuK α radiation. The samples were finely ground and compacted in a sample holder before measurement. The X-ray tube voltage was set to 30 kV and the current to 15 mA.

Phase identification data were collected in the 2θ range from 10-90° using a step size of 0,02 and counting for 10 s at each step. Phases were identified by comparing peaks in the diffraction pattern with standards in a database [40].

Relative γ -alumina particle sizes were determined by applying the Sherrer equation on the (440) diffraction peak located at $2\theta = 66,5^\circ$. To correct for the spherical γ -alumina particles the shape factor was set to 0,89. The X-ray wavelength is 1,54 Å. The instrumental line broadening was not calculated. Normally β in the Sherrer equation is calculated from equation 3.7.

$$\beta = \sqrt{B^2 - b^2} \quad 3.7$$

In equation 3.7, B is the experimental width at half the maximum of the γ -alumina peak at $2\theta = 66,5^\circ$ and b is a correction factor that stems from the instrument contribution to the peak width [41]. b has not been calculated for the Rigaku MiniFlex+ X-ray diffractometer used in this work, but the b -value should be the same for all samples. In this work the value of b is omitted from the calculations, and hence the particle sizes are calculated with the intention of finding relative sizes for the samples tested.

4.2.3 HYDROGEN (H₂) CHEMISORPTION

Chemisorption with H₂ was performed on a Micromeritics ASAP 2020 unit. A U-shaped quartz reactor was loaded with ~0,4 g of catalyst (53 - 90 μm) and mounted inside an electric furnace. Quartz wool was used to keep the catalyst sample in place inside the reactor during evacuation. The sample temperature was measured by mounting a thermocouple outside the reactor in approximately the same height as the catalyst sample. The samples were initially dried in vacuum for two hours at 250 °C. Before the temperature analysis program was started, a vacuum test was performed. This was done to prevent leaks during analysis. The leak test was performed by first



evacuating the samples until the pressure stabilized and then turning off the vacuum pumps and measuring the pressure increase per time. When leaks were excluded the temperature analysis program was started:

The samples were evacuated at 40 °C for one hour before being reduced *in situ* in flowing hydrogen for 16 hours at 350 °C. For the 40 - 350 °C temperature increase, the ramping rate was held constant at 1 °C/min. Following the reduction, the samples were evacuated for 1 hour at 330 °C and then evacuated for 30 min at 100 °C. Lastly the samples were cooled to 40 °C where the adsorption isotherms were obtained.

The adsorbed amount of hydrogen at 11 different pressures in the range 15 - 500 mmHg formed the basis for constructing the adsorption isotherm at 40 °C. By extrapolating the straight-line portion of this isotherm to zero pressure, the amount of hydrogen gas required to form a monolayer on the catalyst surface could be estimated. For the cobalt dispersion calculation equation 3.3 was used. The cobalt dispersion was used to estimate the cobalt particle size by applying equation 3.4.

4.2.4 NITROGEN ADSORPTION/DESORPTION

N₂ adsorption and desorption isotherms were collected for all catalysts and supports at the boiling point of liquid nitrogen (-196 °C) using a Micromeritics TriStar 3000 instrument. ~0, 5 g of catalysts or support (53 - 90 μm) was loaded in a sample tube and dried in vacuum at 250 °C for 2 hours. The samples were subsequently cooled to room temperature before starting the experiment.

The BET specific surface area, A , was calculated from the adsorption isotherm using equation 3.13. The monolayer capacity, V_m , was obtained by plotting $\frac{p}{V_a \cdot (p_0 - p)}$ as a

function of $\frac{p}{p_0}$ in the pressure range $0 < \frac{p}{p_0} < 0,3$. Pore size distribution and the total pore volume were found from the BJH method. Desorption data were used for the pore size analysis.



4.3 FISCHER-TROPSCH SYNTHESIS

The most important aspects with regards to the experimental procedure for the FT-synthesis testing are given in this section. Additions to the procedure, together with certain advices and guidance on how to improve and better understand the procedure are given in Appendix B.

4.3.1 PROCEDURE

The Fischer-Tropsch synthesis was carried out in two parallel fixed-bed reactors. A schematic of the double fixed-bed test unit is presented in Figure 4.4. The feed gases used for this work were pure, and no purification was needed, hence gas driers and oxy-traps installed in the FT-synthesis setup used for this work were redundant. In addition, the feed gases were delivered in aluminium cylinders which mean that the installed carbonyl traps for removal of iron carbonyls were superfluous as well. Mass flow controllers (MFC), used to control the feed gas flow rates, were calibrated using a soap-bubble flow-meter. A detailed description on how to calibrate the MFC's are presented in Appendix B.

Reaction conditions are summarized in Table 4.3

Table 4.3 Reaction conditions used for every experiment conducted in this work.

Temperature [°C]	210
Pressure [bar]	20
Feed gas ratio [H₂/CO]	2,1

A feed gas analysis was performed before each run to obtain accurate feed gas compositions for the Fischer-Tropsch synthesis (FTS) data analysis. A gas chromatograph (GC) HP6890A equipped with a thermal conductivity detector (TCD), a flame ionizing detector (FID) unit and a GS-Alumina PLOT column were used for all gas analyses.

Reactor temperatures and temperatures at several other positions in the setup were logged and monitored. The temperature monitoring was needed to ensure a sufficient viscosity for extraction of the heaviest products and to avoid thermic methanation downstream of the reactors.

The two fixed-bed reactors were constructed in stainless steel with an inner diameter of 10 mm. The reactors were loaded with 1 g of catalyst (53 - 90 μm) diluted with 10 g of inert SiC to ensure proper heat distribution (isothermicity) throughout the



catalyst bed. The catalyst bed was kept in place by quartz wool. Temperature gradients were further minimized by placing the reactor cylinders in aluminium jackets. An electrical furnace connected to a Eurotherm controller was used to heat the reactor systems.

The catalysts were reduced *in situ* with flowing hydrogen at 350 °C and 1,5 bar hydrogen (H₂) pressure. The temperature was ramped at 1 °C/min and kept at 350 °C for 16 hours. The catalyst bed was successively cooled to 170 °C and pressurized to 20 bar using 250 NmL/min helium. Synthesis gas was introduced at 250 NmL/min after turning off the helium flow. The temperature was then ramped at 0,5 °C/min to 190 °C, then 5 °C/h to 200 °C, and finally 0,1 °C/min to 210°C. Temperature profiles for each catalyst bed were monitored to ensure isothermicity.

A constant feed gas flow rate of 250 NmL/min was kept for 30 hours, before it was reduced in order to reach ~50 % CO conversion (measured by the gas chromatograph). The adjusted flow rate was kept at the reduced rate for 24 hours. This corresponds to a total of ~54 hours on stream. Reported data for conversion, reaction rate, olefin/paraffin ratio and turn over frequency (TOF) are acquired after 15 hours of stable operation. Selectivity data are reported after 10 hours of stable operation (after flow adjustments to reach 50 % CO conversion).

To collect the synthesis products, two traps were kept downstream; a hot trap kept at ~90 °C for the collection of heavy products and a cold trap kept at room temperature for the collection of the light liquid products. For each run the heaviest products (wax) were separated out prior to the downstream gas analysis. Gases lighter than C₅ were fed to the Agilent HP6890A gas chromatograph for analysis. Products ranging from C₁ - C₄, together with unconverted CO, were quantified in order to determine the amount of C₅₊ in the product mixture. ~3 vol. % nitrogen (N₂) in the feed gas served as an internal standard for the quantification. The GC quantification is within ±0,5 % uncertainty.

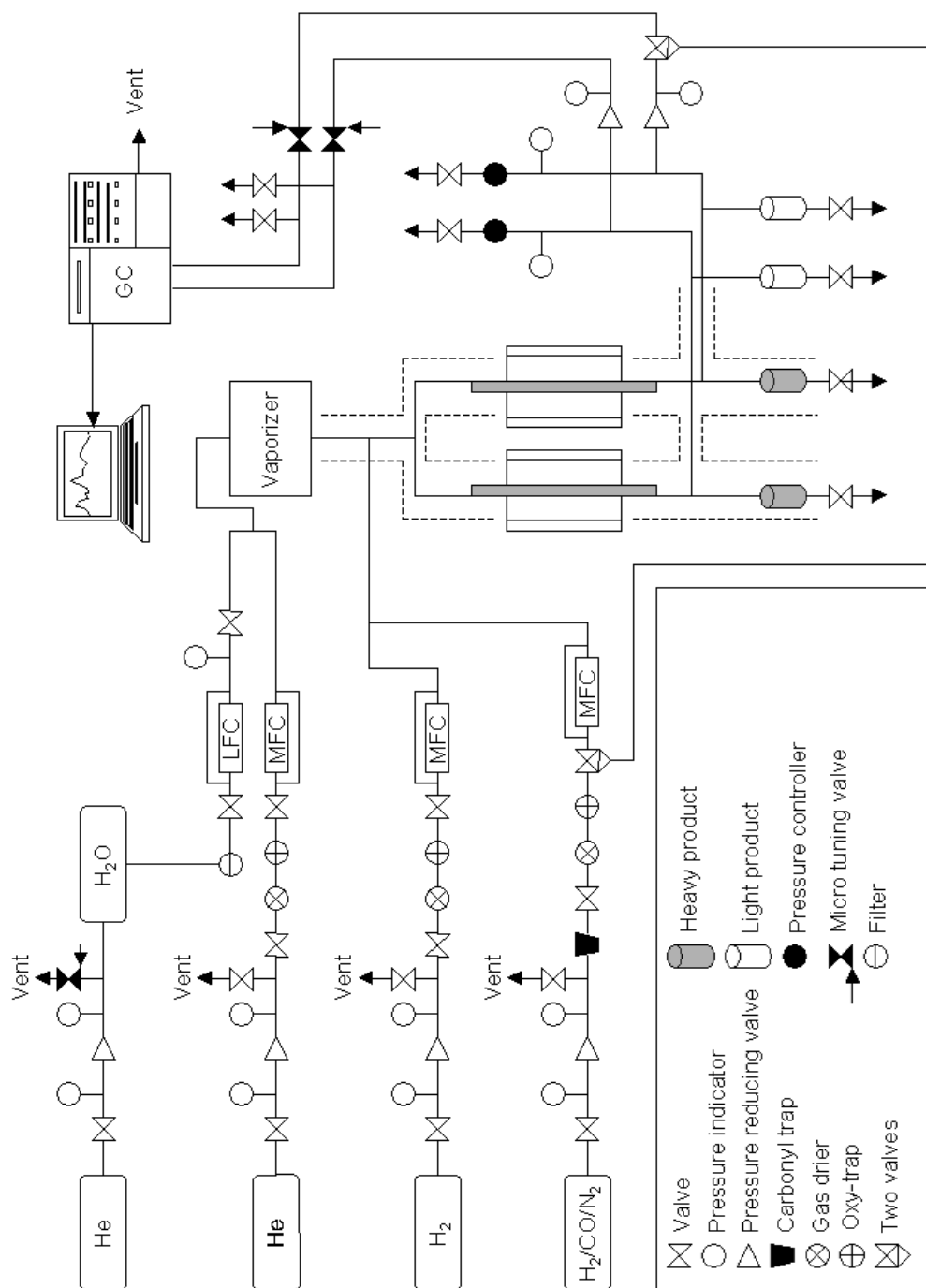


Figure 4.4 The Fischer-Tropsch synthesis apparatus used in this work².

² The schematic of the apparatus is copied from Bjørn Christian Enger's Master thesis. The rig has since that been modified, but the main features are the same.

4.3.2 DATA ANALYSES

Fischer-Tropsch synthesis data is based on gas chromatography of the gas compositions on the inlet and outlet side of the catalyst bed. The amount of data obtained from the GC for each experiment is immense. To avoid time-consuming and tedious calculation work, data analysis was performed using a pre-programmed excel sheet developed by Bjørn Chritian Enger for his PhD thesis in 2007. A detailed description of the theoretical basis for the calculations performed in excel is given in this section. The derivation is based on the work presented in Bjørn Chritian Enger's master thesis (from 2005) and Øyvind Borg's master thesis (from 2003). The pre-programmed excel sheets and data extraction sheets constructed by the author of this thesis are given in Appendix D.

Figure 4.5 depicts the conceptual outline of the analysis unit including the GC. The feed gas mixture was analyzed by reactor by pass.

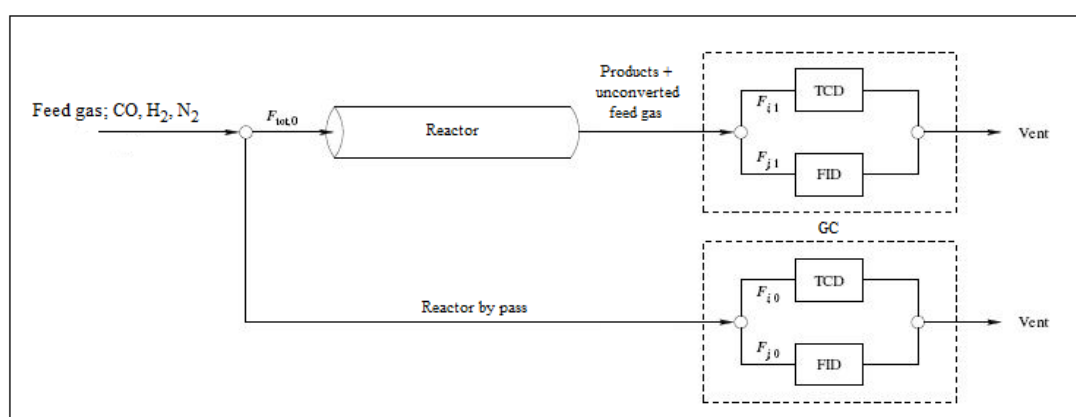


Figure 4.5 Flowsheet for the Fischer-Tropsch synthesis apparatus including the GC equipped with a TCD and a FID.

The GC used two different techniques to analyze the gas compositions. The TCD can detect H₂, N₂, CO, H₂O, CO₂ and CH₄. The FID can detect the hydrocarbon components from CH₄ and heavier. The heaviest hydrocarbon components, typically components with a boiling point above room temperature were removed from the product stream before the GC analysis. The reason for this is to avoid condensation of heavier products inside the lines of the setup. No products lighter than C₅ were removed.

Only a fraction of the FT-products was analyzed by the GC, and in order to get quantitative data for each component it was necessary to incorporate an internal standard which is inert to the reactions in the test unit. As a reference for quantification, a known amount of N₂ was added to the GC feed gas.

Approximately once every hour a sample was injected to the GC. The components in the unknown sample were separated by their different speed of capillary flow though the long column. As mentioned in section 3.1.3, the GC converts amount signals to electrical signals and displays the separation as chromatograms with characteristic peaks for different components. The chromatogram peak area for one component is



proportional to the amount of that specific component in the mixture. By integrating the area under a specific peak it was possible to calculate the amount. However, the GC response to different components may vary, and peak response factors were needed to get accurate results. This is where the internal standard asserts itself. The molar ratio of a specific component to the internal standard can be calculated by knowing the relative peak area of nitrogen and the component peak. The GC needed to be pre-calibrated with response factors ($\varepsilon_{i,0}$, moles per area) and retention times before measurements. A description of how the GC was calibrated with respect to retention times is given in Appendix B.

In the following derivations the inlet side of the reactor is denoted 0 and the outlet side is denoted 1, the subscript i represents the TCD detected components and the subscript j represents the components detected by the FID ($j = 1$ is CH_4).

The CO conversion, X_{CO} , can be calculated from equation 4.1.

$$X_{CO} = \frac{F_{CO,0} - F_{CO,1}}{F_{CO,0}} \quad 4.1$$

Mole fractions and flow rates of each component are closely linked to the total flow rate. On the inlet side the flow of each component can be written

$$F_{i,0} = x_{i,0} \cdot F_{tot,0} \quad 4.2$$

In order to calculate the conversion an expression for the mole fraction of component i needs to be established. The ratio of mole fractions between each component and the internal standard (N_2) at the reactor inlet can be expressed

$$\Psi_{i,0} = \frac{x_{i,0}}{x_{N_2,0}} \quad 4.3$$

As mentioned above, this mole fraction ratio, $\Psi_{i,0}$, is proportional to the relative chromatogram peak area of component i , $A_{i,0}$, and the peak area of nitrogen, $A_{N_2,0}$, detected by the TCD. The proportional constant is the relative response factor, $E_{i,0}$, expressed by equation 4.4.

$$E_{i,0} = \frac{\varepsilon_{i,0}}{\varepsilon_{N_2,0}} \quad 4.4$$

The mole fraction ratio of component i can be written

$$\Psi_{i,0} = \frac{\varepsilon_{i,0}}{\varepsilon_{N_2,0}} \cdot \frac{A_{i,0}}{A_{N_2,0}} = E_{i,0} \cdot \frac{A_{i,0}}{A_{N_2,0}} \quad 4.5$$



Equation 4.3 can be rewritten to express the mole fraction of component i , $x_{i,0}$

$$x_{i,0} = x_{N_2,0} \cdot \Psi_{i,0} \quad 4.6$$

Conservation of mass predicts that

$$\sum_{i=1}^n x_{i,0} = \sum_{i=1}^n x_{i,1} = 1 \quad 4.7$$

Hence equation 4.6 becomes

$$\sum_{i=1}^n x_{N_2,0} \cdot \Psi_{i,0} = 1 \quad 4.8$$

If N_2 is component 1 then equation 4.8 may be written

$$\Psi_{i,0} \cdot x_{N_2,0} + \sum_{i=2}^n x_{N_2,0} \cdot \Psi_{i,0} = 1 \quad 4.9$$

Since $\Psi_{N_2,0} = 1$, equation 4.8 becomes

$$x_{N_2,0} \cdot \left(1 + \sum_{i=2}^n \Psi_{i,0} \right) = 1 \quad 4.10$$

By combining equation 4.3 and 4.10 it follows that

$$x_{i,0} = \frac{\Psi_{i,0}}{1 + \sum_{i=2}^n \Psi_{i,0}} \quad 4.11$$

The molar flow rates at the reactor inlet for H_2 , CO and N_2 can now be determined (the feed gas analysis).

$$F_{i,0} = x_{i,0} \cdot F_{tot,0} = x_{i,0} \cdot \frac{F_{N_2,0}}{x_{N_2,0}} \quad 4.12$$

$$F_{i,0} = \Psi_{i,0} \cdot F_{N_2,0} \quad 4.13$$

The expression for CO conversion still requires the molar flow rate of CO at the outlet (denoted 1) of the reactor. The derivation of an expression describing the mole fraction ratio for a component i to the internal standard on the reactor outlet side is the same as for the reactor inlet side. The results are presented in equation 4.14 and 4.15.



$$\Psi_{i,1} = E_{i,1} \frac{A_{i,1}}{A_{N_2,1}} \quad 4.14$$

$$x_{i,1} = \frac{\Psi_{i,1}}{1 + \sum_{i=2}^n \Psi_{i,1}} \quad 4.15$$

The molar flow rates at the reactor outlet for H₂, CO and N₂ can be determined from

$$F_{i,1} = x_{i,1} \cdot F_{tot,1} = x_{i,1} \cdot \frac{x_{N_2,0}}{x_{N_2,1}} \cdot F_{tot,0} \quad 4.16$$

Nitrogen is inert during FT-synthesis and consequently $F_{N_2,0} = F_{N_2,1}$

$$F_{i,1} = \Psi_{i,1} \cdot F_{N_2,0} \quad 4.17$$

The CO conversion can now be calculated by summarizing the equations above.

$$X_{CO} = \frac{F_{CO,0} - F_{CO,1}}{F_{CO,0}} = 1 - \frac{A_{CO,1}}{A_{CO,0}} \cdot \frac{A_{N_2,0}}{A_{N_2,1}} \quad 4.18$$

Selectivity data can be obtained by applying a carbon count strategy. The FID can not detect nitrogen. Therefore a different reference is needed to quantify C₂₊ products. Methane (CH₄) is detected by both the TCD and the FID; hence CH₄ can be used as a reference to calculate the amounts of C₂ - C₄. The subscript j describes the FID detected components and n describes the total carbon atoms in that component (for CH₄ $j = 1$ and $n = 1$).

The selectivity towards component j with n carbon atoms in the product gas (reactor outlet) can be expressed by equation 4.19.

$$S_j = n \cdot \frac{F_{j,1} - F_{j,0}}{F_{CO,0} - F_{CO,1}} \quad 4.19$$

It is assumed that the feed gas consists merely of CO, H₂ and N₂. Then $F_{j,0} = 0$ and equation 4.19 becomes

$$S_j = n \cdot \frac{F_{j,1}}{X_{CO,0} \cdot F_{CO,1}} \quad 4.20$$

An expression for the calculation of the molar flow rates in the product stream is needed to get selectivity data from equation 4.20. The mole fraction ratio of



component j containing n carbon atoms and the internal standard at the reactor outlet can be calculated from

$$\Psi_{j,1} = \frac{x_{j,1}}{x_{N_2,1}} = \frac{A'_{j,1}}{A'_{1,1} \cdot n} \cdot \Psi_{CH_4,1} \quad 4.21$$

where n accounts for the response area in proportion to the number of carbon atoms present in compound j . The notation ' in $A'_{j,1}$ represent that the area is detected by the FID, hence $A'_{1,1}$ is the CH_4 area detected by the FID.

The molar flow rate of product j in the reactor outlet is thus given by

$$F_{j,1} = \Psi_{j,1} \cdot F_{N_2,0} \quad 4.22$$

The molar flow rates of the hydrocarbon products at the reactor outlet can now be determined. This means that the compositions and flow rates for every components participating in the Fischer-Tropsch synthesis is known, and that selectivities and reaction rates may be calculated.

$$S_j = n \cdot \frac{F_{j,1}}{X_{CO,0} \cdot F_{CO,1}} = \frac{\varepsilon_{CH_4} \cdot A'_{j,1} \cdot A_{CH_4,1} \cdot A_{N_2,0}}{\varepsilon_{CO} \cdot A'_{1,1} \cdot (A_{CO,0} \cdot A_{N_2,1} - A_{CO,1} \cdot A_{N_2,0})} \quad 4.23$$

The selectivity towards carbon dioxide is as follows

$$S_{CO_2} = n \cdot \frac{F_{CO_2,1}}{X_{CO,0} \cdot F_{CO,1}} = \frac{\varepsilon_{CO_2} \cdot A_{CO_2,1} \cdot A_{N_2,0}}{\varepsilon_{CO} \cdot (A_{CO,0} \cdot A_{N_2,1} - A_{CO,1} \cdot A_{N_2,0})} \quad 4.24$$

C_{5+} selectivity can be calculated from equation 4.25, hence selectivity is defined as the fraction of the carbon atoms present in the feed gas that ends up in a product containing five or more carbon atoms.

$$S_{C_{5+}} = 1 - S_{CO_2} - \sum_{j=1}^4 S_j \quad 4.25$$

$$S_{C_{5+}} = 1 - \frac{A_{N_2,0}}{\varepsilon_{CO} (A_{CO,0} \cdot A_{N_2,1} - A_{CO,1} \cdot A_{N_2,0})} \cdot \left(\varepsilon_{CO_2} \cdot A_{CO_2,1} + \frac{\varepsilon_{CH_4} \cdot A_{CH_4,1}}{A'_{1,1}} \cdot \sum_{j=1}^4 A'_{j,1} \right) \quad 4.26$$

The C_{5+} selectivity data reported in this thesis is calculated by neglecting the formation of CO_2 during FT-synthesis. Hence equation 4.25 becomes



$$S_{C_{5+}} = 1 - \sum_{j=1}^4 S_j \quad 4.27$$

Thus the C_{5+} selectivity can be found from

$$S_{C_{5+}} = 1 - \frac{A_{N_2,0} \cdot \varepsilon_{CH_4} \cdot A_{CH_4,1}}{\varepsilon_{CO} \cdot A'_{1,1} (A_{CO,0} \cdot A_{N_2,1} - A_{CO,1} \cdot A_{N_2,0})} \cdot \sum_{j=1}^4 A'_{j,1} \quad 4.28$$

The reaction rate based on CO consumption can be calculated from

$$-r_{CO} = \frac{X_{CO} \cdot F_{CO}}{W} = \frac{F_{tot,0} \cdot \varepsilon_{CO} \cdot A_{N_2,0} \cdot \left(\frac{A_{CO,0}}{A_{N_2,0}} - \frac{A_{CO,1}}{A_{N_2,1}} \right)}{W \cdot (\varepsilon_{N_2} \cdot A_{N_2,0} + \varepsilon_{CO} \cdot A_{CO,0} + \varepsilon_{H_2} \cdot A_{H_2,0})} \quad 4.29$$

Specific catalyst activity or turnover frequency (TOF) is frequently reported in connection with kinetic experiments. The experiments in this study were not specifically tailored to give data in the absence of transport limitations as is usually the case when TOF is reported. TOF were calculated from equation 4.30 and describes the specific reaction rate per cobalt active site

$$TOF = \frac{-r_{CO} \cdot M}{3600 \cdot x \cdot D} \quad 4.30$$

where $-r_{CO}$ is the reaction rate in mol CO converted per gram catalyst and hour, M is the atomic weight of cobalt, x is the weight fraction of cobalt on the catalyst and D is the dispersion of the catalyst obtained from volumetric chemisorption of H_2 . 3600 is the number of seconds per hour.



5 Results and discussion

This section presents the results obtained in this work, together with some associating explanations and discussions. Only key results is presented here while more extensive tables, figures and raw-data files can be found in Appendix D.

Support and catalyst preparation together with nitrogen adsorption/desorption, hydrogen chemisorption and X-ray diffraction characterization were conducted at Statoil R&D centre at Rotvoll. The Fischer-Tropsch synthesis analysis was performed in a doble fixed-bed unit at The Department of Chemical Engineering at NTNU.

5.1 SUPPORT AND CATALYST PREPARATION

Figure 4.1 and Table 4.2 from the experimental procedeeur in included in this section in order to make it easier for the reader to understand the results.

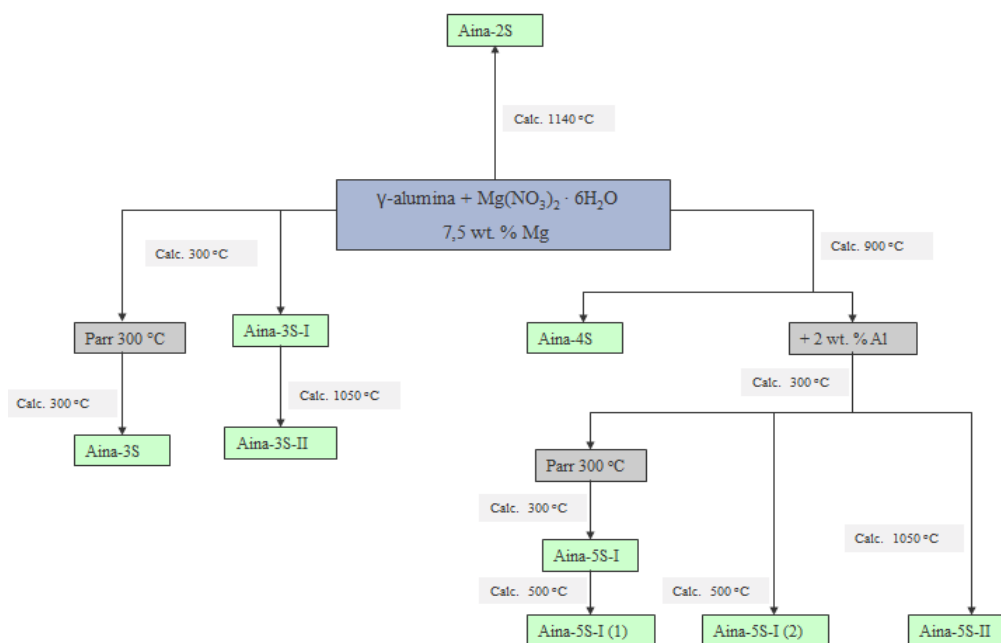


Figure 4.1 Overview of the several preparation steps for the different magnesium modified γ -alumina supports.



Table 4.2 Preparation process for the different supports and catalysts prepared in this work.

Sample	Mg- Al - Co - Re [wt. %]	Hydrothermal support treatment, 300 °C	Support	Support calcination temperature [°C]	Support promoted with 2 wt. % Al	Catalyst calcination temperature [°C]
Aina-2S	7,5-0-0-0	no	γ -alumina	1140	no	-
Aina-3S	7,5-0-0-0	yes	γ -alumina	300,300	no	-
Aina-3S-I	7,5-0-0-0	no	γ -alumina	300	no	-
Aina-3S-II	7,5-0-0-0	no	γ -alumina	300,1050	no	-
Aina-4S	7,5-2-0-0	no	γ -alumina	900	no	-
Aina-5S-I	7,5-2-0-0	yes	γ -alumina	900,300,300	yes	-
Aina-5S-I (1)	7,5-2-0-0	yes	γ -alumina	900,300,300,500	yes	-
Aina-5S-I (2)	7,5-2-0-0	no	γ -alumina	900,300,500	yes	-
Aina-5S-II	7,5-2-0-0	no	γ -alumina	900,300,1050	yes	-
Aina-2A	7,5-0-12-0,5	no	Aina-2S	1140	no	300
Aina-3A	7,5-0-12-0,5	yes	Aina-3S	300,300	no	300
Aina-3A-I	7,5-0-12-0,5	no	Aina-3S-I	300	no	300
Aina-4A	7,5-0-12-0,5	no	Aina-4S	900	no	300
Aina-5A-I	7,5-2-12-0,5	yes	Aina-5A-I	900,300,300	yes	300
Aina-5A-II	7,5-2-12-0,5	no	Aina-5S-II	900,300,1050	yes	300

It was difficult to reach the exact point of incipient wetness in the beginning of the preparation work. A somewhat dry impregnation (not complete capillary condensation) resulted for sample Aina-3A when cobalt and rhenium were added. It is believed that this did not cause any substantial effects on the results.

The incentive for adding extra aluminium to the magnesium modified supports was to investigate if this could lead to formation of α -alumina at lower temperatures. The idea was that the extra 2 wt. % aluminium would act as a growth initiator, as seeds for α -alumina growth.



5.2 SUPPORT AND CATALYST CHARACTERISATION

This section presents the results obtained from the characterization work.

5.2.1 X-RAY DIFFRACTION

X-ray diffraction patterns were recorded for all the supports at ambient temperature on a Rigaku MiniFlex+ X-ray diffractometer using $\text{CuK}\alpha$ radiation. The X-ray diffractograms for the different supports are presented in Figure 5.1 to Figure 5.3. Data retrieved from the Rigaku MiniFlex+ and all the different corresponding diffractograms are presented digitally in Appendix 0. The peaks in the measured diffractograms were compared to standards from a database [40] included in the Rigaku Integrated X-ray Powder Diffraction software. These standards are presented in Appendix C as well. Calculations performed in order to determine the γ -alumina particle size for the samples Aina-3S-I, Aina-3S and pure γ -alumina powder are presented in Appendix A.

The X-ray diffractograms for pure α -alumina is presented in Appendix C. The measured pattern for α -alumina consists of 10 distinct peaks. Figure 5.1 clearly indicates that the 10 distinct peaks observed for pure α -alumina powder are present in Aina-2S. This sample was calcined at 1140 °C. The additional 10 distinct peaks correspond to MgAl_2O_4 spinel. This was observed by comparing the 2θ values in Figure 5.1 with the standards in Appendix C. The diffractograms shows that calcination at this temperature leads to a support material consisting of crystalline α -alumina and MgAl_2O_4 spinel phase. The narrower the peak the more crystalline is the material. The relative intensities of the peaks indicate relative amounts of phases compared to each other. Figure 5.1 then indicates that calcination at higher temperatures (1140 °C for Aina-2S compared to 1050 °C for Aina-3S-II and 5S-II) leads to a support material with more α -alumina compared to MgAl_2O_4 spinel and a more crystalline material (larger crystallite sizes).

All of the detected peaks in Figure 5.1 have been identified as either α -alumina or MgAl_2O_4 spinel. The crystallinity appears to be approximately the same for the two samples Aina-3S-II and Aina-5S-II. These two samples are different in whether or not they have been impregnated with additional 2 wt. % aluminium post magnesium impregnation (Aina-5S-II was promoted with aluminium while Aina-3S-II was not). Peak intensities of these two samples indicate that α -alumina formation is intensified by extra alumina addition. The α -alumina peaks are more intense for 5S-II than for 3-II. All of the peaks are narrow, hence crystal grains are large enough to avoid fractions being missed by the detector (as could be the case for the γ -alumina samples, see Figure 5.2).

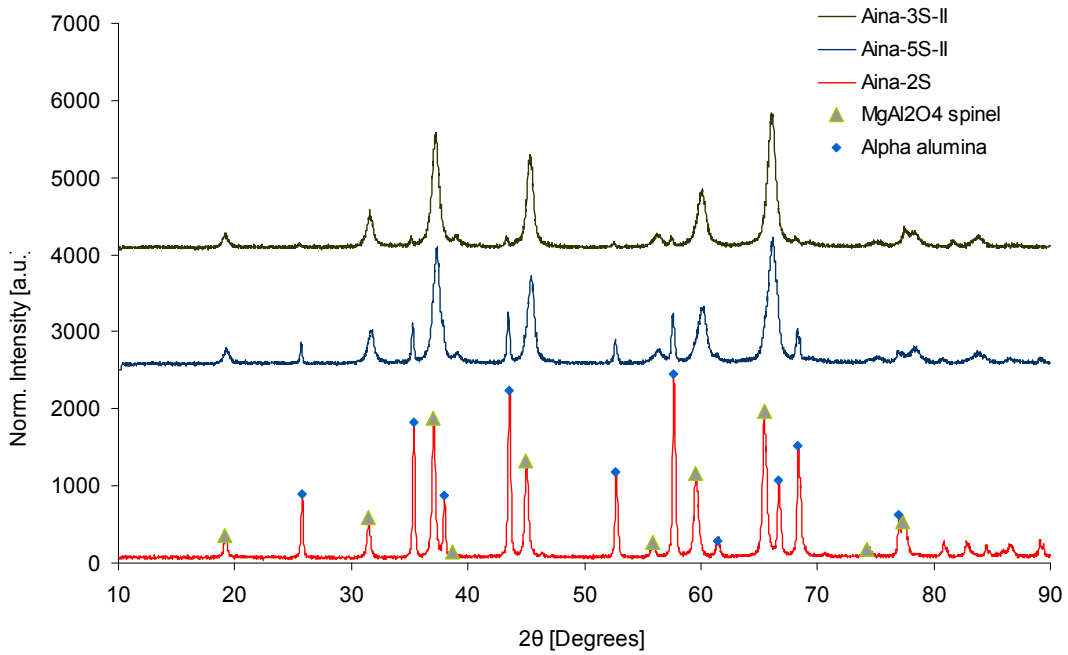


Figure 5.1 The measured XRD patterns for Aina-3S-II, Aina 5S-II and Aina-2S.

In Figure 5.2 the XRD results obtained for Aina-3S, Aina-3S-I and γ -alumina powder are presented. All of the peaks in this figure have been identified as γ -alumina, indicating that hydrothermal treatment of magnesium modified γ -alumina support does not have any effect on phase structure. This is the same result as asserted by Zhang et al. [9] on hydrothermal treatment of γ -alumina with water.

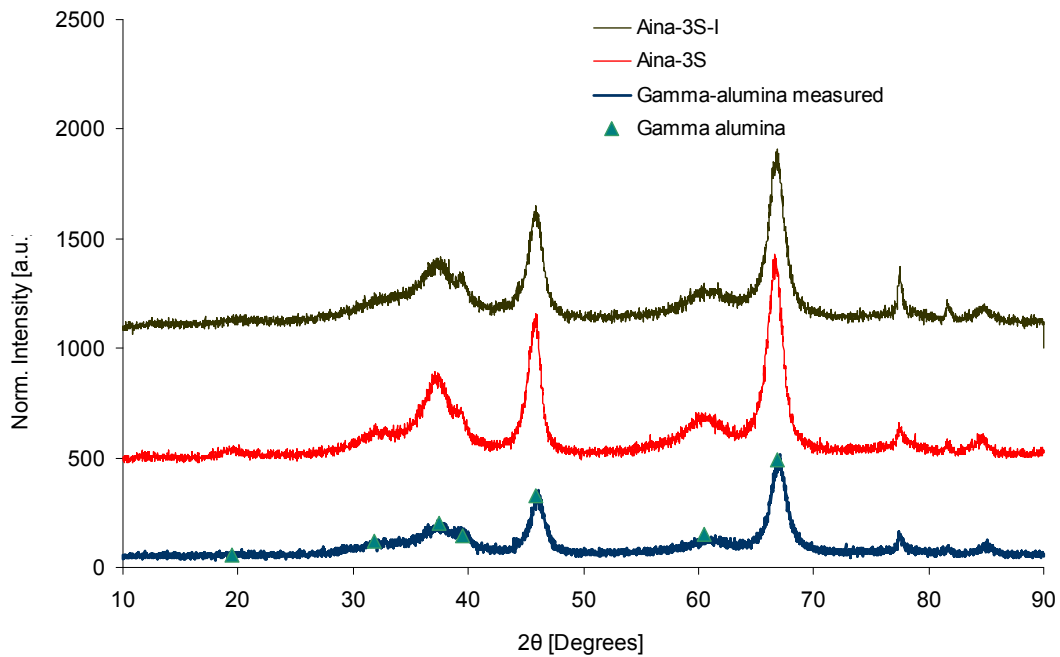


Figure 5.2 The measured XRD patterns for Aina-3S-I, Aina 3S and γ -alumina powder.



Table 5.1 presents the calculated crystallite thicknesses for the samples in Figure 5.2. The results are obtained by applying the Sherrer equation on the most prominent peak located at $2\theta = 66,5^\circ$. Calculation examples are given in Appendix A. As indicated by the diffractograms in Figure 5.2 (broad peaks) the γ -alumina particles are very small (in the range 4,9 - 5,8 nm). The crystallite size variation between the different samples is relatively little, and it is quite possible that it has its origin in random variations between the samples.

The measured diffractograms for Aina-3S and 3S-I did not display any peaks indicating that MgO was present at the surface. This is the same result as reported by Zhang et al. [18], which found that XRD profiles of magnesium modified alumina supported cobalt catalysts displayed no indications of MgO phase at the catalyst surface. This could indicate that the MgO is highly dispersed on the alumina support, i. e. the MgO particles are too small to be detected by X-ray diffraction.

Table 5.1 Calculated crystallite thicknesses by applying the Sherrer equation on the $2\theta = 66,5^\circ$ peak.

Sample	γ -alumina diffraction peak 2θ [°]	γ -alumina particle size [m]
Aina-3S-I	66,5	4,9E-09
Aina-3S	66,5	5,6E-09
γ -alumina measured ³	66,5	5,8E-09

Figure 5.3 display the measured diffractograms for Aina-4S, 5S-I, 5S-I (1) and 5S-I (2). All of these samples have been calcined at maximum 900 °C. Aina-5S-I, 5S-I (1) and 5S-I (2) have in addition been promoted with extra 2 wt. % aluminium post magnesium impregnation. Aina-5S-I and 5S-I (1) was treated hydrothermally in the Autoclave Parr CSTR at 300 °C.

Aina-4S, 5S-I (1) and 5S-I (2) all display the same diffractograms. The peaks are identified as $MgAl_2O_4$ spinel by comparing the measured patterns with the standards in Appendix 0. No α - or γ -alumina were detected for any of the samples in Figure 5.3. This indicates that aluminium promotion does not have the same effect of intensifying α -alumina formation as were the case for samples calcined at higher temperatures. However, at temperatures as low as 900 °C formation of α -alumina is not expected at all (with or without aluminium promotion). In addition the peaks appear to be somewhat less narrow than the ones displayed in Figure 5.1 (compare the scales in the figures), indicating lower crystallinity for samples calcined at lower temperatures.

Addressing the hydrothermal treatment, the sample Aina-5S-I displayed additional peaks in the diffractograms compared to the other samples. The additional peaks were identified as boehmite by comparing with standards in Appendix 0. It has been

³ Sasol Condea Puralox SCCa-45/190 lot 15104



reported previously by Absi-Halabi et al. [45] that aluminium oxides and hydroxides convert to boehmite upon hydrothermal treatment with basic and acidic solutions.

After treatment in Parr reactor Aina-5S-I was first calcined at 300 °C then it was subsequently calcined at 500 °C to yield Aina-5S-I (1). A comparison of the XRD patterns for these two samples indicates that boehmite was formed in the Parr reactor, and that calcination at 500 °C reverses the formation process. Aina-5S-I (2) was not treated hydrothermally, but the preparation sequence is otherwise identical to that of Aina-5S-I (1). The diffractograms are almost identical as well, thus strengthening the suggestion that hydrothermal formation of boehmite is reversed by calcination at 500 °C. The hydrothermal synthesis of boehmite is a very interesting result as it indicates that hydrothermal treatment with water has the ability to alter the support surface acidity. Zhang et al. [9] reported that hydrothermal treatment with water did not affect the hydroxylation and dehydroxylation of alumina, whereas the acid or base did have a significant influence on the composition of the support. Upon XRD analysis of the hydrothermally treated support material, Zhang et al. observed no peaks indicating boehmite. However, Zhang et al. did not calcine their γ -alumina samples pre hydrothermal treatment nor did they modify the supports with magnesium. Their XRD results resemble that of Aina-3S and Aina-3S-I. This could indicate that magnesium modification to yield MgAl_2O_4 spinel support material results in the formation of boehmite upon hydrothermal treatment.

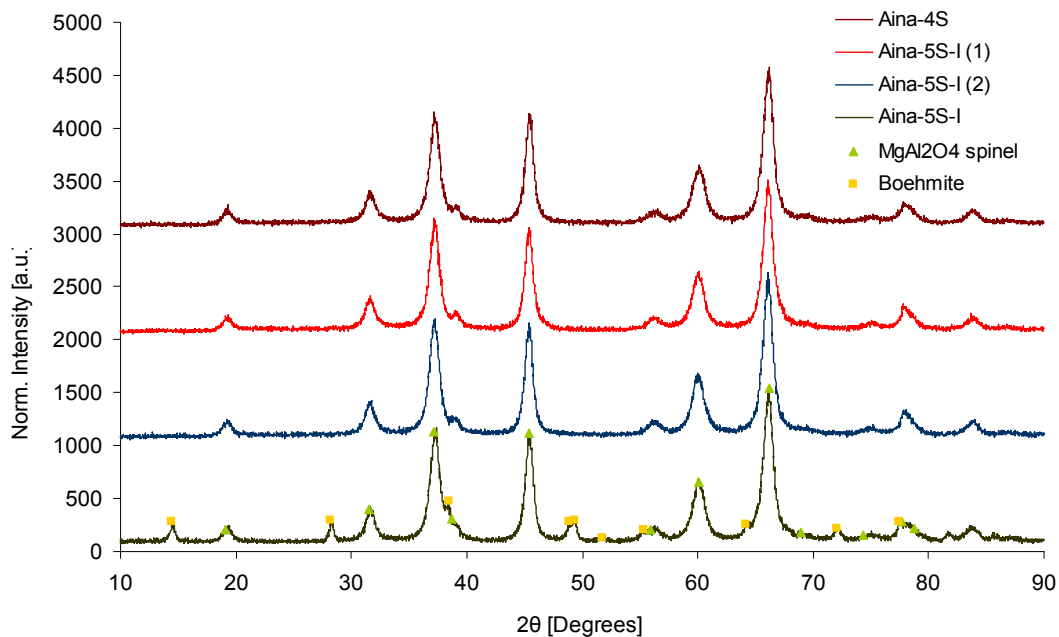


Figure 5.3 The measured XRD patterns for Aina-4S, Aina-5S-I (1), Aina-5S-I (2) and Aina-5S-I.

It is worth noting that no MgO was detected for any of the samples tested. It might be difficult to determine the MgO phase based on the XRD characteristic alone for the high to medium temperature calcined samples however, because both MgO and MgAl_2O_4 have cubic structure with almost identical diffraction peak positions.



5.2.2 NITROGEN (N₂) ADSORPTION/DESORPTION

BET surface areas together with pore volumes and estimated pore sizes for the different supports and catalysts are given in Table 5.2. The results were all retrieved from calculations performed by the Micromeritics Tristar 3000 software program. The computational algorithm that forms the basis for the method (BJH) used to calculate the pore sizes and pore volumes frequently leads to inconsistencies when carried out to low surface area materials. This often leads to the calculation of a too large volume of small pores. However, it was observed from the pore size distribution plots (pore volume vs. pore size) that all of the distributions converged to zero pore volume at both the start and the end of the size interval (from 1,7 – 300 nm).

It is worth noting that although the assumptions used to derive the BET-isotherm and the BET method generally are valid for Al₂O₃ which is a porous structure with medium to large pore sizes, the heat of adsorption is not necessarily constant on the whole surface. Trace amount of other substances often present in alumina would modify the adsorption properties of the surface to some degree. In addition, the BET theory does not account for capillary condensation, which will occur at high partial pressures. However, retrieving the BET-isotherm in the pressure range $0 < \frac{p}{p_0} < 0,3$ ensures multilayer adsorption and negligible capillary condensation.



Table 5.2 Results from the nitrogen adsorption/desorption analysis for all the different samples tested.

Sample	Support calcination temperature [°C]	Support treatment in Parr-reactor at 300 °C	Support promoted with 2 wt. % Al	BET Surface area [m ² /g]	Pore volume [cm ³ /g]	Pore size [nm]
γ -alumina ⁴	500	no	no	174	0,7	12
Aina-2S	1140	no	no	13	0,1	23
Aina-3S	300, 300	yes	no	122	0,5	12
Aina-3S-I	300	no	no	146	0,6	11
Aina-3S-II	300, 1050	no	no	68	0,4	16
Aina-4S	900	no	no	103	0,5	15
Aina-5S-I	900, 300, 300	yes	yes	99	0,5	16
Aina-5S-I (1)	900, 300, 300, 500	yes	yes	103	0,6	17
Aina-5S-I (2)	900, 300, 500	no	yes	107	0,5	15
Aina-5S-II	900, 300, 1050	no	yes	50	0,3	16
Aina-2A	1140	no	no	24	0,1	17
Aina-3A	300, 300	yes	no	135	0,5	12
Aina-3A-I	300	no	no	-	-	-
Aina-4A	900	no	no	94	0,4	15
Aina-5A-I	900, 300, 300	yes	yes	86	0,4	15
Aina-5A-II	900, 300, 1050	no	yes	38	0,2	15
Standard ⁵ 20 wt. % Co, 1 % wt. Re	500	no	no	144	0,5	11
Standard ⁶ 20 wt. % Co, 0,5 % wt. Re	500	no	no	132	0,4	12

The calcination temperature effect

The results indicate that high temperatures calcination leads to low surface areas, small pore volumes and large pore diameters. This typically indicates a collapse of the pore structure and the small pores, and can be observed for the samples Aina-2S and Aina-5S-II calcined at 1140 °C and 1050 °C respectively. The samples that were calcined at lower temperatures show larger surface areas. The effect of calcination temperature is presented in Figure 5.4 where the measured BET surface area is plotted against the highest support calcination temperature.

⁴ Sasol Condea Puralox SCCa-45/190 lot 15104: The values are retrieved from Statoil ASA

⁵ Standard 20177/170: The values are retrieved from Statoil ASA

⁶ Standard 13-33: The values are retrieved from Statoil ASA

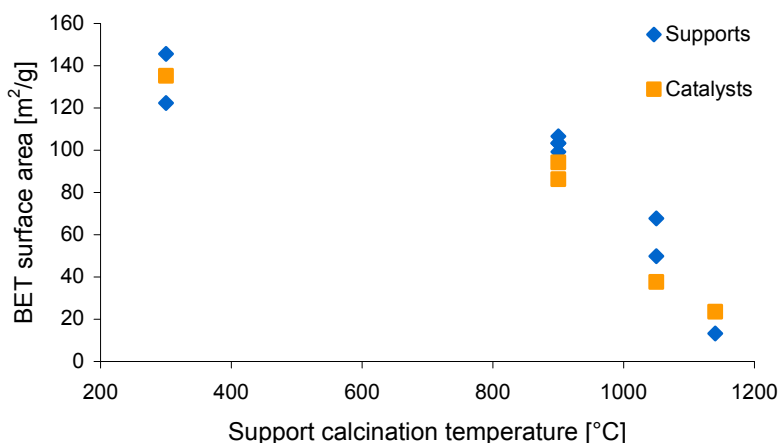


Figure 5.4 The effect of support calcination temperature on the BET surface area for all the different samples tested.

The hydrothermal treatment effect

The effect of hydrothermal treatment appears to be a decrease in surface area. This effect can be observed by comparing the samples Aina-3S and Aina-3S-I. The high pressure observed at 300 °C in the Parr reactor (~30 bar) could cause a collapse of pore structure in the highly porous γ -alumina material. However, more data are needed to get a full understanding of the effect. The difference in surface area for Aina-5S-I (1) compared to Aina-5S-I (2) is too small to draw any conclusions upon, but a comparison of Aina-5S-I (with boehmite) and 5S-I (1) (without boehmite) indicates that the presence/formation of surface hydroxyls groups does not affect the surface area.

The effect of adding extra aluminium

By comparing the Aina-3S-II (without aluminium) and Aina-5S-II (with aluminium) supports a small decrease in surface area can be observed upon addition of extra aluminium. The reduction in pore volume and surface area could be a result of pore blocking by the extra aluminium added. Another explanation, as described in a previous section, could be the formation of relatively more α -alumina as a result of extra aluminium addition in Aina-5S-II compared to Aina-3S-II. Since α -alumina has a low surface area, the presence of a larger amount of this phase will result in a decrease of the total surface area in the support. This explanation seems more probable if Aina-4S (without aluminium) is compared to Aina-5S-I (2) (with aluminium). The difference in surface area is too small to yield any indications on the effect of extra aluminium addition. For these supports the temperature at which they were calcined (900 °C) is too low to form any α -alumina and thus adding extra aluminium does not have any effect.

The effect of magnesium moderation

Moderation of γ -alumina with magnesium resulted in support materials with lower surface areas, smaller pore volumes and larger pore diameters. This is the same trend



as reported by Zhang et al. [18]. They observed that the BET surface area and the total pore volume decreased with increasing magnesia content, while the average pore diameter slightly increased. The results indicate that the small pores of the γ -alumina support are blocked by magnesia.

α -alumina has a low surface area, typically ~ 15 m²/g [10]. XRD analysis indicated that Aina-2S consisted of a large fraction of α -alumina and thus the low surface area observed for this support material can be explained. In this case magnesium modification did not have a positive effect on the surface area as it did not counteract the collapse of pore structure. The XRD analysis also indicated that Aina-3S-II and Aina-5S-II contained a smaller fraction of α -alumina and more MgAl₂O₄ spinel. These two support materials have a larger surface area than Aina-2S and pure α -alumina indicating that the collapse of pore structure might be counteracted by introducing a 2-valent metal in the support material. However, Aina-3S-II and Aina-5S-II were calcined at 1050 °C thus a sample of pure γ -alumina should be calcined at 1050 °C to be able to compare the surface areas.

For the samples calcined at 900 °C introducing magnesium into the support material resulted in samples with relatively high surface areas compared to the high temperature calcined samples. It would be interesting to investigate samples of γ -alumina calcined at 900 °C without magnesium moderation to find out if it is the magnesium moderation effect that counteracts the collapse of pore structure.

The effect of cobalt and rhenium impregnation

Table 5.3 Percentual change in BET surface areas upon cobalt and rhenium impregnation

Samples to be compared	Difference in BET Surface area [m²/g]	Percentual change upon impregnation
Aina-2S and Aina-2A	13-24	+ 85
Aina-3S and Aina-3A	122-135	+ 11
Aina-4S and Aina-4A	103-94	- 9
Aina-5S –I and Aina-5A-I	99-86	- 13
Aina-5S-II and Aina-5A-II	50-38	- 24
Standard 20177/170 and γ-alumina	174-144	- 17
Standard 13-33 and γ-alumina	144-132	- 24

Table 5.3 presents the percentual change in BET surface area upon cobalt and rhenium impregnation. Cobalt and rhenium impregnation of γ -alumina resulted in a 17 % and 24 % decrease in surface area for the standard catalysts (for standard 20177/170 and 13-33 respectively). The reduction in pore volume and surface area upon impregnation was most likely due to cobalt oxide particles taking up space in the porous support structure (the pores were blocked by cobalt oxide particles). The change is in the same range and direction for most of the catalysts prepared in this



work, except for Aina-2A and Aina-3A. Aina-2S have a very low surface area and upon cobalt and rhenium impregnation cobalt and rhenium oxide particles will add to the total surface area and thus an increase upon impregnation can be observed.

If the results can be trusted, and there are no indications of the contrary, Aina-3S displays a somewhat strange behaviour upon cobalt and rhenium impregnation. Aina-3S have a relatively high surface area. Impregnation of this support material yields a catalyst with even higher total surface area. This is a strange result, and no clear explanation has been found. It is interesting to note that Aina-3A in addition exhibited low cobalt dispersion (6,1 % a result retrieved from hydrogen chemisorption data) and very low FT activity (CO conversion was 2 %). Aina-3S was treated hydrothermally in the autoclave Parr CSTR prior to cobalt and rhenium impregnation. The results for Aina-3S should be confirmed by more experiments, and the effect of hydrothermal treatment should be investigated further by preparing samples with isolated differences. Surface acidity should be investigated after hydrothermal treatment as the author of this work suspects that such parameters are altered by such a treatment. Like Aina-5S-I, Aina-3S could contain boehmite phase. Boehmite was not detected by XRD of Aina-3S, however this could be a result of low crystallinity in this support material due to low temperature calcination. XRD analysis of Aina-3S revealed the presence of very small γ -alumina particles.



5.2.3 HYDROGEN (H₂) CHEMISORPTION

Dispersion together with cobalt metal surface area and particle size for all the catalysts tested are given in Table 5.4. The dispersion and metallic surface area were retrieved from calculations performed by the Micromeritics ASAP 2020 software program. They are calculated from the total hydrogen uptake by extrapolating the linear parts of the adsorption isotherms to zero pressure as described in section 3 and 4. Cobalt metal particle size is calculated from the dispersion and a calculation example is given in Appendix A. The assumptions made to arrive at equations 3.4 are not entirely valid. Depending on how the cobalt phases are dispersed the degree of reduction may have a significant effect on the actual average particle diameter. Dispersions and particle diameters were calculated using the standard procedure in order to be comparable with previous experiments.

Table 5.4 Results from the hydrogen chemisorption analysis for all the different samples tested.

Sample	Support calcination temperature [°C]	Hydrothermal treatment of support, 300 °C	Support promoted with 2 wt. % Al	Dispersion [%]	Metallic surface area [m ² /g _{sample}]	Cobalt metal particle size [nm]
Aina-2A	1140	no	no	5,2	4	18
Aina-3A	300,300	yes	no	6,1	5	16
Aina-3A-I	300	no	no	2,4	2	40
Aina-4A	900	no	no	11,2	9	9
Aina-5A-I	900,300,300	yes	yes	11,4	9	8
Aina-5A-II	900,300,1050	no	yes	9,2	7	10
Standard ⁷ 20 wt. % Co, 1 % wt. Re	500	no	no	8,4	11	11
Standard ⁸ 20 wt. % Co, 0,5 % wt. Re	500	no	no	7,8	-	12

The effect of magnesium moderation

The low dispersion in Aina-2A can be explained by the low surface area of the support material. In this catalyst all of the magnesium added is most certainly chemically bonded in the MgAl₂O₄ spinel structure, thus no magnesium is present at the catalyst surface to exert any potential site blocking or electronic effects.

⁷ Standard 20177/170

⁸ Standard 13-33: The values are retrieved from Statoil ASA

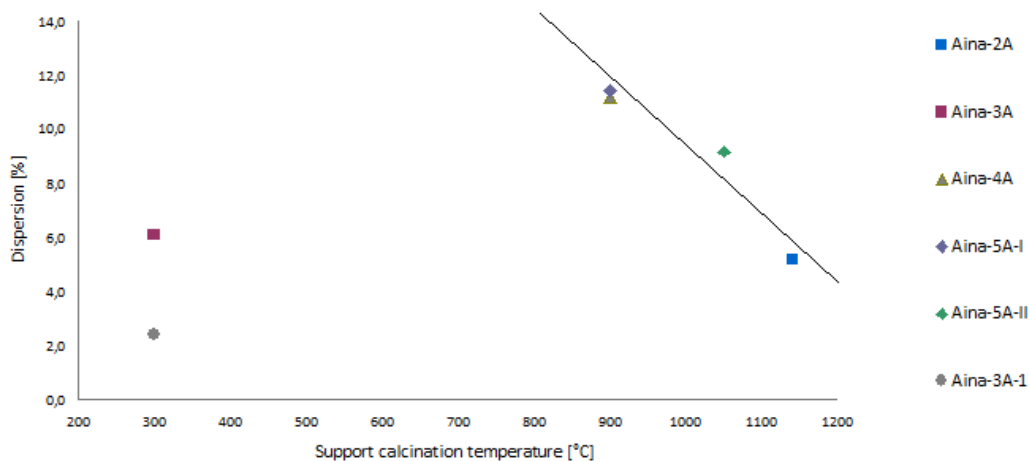


Figure 5.5 The effect of support calcination temperature on the cobalt metal dispersion for all the different samples tested.

It is suggested by Zhang et al. that small amounts of MgO can suppress the cobalt support interaction (to yield cobalt spinel) and thereby increase the reducibility. This would lead to higher dispersion. For the medium temperature (900 °C) calcined samples; Aina-4A and 5A-I this appears to be a reasonable explanation to the relatively high calculated dispersion for these two samples (11,2 and 11,4 % respectively) compared to the high temperature calcined samples (Aina-2A and Aina-5A-II) and the low temperature calcined samples (Aina-3A and 3A-I). However, as will be explained below, dispersion data that are not corrected for degree of reduction could give a wrong picture. The effect of support calcination temperature is displayed in Figure 5.5. It appears that optimal cobalt dispersion is achieved for medium temperature calcined samples, in which it is reasonable to believe that the formation of $MgAl_2O_4$ suppresses the formation of cobalt spinel and thus increases reducibility. Aina-3A and 3A-I have been calcined at a low temperature post magnesium impregnation, thus it is very possible that most of the magnesium is present at the support surface (also indicated by the XRD analysis) i. e not chemically bonded in the support. Borg et al. recently reported in [19] that magnesium post impregnation of Ni-aluminate supported cobalt/rhenium catalysts yielded catalysts with lower activity. The activity decrease was ascribed to physical blocking of cobalt sites. Borg et al. did however not report any decrease in dispersion. It should be mentioned that the amount of magnesium added was far less than what is the case for the support materials prepared in this work.

As mentioned above the dispersion data and the cobalt metal particle size data presented in this thesis were not corrected for degree of reduction. Also indicated above is that in supported cobalt catalysts, the reducibility of the cobalt species often depends on the extent of the metal support interaction. Reduction temperature of the cobalt species depends on the nature and the amount of other cations in the catalyst. This is because cobalt has a tendency to form spinel-like phases, and this is particularly true when the neighbouring cations are aluminium and magnesium. Results obtained by Zhang et al. [18] indicated that CoO–MgO solid solution was formed in the magnesium modified alumina supported cobalt catalysts. Formation of CoO–MgO solid solution affects the reducibility of the cobalt catalysts, because this



kind of cobalt species could only be reduced at an elevated temperature. The results also indicated a surface enrichment of magnesium in these catalysts. With increasing magnesium content (more than 5 wt. %) the interaction between MgO and CoO was enhanced with the formation of CoO–MgO solid solution. In the studies presented by Zhang et al. there were no indications of magnesium forming a spinel structure with alumina (MgAl_2O_4). This was probably due to the low calcination temperature for the magnesium modified supports in this work.

For the low temperature calcined samples prepared for this thesis the hydrogen chemisorption was very low. These catalysts are similar to those prepared by Zhang et al. and the results can therefore be compared.

Zhang et al. showed that hydrogen chemisorption decreased significantly with increasing magnesia content, indicating that the amount of cobalt active sites decreased when large amounts of magnesia were added to the catalysts. In addition the reducibility of the catalyst decreased significantly for the catalysts containing more than 5 wt. % magnesium. It was suggested that small amounts of magnesium could suppress the interaction between cobalt and the support and thus increase the reducibility. Interactions between magnesia and cobalt oxide with formation of CoO–MgO solid solution and with corresponding reduced degree of reduction for the catalysts can explain the low dispersion observed for Aina-3A and 3A-I. If the dispersion was to be corrected for degree of reduction, then the calculated percentage dispersion would increase for these samples. For the medium temperature calcined samples, if reducibility is increased, then correcting for reducibility would lead to decreased dispersion values compared to the calculated ones presented in this thesis. Thus the calculated cobalt metal particle sizes and the dispersion can not be trusted as degree of reduction has not been taken into account.

The hydrothermal treatment effect

The effect of hydrothermal treatment on low temperature calcined samples appears to be an increase in cobalt dispersion. This effect can be observed by comparing the samples Aina-3S and Aina-3S-I. The decrease is substantial leaving Aina-3A-I probably completely inactive to hydrogen chemisorption. As will be presented in section 5.3 Aina-3A exhibited very low FT activity (CO conversion was 2 %). And as mentioned above, these two samples have been calcined at a low temperature post magnesium impregnation, thus it is very possible that most of the magnesium is present at the support surface (i. e. not in magnesium spinel). The fact that the hydrothermally treated support sample exhibited higher dispersion than the untreated one indicates that some of the magnesium was “washed off” during hydrothermal treatment in the Parr reactor.

The effect of adding extra aluminium can not be determined because too many variables exist for the samples tested.



5.3 FISHER-TROPSCH SYNTHESIS

Fischer-Tropsch catalytic performance data were obtained in an isothermal dual fixed-bed unit at 20 bar, 210 °C and $H_2/CO = 2,1$. The results are presented in Table 5.5. Selected results are presented graphically in Figure 5.6 to Figure 5.11. The main source of error for the FT synthesis was attributed to temperature variations in the catalyst bed. The temperature varied with ~ 1 °C throughout the bed, and the average bed temperature deviated from 210 °C with no more than $\pm 0,5$ °C. The difference between the two fixed-bed reactors was found by testing a standard catalyst in both beds. This error was found to be within ± 1 % in CO conversion.

It is worth noting that the reason for not obtaining data for the selectivities for Aina-3A is that this catalyst was essentially inactive for the FT synthesis and 50 % CO conversion could therefore not be reached. Selectivity data (at 50 % CO conversion) for Aina-2A was not obtained due to troubles with the GC. In addition for the standard catalyst 13-33, no selectivity data (at 50 % CO conversion) were retrieved either. The reason for running this catalyst in the fixed-bed rig was merely to estimate the error associated with the two different fixed-bed reactors. For the other samples the space velocity was adjusted to give an estimated CO conversion level of 50 %. This was done because C_{5+} selectivity is strongly dependent on conversion. The FT reactions yield water and so an increase in CO conversion will lead to a rise in C_{5+} selectivity due to an elevated amount of water present at the catalyst surface [46].



Table 5.5 Relevant results obtained from the catalytic activity analysis for all the different catalysts tested.

Sample	Conversion, X_{CO} [%]	C_{5+} selectivity [%]	C_3 Olefin/paraffin	TOF [s^{-1}]
Aina-2A	7	-	3,8	0,037
Aina-3A	2	-	3,5	0,009
Aina-3A-I	-	-	-	-
Aina-4A	13	84,7	3,7	0,033
Aina-5A-I	13	87,4	3,9	0,032
Aina-5A-II	14	86,7	3,7	0,045
Standard ⁹ 20 wt. % Co, 1 % wt. Re	24	82,2	2,7	0,049
Standard ¹⁰ 20 wt. % Co, 0,5 % wt. Re	24	91	2,9	0,051
Standard ¹⁰ 20 wt. % Co, 0,5 % wt. Re	23	91	2,8	0,049
Sample	Rate [molCO/g·h]	Dispersion [%]	Metallic surface area [m^2/g_{sample}]	Cobalt metal particle size [nm]
Aina-2A	0,014	5,2	4	18
Aina-3A	0,004	6,1	5	16
Aina-3A-I	-	2,4	2	40
Aina-4A	0,027	11,2	9	9
Aina-5A-I	0,027	11,4	9	8
Aina-5A-II	0,027	9,2	7	10
Standard ⁹ 20 wt. % Co, 1 % wt. Re	0,050	8,4	11	11
Standard ¹⁰ 20 wt. % Co, 0,5 % wt. Re	0,049	7,8	-	12
Standard ¹⁰ 20 wt. % Co, 0,5 % wt. Re	0,047	7,8	-	12

⁹ Standard 20177/170: Catalyst retrieved from Statoil ASA¹⁰ Standard 13-33: Catalyst and values for chemisorption and selectivity are retrieved from Statoil ASA.



Catalytic activity

Aina-3A display a very low TOF compared to the other catalysts. It is substantially lower than for Aina-2A despite having higher dispersion. Aina-2A, 4A and 5A-I display similar TOF values, while Aina-5A-II exhibits approximately the same TOF value as the standards. As mentioned in previous sections, the dispersion data obtained from hydrogen chemisorption should probably not be trusted as the author of this thesis suspect that magnesium moderation causes differences in reducibility for the different samples. Some samples are believed to have received increased reducibility upon magnesium moderation, while some (especially Aina-3A) suffer from a decrease. This would influence the calculated dispersion. Was the degree of reduction to be taken into account then for Aina-3A it would lead to an increase in the dispersion. For Aina-4A, 5A and 5A-I it would cause a decrease in dispersion, thus the differences in dispersion for the different samples with magnesium moderation might be approximately annihilated. Since the TOF values are based on hydrogen chemisorption data this would lead to completely different values. In addition, the term turnover frequency is misleading as the number of sites is measured *ex situ* under a nonreactive Fischer-Tropsch gaseous environment. The TOF data calculated in this work may not be trusted. The CO conversions and the reaction rates are more reliable activity expressions.

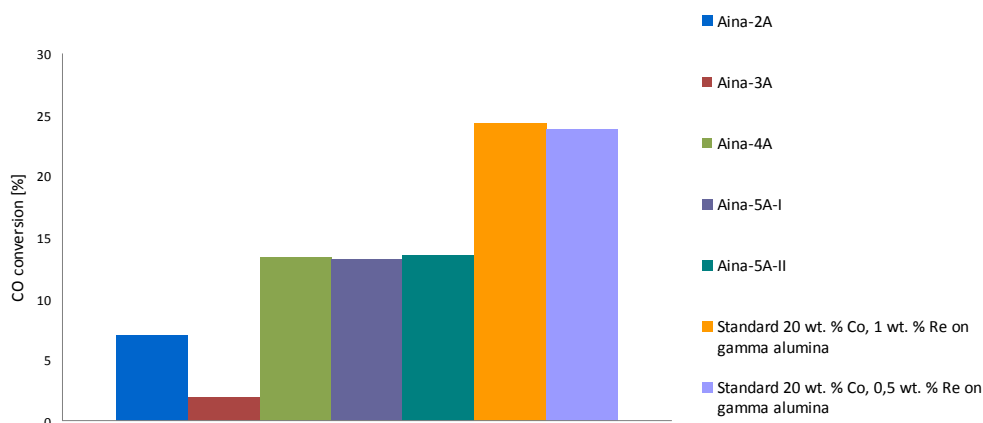


Figure 5.6 CO conversion for the different catalysts tested.

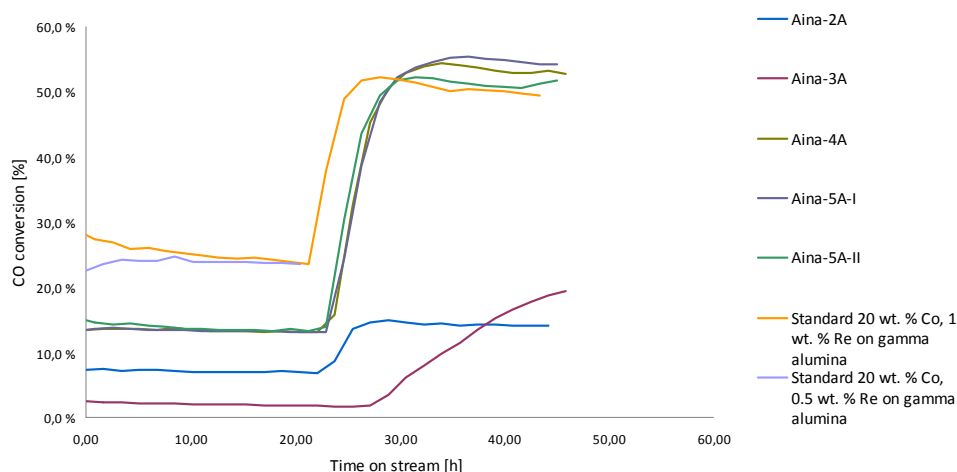


Figure 5.7 CO conversion as a function of time on stream for the different catalysts tested.

Figure 5.6 and Figure 5.7 display the catalytic activity, expressed in CO conversion for the different samples tested in the dual fixed-bed unit. All of the samples modified with magnesium show a decrease in activity compared to the standard catalysts. However, it is not reasonable to compare the activity for these samples. The samples prepared for this work contain ~12 wt. % cobalt, while the standards were both impregnated with ~20 wt. % cobalt thus a higher activity is expected for these catalysts. It would be interesting to investigate the activity of cobalt/rhenium catalysts supported on both pure α - and γ -alumina with 12 wt. % cobalt and 0,5 wt. % rhenium for comparison.

As mentioned in section 2, Enger et al. [13] found that magnesium modification before high temperature calcination of the support yielded catalysts with reduced C_{5+} selectivity and turnover frequency (TOF) compared to low surface area α -alumina supported catalysts. XRD analysis revealed the presence of Mg/Ni - Al_2O_4 spinel structures. For further work, it would be interesting to investigate these results and compare low surface area alumina supported catalysts with 12 wt. % cobalt and 0,5 wt. % rhenium in order to study the effect of magnesium modification with subsequent high temperature calcination.

The low FT-activity for Aina-2A can be explained with the low surface area of the support material in this catalyst and the resulting low dispersion. In this catalyst most of the magnesium added is likely to be chemically bonded in the $MgAl_2O_4$ spinel structure, thus no magnesium is present at the catalyst surface to exert any site blocking or electronic effects.

The complete deactivation of Aina-3A needs to be addressed. It has been suggested that the activity of cobalt catalyst is directly dependent on the catalyst reducibility [47]. If this is true then variations in CO conversion with magnesia content should correspond to the degree of reduction of the catalysts. If the suggestion that Aina-3A has a low reducibility is true then this could explain the low activity. It would be interesting to investigate the reducibility of this catalyst with temperature



programmed reduction and O₂ titration in order to either confirm or reject this hypothesis.

In addition, even though selectivity data could not be retrieved for Aina-3A product flow data indicates that this catalyst has a much higher CH₄ and CO₂ selectivity than the other catalysts tested. Even at the very low CO conversion detected for this catalyst the production of CO₂ is in the same order or higher as for catalysts with 10 times higher conversion. This could indicate higher water-gas-shift (WGS) activity. Or; if unreduced magnesium are present at the catalyst surface, and there is a large possibility that there are due to the difficulty of reducing magnesium, then the electropositive Mg could transfer charge to the catalytic surface through the accompanying oxygen ion. According to Balonek et al. [48], transfer of charge from calcium to the catalytic surface changes the adsorption and dissociation properties of the reactants. The authors suggested that the observed decrease in activity upon addition of Li, Na, K, and Ca to a cobalt and rhenium catalyst supported on γ -alumina was a result of decreased surface hydrogen concentrations and increased CO adsorption and dissociation. If more adsorbed oxygen is present at the catalyst surface then this could explain the increase in CO₂ and possibly CH₄ formation given that the adsorbed carbon is hydrogenated.



C₅₊ selectivity

Figure 5.8 displays the trend of increased C₅₊ selectivity accompanied an increase in CO conversion. More water is formed by the FT reactions with an increase in CO conversion. This leads to a rise in C₅₊ selectivity due to an elevated amount of water present at the catalyst surface [46]. Several different theories were considered by Borg et al. [46] to explain the effect of water on the selectivity. The authors looked into the possibility that water can influence the relative concentrations of active and inactive species of carbon present at low concentrations on cobalt surfaces. Interactions between water and co-adsorbed CO to lower the barrier for CO dissociation were mentioned. C₅₊ selectivity data at 50 % conversion were not obtained for Aina-3A.

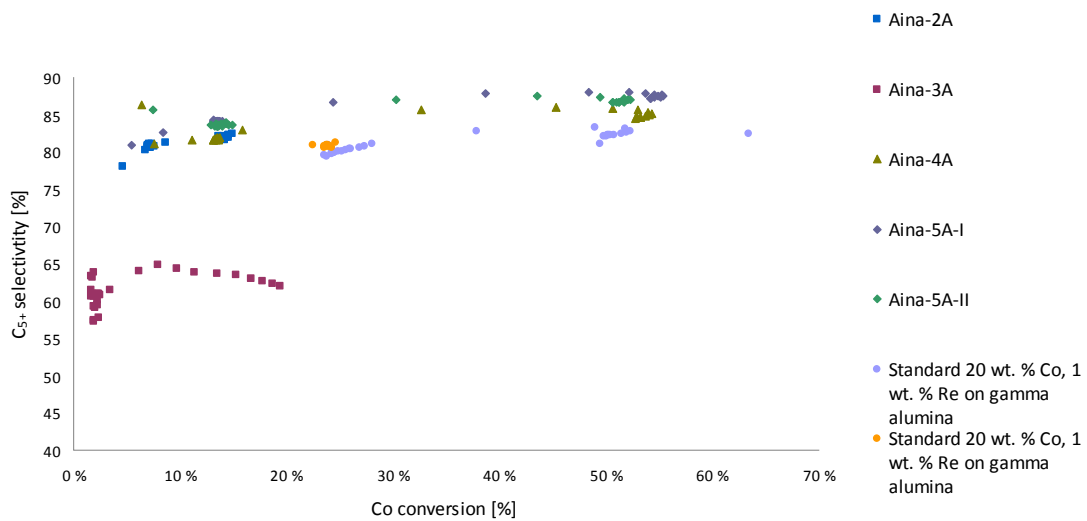


Figure 5.8 C₅₊ selectivity as a function of CO conversion for the different catalysts tested.

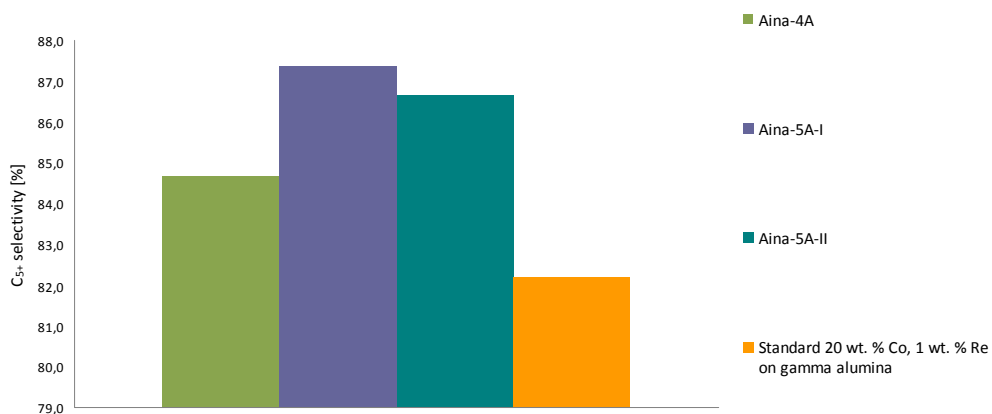


Figure 5.9 C₅₊ selectivity for the different catalysts tested.

Figure 5.9 indicates that C₅₊ selectivity is increased upon magnesium modification of the γ -alumina support to yield MgAl₂O₄ spinel and α -alumina formation compared to



the standard. This is in agreement with the result reported by Schanke et al. [10] that high temperature calcination accompanied with partial transformation of γ -alumina to α -alumina yielded catalysts with improved C_{5+} selectivity. The relatively high calcination temperature (1050 °C) and consequently the formation of some α -alumina phase (as indicated by the XRD analysis) might explain the high C_{5+} selectivity for Aina-5A-II. Aina-2A should be tested again in the fixed-bed unit to find the selectivities. For the completely inactive catalyst, Aina-3A, measuring selectivity data does not serve any purpose.

Aina-5A-I is the catalyst prepared on the support with boehmite on the surface. Zhang et al. [9] reported that surface acidity could have an influence on the interactions between cobalt and the support. Increased support acidity (more hydroxyl groups at the surface) has been found to decrease the C_{5+} selectivity. The observed effect is opposite for the sample tested in this work (Aina-5A-I with boehmite on the support surface exhibited the highest C_{5+} selectivity).

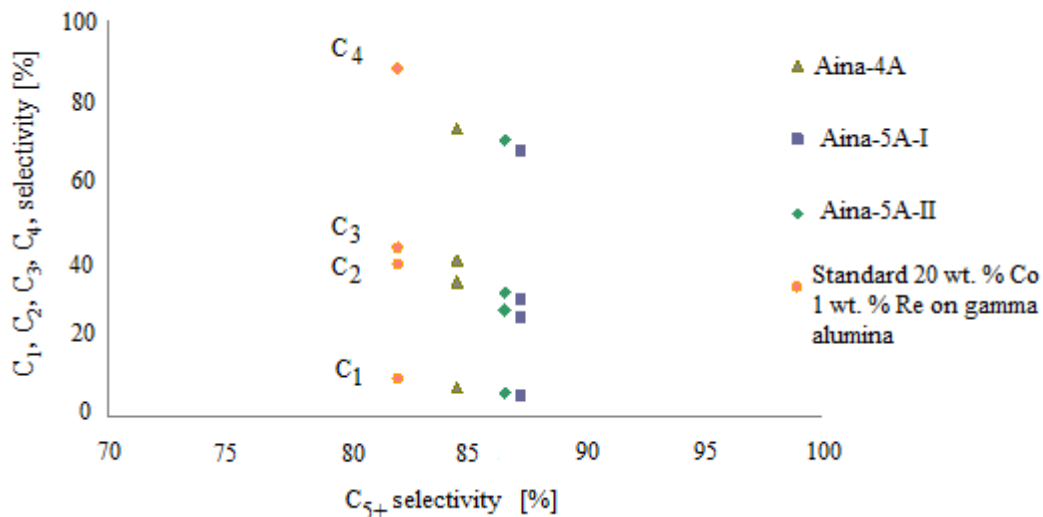


Figure 5.10 C_1 , C_2 , C_3 and C_4 selectivity as a function of C_{5+} selectivity for Aina-4A, 5A-I, 5A-II and standard catalysts.

The Fischer-Tropsch reaction is believed to be non-structure sensitive, hence dispersion should not significantly influence the selectivity. However dispersion data obtained from hydrogen chemisorption without correcting for differences in reducibility does not give a clear picture of the structure sensitivity. Figure 5.10 indicates that the increase in C_{5+} selectivity is mostly at the expense of C_4 (this slope is more steep in Figure 5.10). As mentioned in a previous section Pankina et al. [17] found that a considerable fraction of superparamagnetic cobalt particles, which increase selectivity for C_{5+} hydrocarbons and decrease the yield of methane in the FT synthesis, was present in magnesium modified ruthenium containing cobalt catalysts. The results in Figure 5.10 indicate that magnesium moderation does not cause any changes in methane selectivity.

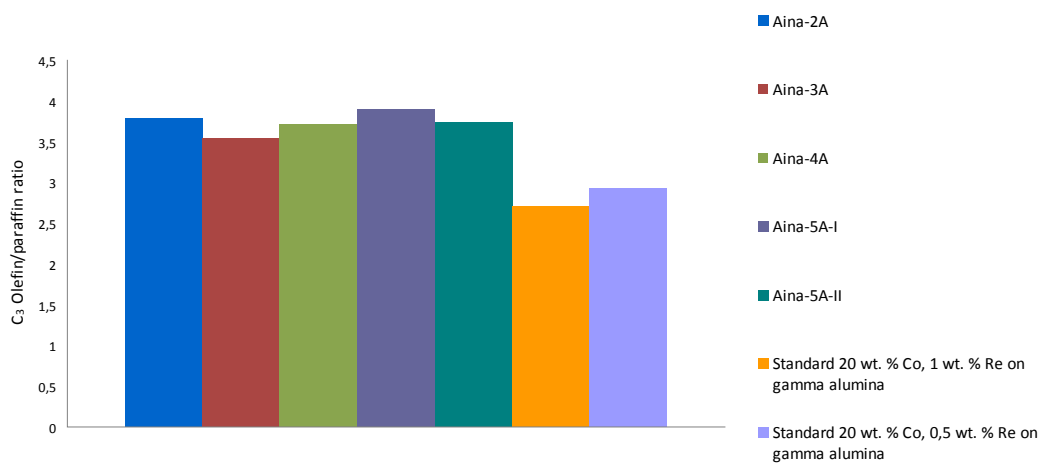
*Olefin/paraffin ratio*

Figure 5.11 C₃ olefin/paraffin ratio for all the different samples tested.

Figure 5.11 displays the ratio between C₃ olefin production to C₃ paraffin production. It appears that the magnesium modified catalysts produce more olefins than the standard catalysts, however no conclusions can be drawn upon the effect of magnesium moderation as the catalysts supported on these materials are lower in cobalt loading together with other substantial differences.



6 Further work

More experiments should be conducted in the autoclave Parr CSTR to get a better understanding of the effects of hydrothermal treatment on the physical and chemical support parameters. The hydrothermal synthesis of boehmite is a very interesting result as it indicates that hydrothermal treatment with water has the ability to alter the support surface acidity. To the authors' knowledge this result has not previously been reported in the literature, however the same effect has been reported upon hydrothermal treatment with acidic and basic solution. This could indicate that magnesium modification to yield MgAl_2O_4 spinel support material results in the formation of boehmite upon hydrothermal treatment and should be investigated further. The effect of hydrothermal treatment on low temperature calcined samples should also be investigated further by preparing samples with isolated differences. Surface acidity should then be investigated after hydrothermal treatment as the author of this work suspects that such parameters are altered by such a treatment even if boehmite was not detected in these samples.

The effect of modifying the supports with extra aluminium post magnesium moderation of γ -alumina should be further investigated. Magnesium modified supports should be impregnated with extra aluminium and then calcined at lower temperatures, for example 1000 °C. Then a XRD analysis could reveal if the extra wt. % aluminium actually acts as a growth initiator for α -alumina.

The counteracting effect on pore structure collapse of introducing magnesium in the support material should also be investigated further. This could be done by calcining a sample of pure γ -alumina at 1050 °C in order to compare the surface area of this sample to the sample containing magnesium. For the samples calcined at 900 °C introducing magnesium into the support material resulted in samples with relatively high surface areas compared to the high temperature calcined samples. It would be interesting to investigate samples of γ -alumina calcined at 900 °C without magnesium moderation to find out if it is the magnesium moderation effect that counteracts the collapse of pore structure.

In addition, as one of the incentives for modifying alumina supports with magnesium was to improve mechanical and chemical catalyst stability, attrition tests should be



performed in order to determine support and catalyst strength. Catalyst stability FT tests could also be performed over a longer time period to determine stability.

It is worth noting that no MgO was detected for any of the samples tested. It might be difficult to determine the MgO phase based on the XRD characteristics alone, and efforts should be made to try to characterize support surface species.

The author of this thesis suspects that the catalyst reducibility and thus FT activity is affected by modifying alumina with magnesium and that it depends on whether or not magnesium gets incorporated into the support structure (as spinel) or not. The reduction level of the catalysts should therefore be determined by oxygen titration and temperature programmed reduction (TPR) and all of the different catalysts prepared should be subjected to a XRD analysis in order to identify surface species. The calculated dispersion data reported in this work can not be trusted and should be corrected with degree of reduction.

Additional FT synthesis analysis should be performed. Many support samples prepared for this work did not get impregnated with cobalt and rhenium and thus further work should focus on preparing catalysts on these supports and subsequently perform FT synthesis. Standards with 12/0,5 wt. % Co/Re on both γ - and α -alumina should be prepared as references and tested for FT activity in order to get comparable data. Selectivity data (at 50 % CO conversion) for the high temperature calcined magnesium modified γ -alumina supported catalyst was not obtained due to troubles with the GC. This experiment should be repeated in order to study the effect of magnesium modification with subsequent high temperature calcination.

The high C_{5+} selectivity observed for some of the samples should be verified. If the results are valid, this is an interesting feature. Even though the activities for these samples were not as high as the standards they exhibited sufficiently high activity to make them interesting. If the goal was to maximise heavy wax production and not product volumes then activity would be of less concern (for example in cosmetics production) and this type of catalysts would in that respect become interesting.



7 Conclusions

It has been found that high temperature calcination of magnesium modified γ -alumina leads to a support material consisting of crystalline α -alumina and MgAl_2O_4 spinel phases. α -alumina formation was intensified by the addition of extra aluminium post magnesium impregnation for these samples. For the low temperature calcined magnesium modified γ -alumina supports only γ -alumina was detected, and for the medium temperature calcined supports only MgAl_2O_4 spinel was detected. This indicates that aluminium promotion does not have the ability to induce α -alumina formation at lower temperatures. Hydrothermal treatment with water appeared to induce boehmite formation in the magnesium modified support material. This indicates that hydrothermal treatment with water has the ability to alter the support surface acidity when MgAl_2O_4 spinel is present at or near the surface.

The results indicate that high temperature calcination leads to low surface areas, small pore volumes and large pore diameters and that magnesium modification does not have the ability to counteract this effect. The samples that were calcined at high to medium temperatures show larger surface areas, indicating that the collapse of pore structure to a certain degree is counteracted by introducing a 2-valent metal in the support material. The effect of hydrothermal treatment of the high surface area magnesium modified supports appears to be a decrease in surface area and can be explained by high water vapour pressures to cause a collapse of pore structure in the highly porous γ -alumina material. A small decrease in surface area was observed upon addition of extra aluminium due to the initiating effect of extra aluminium addition to form low surface area α -alumina.

The low temperature calcined magnesium modified alumina supported cobalt/rhenium catalyst was essentially inactive for the Fischer-Tropsch synthesis. This is can be explained by either a reduction in reducibility due to MgO-CoO solid solution formation, by charge transfer from magnesium to the catalytic surface and corresponding changes in the adsorption and dissociation properties of the reactants, by physical site blocking or a combination of these factors. The high temperature calcined magnesium modified alumina supported cobalt/rhenium catalyst also displayed a very low Fischer-Tropsch activity. This can be explained by the low surface area of the support material in this catalyst and the resulting low dispersion. In this catalyst most of the magnesium added is likely to be chemically bonded in the MgAl_2O_4 spinel structure, thus no magnesium is present at the catalyst surface to exert any site blocking or electronic effects.



Increased C_{5+} selectivity was observed accompanying an increase in CO conversion. More water being formed at the catalyst surface is believed to be the reason for the increase in C_{5+} selectivity. In addition, an increase in C_{5+} selectivity was observed upon magnesium modification of the γ -alumina support compared to the standard when $MgAl_2O_4$ spinel and/or α -alumina were present. The formation of boehmite at the support surface upon hydrothermal treatment with water yielded a catalyst with relatively high C_{5+} selectivity. The effect of increased surface acidity upon C_{5+} selectivity observed is opposite to that reported in the literature. The increase in C_{5+} selectivity observed between catalysts prepared in this work and standards was mostly at the expense of C_4 . It appears that magnesium moderation does not cause any changes in methane selectivity.



List of symbols

Symbol	Unit	Description
α	-	Chain growth probability
β	-	Diffraction line broadening
θ	rad	Bragg angle
λ	nm	Wave length
σ	m ²	Area occupied by one adsorbed molecule
ΔH_1^0	kJ/mol	Heat of adsorption of layer 1
ΔH_i^0	kJ/mol	Heat of liquefaction of the adsorbate gas
ΔH_0^{298}	kJ/mol	Enthalpy at 1 bar and 25 °C
a	-	slope
$A_{i,1}$	-	TCD area of component j at the reactor outlet
$A_{i,0}$	-	TCD area of component i at the reactor inlet
$A'_{j,1}$	-	FID area of product containing j carbon atoms at the reactor outlet
b	rad	Instrumental contribution to peak width
b		intercept
B	rad	Experimental peak width
C	-	BET constant
d	nm	Particle diameter
D	%	Dispersion
E_a	J/mol	Activation energy
E_d	J/mol	Desorption energy
$E_{i,0}$	-	Relative response factor of component i at the reactor inlet
$E_{i,1}$	-	Relative response factor of component i at the reactor outlet
$\varepsilon_{i,0}$	mol i / area i	Response factor of component i at the reactor inlet
F	-	Stoichiometric coefficient
$F_{tot,0}$	mol/s	Total flow rate at the reactor inlet
$F_{tot,1}$	mol/s	Total flow rate at the reactor outlet



$F_{i,0}$	mol/s	Flow rate of component i at the reactor inlet
$F_{j,1}$	mol/s	Flow rate of a component containing j carbon atoms at the reactor outlet
$F_{i,1}$	mol/s	Flow rate of component i at the reactor outlet
i	-	Specie
j	-	Number of carbon atoms
K	-	Equilibrium constant
k	h^{-1}	Adsorption constant
K	-	Sherrer constant
M	g/mol	Molecular weight
m_s	g	Weight of sample being impregnated
N_A	mol^{-1}	Avogadro's constant
n	-	Stoichiometric coefficient
n	-	Number of carbon atoms
n	-	Integer, order of reflection
N_s	-	Surface metal atoms
N_t	-	Total number of metal atoms
p	Pa	Equilibrium pressure of adsorbed gas
P_0	Pa	Saturation pressure of adsorbed gas
P_{CO}	Pa	Partial pressure of CO
P_{H_2}	Pa	Partial pressure of H ₂
R	$\text{JK}^{-1}\text{mol}^{-1}$	Gas constant
$-r_{CO}$	$\text{mol}_{CO}/\text{g}\cdot\text{h}$	Reaction rate
S_j	%	Selectivity of product containing j carbon
t	nm	Crystallite thickness
T	K/°C	temperature
V_a	m^{-3}	Volume of gas adsorbed at equilibrium pressure p
V_m	m^{-3}	Adsorbed at monolayer
V_{ig}	m^3/mol	Volume of one mole ideal gas at 1 atm and 0 °C
W	g	Catalyst mass
x	-	Weight fraction of metal
$x_{i,1}$	-	Mole fraction of component i at the reactor outlet
$x_{i,0}$	-	Mole fraction of component i at the reactor inlet
$x_{j,1}$	-	Mole fraction of a component containing j carbon atoms at the reactor outlet
$\Psi_{j,1}$	-	Mole fraction ratio of a component containing j carbon atoms at the reactor outlet
$\Psi_{i,1}$	-	Mole fraction ratio of component i at the reactor outlet
$\Psi_{i,0}$	-	Mole fraction ratio of component i at the reactor inlet



List of abbreviations

Abbreviation	Description
ASA	Allmennaksjeselskap
ASF	Anderson-Schulz-Flory
BET	Brunauer, Emmet and Teller
BJH	Barrett, Joyner, Halenda
Calc.	Calcined
CSTR	Continuous stirred tank reactor
FT	Fischer-Tropsch
FTS	Fischer-Tropsch synthesis
FID	Flame ionizing detector
GC	Gas chromatograph
GTL	Gas-to-liquids
ICDD	The International Centre for Diffraction Data
MFC	Mass flow controller
MSc	Master of Science
NTNU	Norwegian University of Science and Technology
PDXL	Integrated X-ray powder diffraction software
PhD	Philosophiae doctor
STP	Standard temperature and pressure
SMDS	Shell Middle Distillates Synthesis
TCD	Thermal conductivity detector
TOF	Turn over frequency
TOS	Time on stream
TPR	Temperature programmed reduction
Vol. %	Volume percentage
Wt. %	Weight percentage
WGS	Water-gas-shift
XRD	X-ray diffraction



References

1. Ø. Borg, M. Rønning, S. Storsæter, W. van Beek and A. Holmen, *Identification of cobalt species during temperature programmed reduction of Fischer-Tropsch catalysts*. *Studies in Surface Science and Catalysis*, 2007. **163**: p. 255-272.
2. S. Barradas, E.A. Caricato, P.J. van Berge and J. van de Loosdrech, *Support Modification of Cobalt based Slurry Phase Fischer-Tropsch Catalysts*. *Studies in Surface Science and Catalysis*, 2000. **143**: p. 55-65.
3. R. H. Matjie, M. S. Scurrrell and J. Bunt, *The selective Dissolution of Alumina, Cobalt and Platinum from a calcined spent Catalyst using different Lixivians*. *Minerals Engineering*, 2005. **18**: p. 801-810.
4. F. Rohr, O. A. Lindvåg, A. Holmen and Edd A. Blekkan, *Fischer-Tropsch synthesis over cobalt catalysts supported on zirconia-modified alumina*. *Catalysis Today*, 2000. **58**: p. 247-254.
5. Ø. Borg, N. Hammer, S. Eri, O. A. Lindvåg, R. Myrstad, E. A. Blekkan, M. Rønning, E. Rytter and A. Holmen, *Fischer-Tropsch synthesis over un-promoted and Re-promoted γ -Al₂O₃ supported cobalt catalysts with different pore sizes*. *Catalysis Today*, 2009. **142**: p. 70-77.
6. W. L. Suchanek, *Hydrothermal Synthesis of Alpha Alumina (α -Al₂O₃) Powders: Study of the Processing Variables and Growth Mechanisms*. *Journal of the American Ceramic Society*, 2010. **93**(2): p. 399-412.
7. L. K. Hudson and Aluminum-Company, *Aluminum Oxide*, in *Ullmanns Encyclopedia of Industrial Chemistry*. 1802. p. 339-43.
8. W. L. Suchanek, J. M. Garcés, P. F. Fulvio and M. Jaroniec, *Hydrothermal Synthesis and Surface Characteristics of Novel Alpha Alumina Nanosheets with Controlled Chemical Composition*. *Chemistry of Materials*, 2010. **22**(24): p. 6564-6574.



9. J. Zhang, J. Chen, J. Ren and Y. Sun, *Chemical treatment of γ - Al_2O_3 and its influence on the properties of Co-based catalysts for Fischer-Tropsch synthesis*. Applied Catalysis A., 2003. **243**(1): p. 121-133.
10. D. Schanke, S. Eri, E. Rytter, C. Aaserud, A. M. Hilmen, O. A. Lindvåg, E. Bergene and A. Holmen, *Fischer-Tropsch Synthesis on Cobalt Catalysts Supported on Different Aluminas*. Studies in Surface Science and Catalysis, 2004. **147**: p. 301.
11. E. Rytter, T. H. Skagseth, S. Eri and A. O. Sjøstad, *Cobalt Fischer-Tropsch Catalysts Using Nickel Promoter as a Rhenium Substitute to Suppress Deactivation*. Industrial & Engineering Chemistry Research, 2010. **49**: p. 4140-4148.
12. Ø. Borg, P. D. C. Dietzel, A. I. Spjelkavik, E. Z. Tveten, J. C. Walmsley, S. Eri, A. Holmen and E. Rytter, *Fischer-Tropsch Synthesis: Cobalt Particle Size and Support Effects on Intrinsic Activity and Product Distribution*. Journal of Catalysis, 2008. **259**: p. 161.
13. B. C. Enger, Ø. Borg, Å L. Fossan, O. A. Lindvåg, R. Myrstad, E. Rytter and A. Holmen. *Fischer-Tropsch synthesis on Co supported on modified alumina*. in *236th National Meeting and Exposition of the American Chemical Society, ACS 2008*. 2008. Philadelphia.
14. E. Rytter, *Promoted Fischer-Tropsch Catalysts*. 2008. **US 2008/0255256 A1**(11/663,663): USA.
15. D. Schanke, S. Vada, E. A. Blekkan, A. M. Hilmen, A. Hoff and A. Holmen, *Study of Pt-Promoted Cobalt CO Hydrogenation Catalysts*. Journal of Catalysis, 1995. **156**(1): p. 85-95.
16. P. A. Chernavskii, G. V. Pankina and V. V. Lunin, *The influence of oxide-oxide interaction on the catalytic properties of Co/ Al_2O_3 in CO hydrogenation*. Catalysis Letters, 2000. **66**(3): p. 121-124.
17. G. Pankina, P. Chernavskii, A. Krylova and V. Lunin, *Formation of Co-Ru/MgO/ Al_2O_3 catalysts for the Fischer-Tropsch synthesis: A magnetic method for the estimation of cobalt particle size*. Kinetics and Catalysis, 2007. **48**(4): p. 567-571.
18. Y. Zhang, H. Xiong, K. Liew and J. Li, *Effect of magnesia on alumina-supported cobalt Fischer-Tropsch synthesis catalysts*. Journal of Molecular Catalysis A., 2005. **237**: p. 172-181.
19. Ø. Borg, N. Hammer, B. C. Enger, R. Myrstad, O. A. Lindvåg, S. Eri, T. H. Skagseth and E. Rytter, *Effect of biomass-derived synthesis gas impurity elements on cobalt Fischer-Tropsch catalyst performance including in situ sulphur and nitrogen addition*. Journal of Catalysis, 2011. **279**(1): p. 163-173.



20. A. M. Hilmen, O. A. Lindvåg, E. Bergene, D. Schanke, S. Eri and A. Holmen, *Selectivity and Activity Changes upon Water addition during Fischer-Tropsch Synthesis*. Studies in Surface Science and Catalysis, 2001. **136**: p. 245-300.
21. G. P. Van der Laan and A. A. C. M. Beenackers, *Kinetics and selectivity of the Fischer-Tropsch synthesis: A literature review*. Catalysis Reviews Science and Engineering, 1999. **41**: p. 255-318.
22. M. E. Dry, *Fischer-Tropsch Synthesis*. 2003, New York: Wiley.
23. H. H. Storch, N. Golombic and R. B. Anderson, *The Fischer-Tropsch and Related Synthesis*. 1951, New York: John Wiley and Sons Inc.
24. J. A. Moulijn, M. Makkee and A. van Diepen, *Chemical Process Technology*. 2008, Chichester: John Wiley & Sons Ltd.
25. (ZERO), Z.E.R.O. *Fischer- Tropsch reactor fed by syngas*. 2011 [cited 2011 Jun 1st]; Available from: <http://www.zero.no/transport/biodrivstoff/hva-er-biodrivstoff/fischer-tropsch-reactor-fed-by-syngas/>.
26. M. Ojeda, R. Nabar, A. U. Nilekar, A. Ishikawa, M. Mavrikakis and E. Iglesia, *CO activation pathways and the mechanism of Fischer-Tropsch synthesis*. Journal of Catalysis, 2010. **272**(2): p. 287-297.
27. H. Pichler and H. Schultz, *Recent results in the synthesis of hydrocarbons from carbon monoxide and hydrogen*. Chem. Ing. Tech., 1970. **42**: p. 1162-1174.
28. S. Storsæter, D. Chen and A. Holmen, *Microkinetic Modelling of the Formation of C₁ and C₂ products in the Fischer-Tropsch Synthesis over Cobalt Catalysts*. Surface Science, 2006. **600**: p. 2051-2063.
29. S. Storsæter, Ø. Borg, E. A. Blekkan and A. Holmen, *Study of the effect of water on Fischer-Tropsch synthesis over supported cobalt catalysts*. Journal of Catalysis, 2005. **231**(2): p. 405-419.
30. I. C. Yates and C. N. Satterfield, *Intrinsic Kinetics of the Fischer-Tropsch Synthesis on a Cobalt Catalyst*. Energy & Fuels, 1991 **5**: p. 168-173.
31. T. Greibrokk, E. Lundanes, K. E. Rasmussen and J. Karlsen, *KROMATOGRAFI, Separasjon og deteksjon*. 3rd ed. 1994, Oslo: Universitetsforlaget.
32. I. Chorkendorff and J. W. Niemantsverdriet, *Concepts of Modern Catalysis and Kinetics*. 2nd edition ed. 2007, Weinheim: WILEY-VCH.
33. P. C. Hiemenz and R. Rajagopalan, *Principles of Colloid and Surface Chemistry*. 3rd edition ed. 1997, New York: Marcel Dekker Inc.
34. H. S. Fogler, *Elements of Chemical Reaction Engineering*. 4th ed. 2006, Westford: Prentice Hall PTR.



35. P. A. Webb and C. Orr, *Analytical Methods in Fine Particle Technology*. 1st ed. 1997, Norcross: Micromeritics Instrument Corporation.
36. M. A. Vannice, *Kinetics of Catalytic Reactions*. 2005, New York: Springer.
37. R. D. Jones and C. H. Bartholomew, *Improved Flow Technique for Measurement of Hydrogen Chemisorption on Metal Catalysts*. Applied Catalysis, 1988. **39**: p. 77-88.
38. H. P. Klug and L. E. Alexander, *X-ray Diffraction Procedures for Polycrystalline and Amorphous Materials*. 2nd ed. 1974, New York: John Wiley & Sons.
39. J. W. Niemantsverdriet, *Spectroscopy in Catalysis, An Introduction*. 2nd ed. 2000, Weinheim: WILEY-VCH.
40. ICDD Organization, *The International Centre for Diffraction Data*. 2011: Philadelphia.
41. Ø. Borg, *Role of Alumina Support in Cobalt Fischer-Tropsch Synthesis*, in *Faculty of Natural Sciences and Technology-Department of Chemical Engineering*. 2007, Norwegian University of Science and Technology: Trondheim. p. 99.
42. J. M. Thomas and W. J. Thomas, *Principles and practice of heterogeneous catalysis*. 2005, New York & Weinheim: VCH.
43. O. Tronstad, *Overflate of porefordelingsmålinger*. 1995, Trondheim: Institutt for industriell kjemi, Norges Tekniske Høgskole.
44. Parr-Instrument-Company. *Stirred Reactor & Pressure Vessels Homepage*. 2010 [cited 2010 August 1st]; Available from: Parrinst.com.
45. M. Absi-Halabi, A. Stanislaus and H. Al-Zaid, *Effect of Acidic and Basic Vapors on Pore Size Distribution of Alumina Under Hydrothermal Conditions*. Applied Catalysis A, 1993. **101**: p. 117-128.
46. Ø. Borg, S. Storsæter, S. Eri, H. Wigum, E. Rytter and A. Holmen, *The Effect of Water on the Activity and Selectivity for γ -Alumina Supported Cobalt Fischer-Tropsch Catalysts with Different Pore Sizes*. Catalysis Letters, 2006. **107**(1-2): p. 95-102.
47. A. R. Belambe, R. Oukaci and J. G. Goodwin Jr, *Effect of pretreatment on the activity of a Ru-promoted Co/Al₂O₃ Fischer-Tropsch catalyst*. Journal of Catalysis, 1997. **166**(1): p. 8-15.
48. C. Balonek, A. Lillebø, S. Rane, E. Rytter, L. Schmidt and A. Holmen, *Effect of Alkali Metal Impurities on Co-Re Catalysts for Fischer-Tropsch Synthesis from Biomass-Derived Syngas*. Catalysis Letters, 2010. **138**(1): p. 8-13.
49. Parr-Instrument-Company. *4848 Reactor Controller Operating Instruction Manual*. 2010 [cited 2010 August 1st]; Available from: Parrinst.com.





Appendices



A Derivations and calculations

A.1 SUPPORT AND CATALYST PREPARATION

A.1.1 WATER ABSORPTIVITY

When metals are impregnated upon a support via the incipient wetness method, a mixture of metal nitrate dissolved in water is thoroughly homogenized with the sample being impregnated. The amount of water needed to obtain the point of incipient wetness is called the water absorptivity measured in mL/g. It is identified by weighing out ~2 g catalyst or support in a beiger and then adding water drop wise until total capillary condensation is achieved. The water absorptivity is then measured as the weight of water needed to achieve the point of incipient wetness divided by the weight of the sample, $\frac{m_{H_2O_{abs}}}{m_s}$. The total amount of water needed to reach the incipient wetness point for a given sample with a total mass of m_s is thus given by

$$m_{H_2O} = \left(\frac{m_{H_2O_{abs}}}{m_s} \right) m_s \quad A.1$$

A.1.2 METAL NITRATE X HYDRATE NEEDED FOR IMPREGNATION

In order to determine the amount of metal nitrate hydrate needed to obtain the desired weight fraction of that metal in a sample equation A.2 was used.

$$m_{\text{metal nitrate hydrate}} = \frac{x_{\text{metal}}}{M_{\text{metal}}} \cdot \frac{m_s}{1 - x_{\text{metal}}} \cdot M_{\text{metal nitrate hydrate}} \quad A.2$$

where $m_{\text{metal nitrate hydrate}}$ is the weight of metal nitrate needed to obtain the desired weight fraction, x_{metal} , M_{metal} is the molecular mass of the metal. $M_{\text{metal nitrate hydrate}}$ is the molecular mass of the metal nitrate hydrate and m_s is the weight of the support being impregnated.

When 12 wt. % Co is desired for a support weighing 30 g, then the amount of cobalt nitrate hexahydrate needed is



$$m_{\text{Co}(\text{NO}_3)_2 \cdot 6\text{H}_2\text{O}} = \frac{0,12}{58,93 \frac{\text{g}}{\text{mol}}} \cdot \frac{30 \text{ g}}{1-0,12} \cdot 292,03 \frac{\text{g}}{\text{mol}} = 20,273 \text{ g}$$

A.1.3 PERRHENIC ACID NEEDED FOR IMPREGNATION

In order to determine the amount of 75-85 % perrhenic acid needed to obtain catalysts with 0,5 wt. % equation A.3 is applied

$$m_{\text{HReO}_4} = \frac{x_{\text{Re}}}{M_{\text{Re}}} \cdot \frac{m_s}{(1-x_{\text{Re}}) \cdot 0,775} \cdot M_{\text{HReO}_4} \quad \text{A.3}$$

where m_{HReO_4} is the weight of perrhenic acid needed to obtain the desired weight fraction of rhenium, x_{Re} , M_{Re} is the molecular mass of rhenium, M_{HReO_4} is the molecular mass of perrhenic acid and m_s is the weight of the support being impregnated.

When 0,5 wt. % Re is desired for a support weighing 10 g, then the amount of perrhenic acid needed is

$$m_{\text{HReO}_4} = \frac{0,005}{251,21 \frac{\text{g}}{\text{mol}}} \cdot \frac{10 \text{ g}}{(1-0,005) \cdot 0,775} \cdot 186,2 \frac{\text{g}}{\text{mol}} = 0,0481 \text{ g}$$

Table A.1 shows the molecular masses needed in the catalyst preparation procedure.

Table A.1 Relevant molecular masses used for catalyst preparation.

Compound	Molecular weight [g/mol]
Co	58,93
Al	26,98
Mg	24,31
Re	186,20
Co(NO₃)₂·6H₂O	251,21
HReO₄	186,2
Mg(NO₃)₂·6H₂O	256,4
Al(NO₃)₃·9H₂O	375,13



A.2 COBALT METAL PARTICLE SIZE FROM HYDROGEN CHEMISORPTION DATA

Cobalt metal particle sizes were estimated from the cobalt dispersion. For monodisperse spherical particles with a site density of 14, 6 atoms/nm², the relation between cobalt dispersion and cobalt metal particle diameter is given by equation 3.4 as described in section 3.

$$d(\text{Co}^0) = \frac{96}{D} \quad 3.4$$

where d is given in nanometres and D in percent.

For the catalyst Aina-4A with a dispersion of 11,2 % the cobalt metal particle size is

$$d(\text{Co}^0) = \frac{96}{11,2} = 9 \text{ nm}$$

The results obtained by this equation are given in Table A.2.

Table A.2 The calculated cobalt metal particle size from dispersion obtained from hydrogen chemisorption.

Sample	Dispersion [%]	Cobalt metal particle size [nm]
Aina-2A	5,2	18
Aina-3A	6,1	16
Aina-3A-I	2,4	40
Aina-4A	11,2	9
Aina-5A-I	11,4	8
Aina-5A-II	9,2	10
Standard ¹¹		
20 wt. % Co, 1 % wt. Re	8,4	11
Standard ¹²		
20 wt. % Co, 0,5 % wt. Re	7,8	12

¹¹ Standard 20177/170

¹² Standard 13-33: The values are retrieved from Statoil ASA



A.3 GAMMA ALUMINA PARTICLE SIZE FROM X-RAY DIFFRACTION DATA

Relative γ -alumina particle sizes were determined by applying the Sherrer equation on the (440) diffraction peak located at $2\theta = 66,5^\circ$. To correct for the spherical γ -alumina particles the shape factor was set to 0,89. The X-ray wavelength is 1,54 Å. Table A.3 presents the results obtained by the Sherrer equation. Figure A.1, Figure A.2 and Figure A.3 show the most intense γ -alumina XRD peak for the measured samples.

Table A.3 Information obtained from the measured diffractograms used to calculate the relative γ -alumina particle sizes and the results from applying the Sherrer equation.

Sample	γ -alumina diffraction peak 2θ [°]	γ -alumina diffraction peak 2θ [rad]	Maximum intensity	Half maximum	$2\theta_1$
Aina-3S-I	66,5	1,16	906	453	65,36
Aina-3S	66,5	1,16	1031	515,5	65,34
γ -alumina measured ¹³	66,5	1,16	516	258	65,68
Sample	$2\theta_2$	β [rad]	X-ray wavelength [Å]	Sherrer constant	Particle size [m]
Aina-3S-I	67,28	0,034	1,54	0,89	4,9E-09
Aina-3S	67,02	0,0294	1,54	0,89	5,6E-09
γ -alumina measured	67,30	0,0284	1,54	0,89	5,8E-09

Equation 3.6 is used to calculate the crystallite thickness.

$$t = \frac{K\lambda}{\beta \cos \theta} \quad 3.6$$

In order to determine β , the intercept between the measured diffractograms and the line corresponding to half maximum of the peak is needed. The two intercepts in Figure A.1, for γ -alumina are located at $2\theta_1 = 65,68^\circ$ and $2\theta_2 = 67,30^\circ$. β then becomes

$$\beta = (67,30^\circ - 65,68^\circ) \cdot \frac{\pi}{180} = 0,0284 \text{ rad} \quad A.1$$

¹³ Sasol Condea Puralox SCCa-45/190 lot 15104 retrieved from Statoil ASA



The crystallite size can then be estimated

$$t(\gamma\text{-alumina})_{\gamma\text{-alumina measured}} = \frac{0,89 \cdot 1,54 \text{ \AA} \cdot 10^{-1} \frac{nm}{\text{Å}}}{0,0284 \cdot \cos\left(\frac{1,16}{2}\right)} = 4,9 \text{ nm} \quad \text{A.2}$$

The same procedure is used to estimate the crystallite thickness for Aina-3S and Aina-3S-I. The results are given in Table A.3.

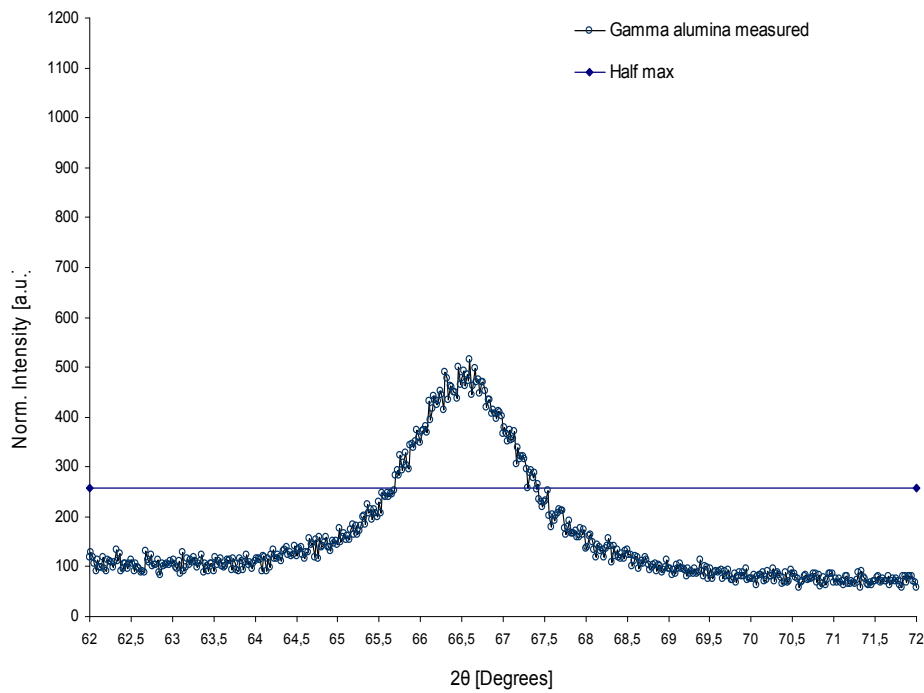


Figure A.1 The (440) γ -alumina diffraction peak located at $2\theta = 66,5^\circ$ for γ -alumina powder.

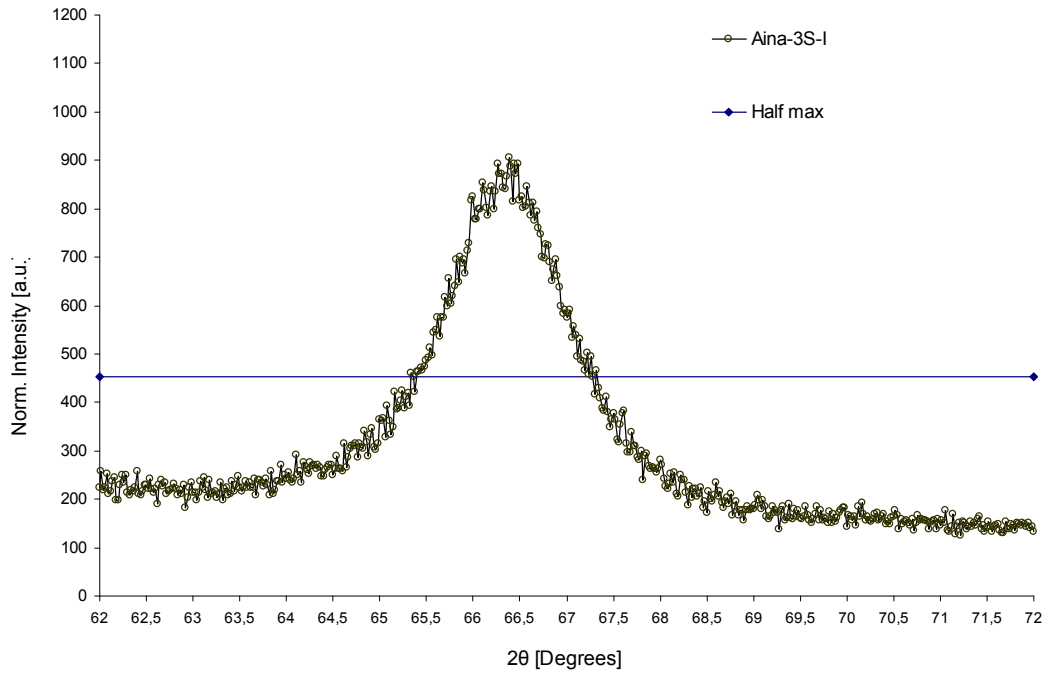


Figure A.2 The (440) γ -alumina diffraction peak located at $2\theta = 66,5^\circ$ for Aina-3S-I.

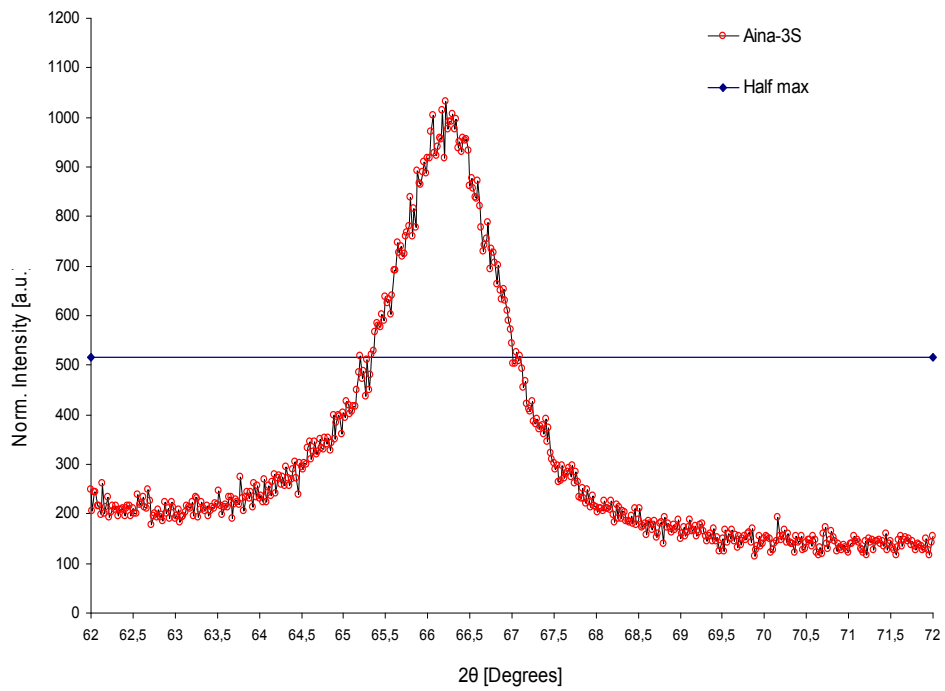


Figure A.3 The (440) γ -alumina diffraction peak located at $2\theta = 66,5^\circ$ for Aina-3S.



B Additions to the procedure

B.1 HYDROTHERMAL TREATMENT IN THE AUTOCLAVE PARR CSTR

B.1.1 MOUNTING THE AUTOCLAVE PARR REACTOR

The two ring sections with bolts were slid into place and positioned so that the drilled shallow socket in the outer surface of one of the ring sections was pointing directly towards the operator. The outer drop band was raised into place around the two ring sections so that the cone pointed screw could be tightened towards the socket to hold the band in place. Each of the six cap screws was tightened in a criss-cross pattern. All the valves were checked carefully (all valves should be closed). [44]

B.1.2 APPLYING TEMPERATURE AND RATE OF ROTATION

The rate of rotation was carefully adjusted by turning the speed control knob on the front panel. The speed control knob was turned slowly until the display showed 500 rpm. This value was the same for every experiment.

The temperature control interface labelled Primary Temperature was adjusted to the desired temperature by pressing the up or down arrow until the lower display showed the desired temperature. The **set** button was pressed to set the value [49]. When applying 300 °C, the temperature set point was first adjusted to 285 °C to avoid overshoot. As the temperature reached the set point, the temperature was set to 300 °C. After 5 min the temperature reached 300 °C. The above mentioned conditions were held constant for 1 h.

B.2 MASS FLOW CONTROLLER CALIBRATION

The mass flow controllers for the synthesis gas had recently been sent to maintenance/service in The Netherlands and in order to obtain accurate gas flows through the catalyst bed, the mass flow controllers needed to be calibrated. The calibration was performed with a soap bubble flow meter of 400 mL. By manually adjusting the mass flow controller valve opening (in intervals from 30 - 100 %) and measuring the time it takes to fill 400 mL in the bubble column with synthesis gas, the mass flow through the controllers could be adjusted with respect to the ambient temperature (19 °C) and pressure (755,6 mmHg) in the laboratory. The adjusted flow (mL/min) was calculated from equation B.1.



$$F_c = \frac{V \cdot \left(\frac{273 \text{ K}}{T}\right) \cdot \left(\frac{760 \text{ mmHg}}{P}\right)}{t} \quad \text{B.1}$$

where V is the volume of the column (400 mL), T is the temperature in the lab measured in kelvin, P is the pressure in the lab measured in mmHg and t is the measured time to fill the column with synthesis gas. The result is presented in Figure B.1 and Figure B.2 where MFC-1 and MFC-2 represent mass flow controller for fixed-bed reactor 1 and 2 respectively.

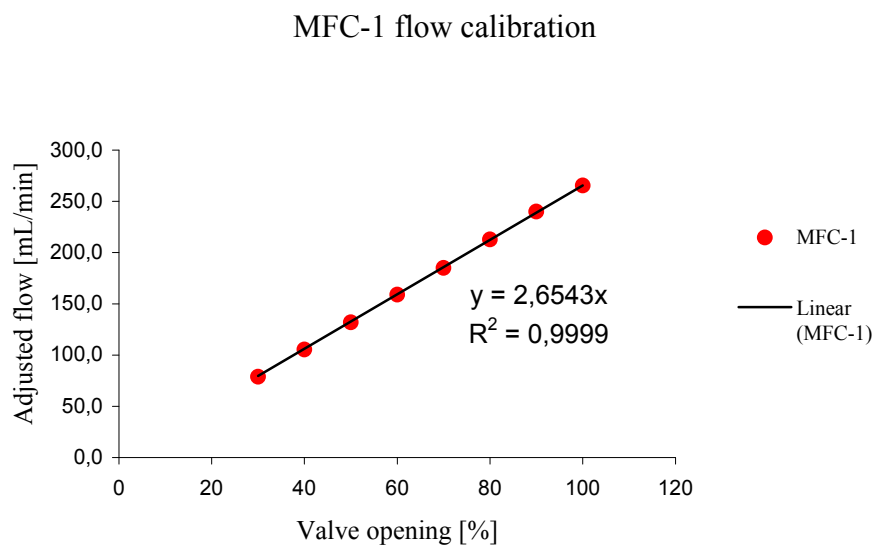


Figure B.1 Gas flow calibration curve for mass flow controller 1.

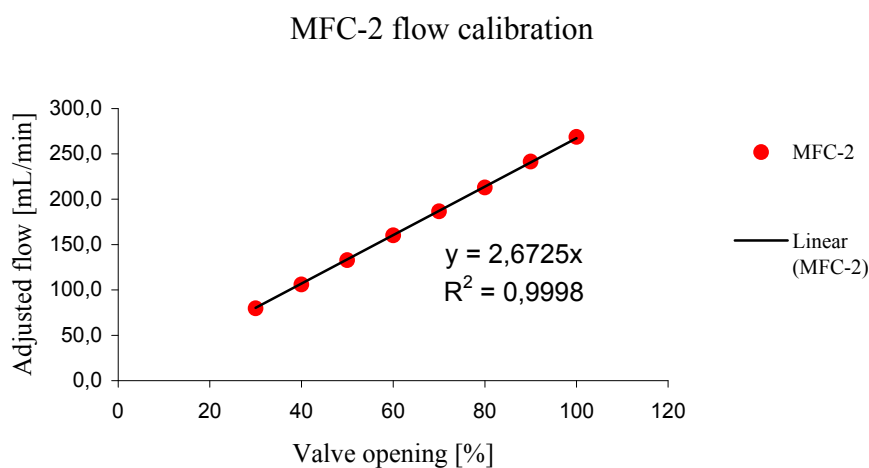


Figure B.2 Gas flow calibration curve for mass flow controller 2.



The mass flow controller valve opening needed to reach a desired flow through the catalyst bed could now be calculated. If 250 NmL/min is desired then the required valve opening for mass flow controller 1 is

$$\text{Valve opening [\%]} = \frac{250 \frac{\text{NmL}}{\text{min}}}{2,65} = 94,2$$

And for controller 2

$$\text{Valve opening [\%]} = \frac{250 \frac{\text{NmL}}{\text{min}}}{2,67} = 93,5$$



B.3 FISCHER-TROPSCH SYNTHESIS

In this appendix additions to the procedure applied for the FT synthesis analysis, together with certain advices and guidance on how to improve and better understand the procedure are given.

B.3.1 PRESSURE TESTING

Before each experiment the rig needed to be examined for any leaks. The feed for the FT synthesis is synthesis gas consisting of CO and H₂. This gas mixture can be both explosive and poisonous to people if released to the surroundings.

Pressure testing was performed by pressurising the rig to FT synthesis operating pressure (20 bar) with helium. The outlet was closed before slowly increasing the inlet pressure. When the inlet flow rate approached zero then no major leaks were present and the rig could be left overnight at 20 bar pressure to complete the pressure test. The maximum allowed leak rate was set to be 1 mL/min which corresponds to a 0, 8 bar pressure drop over 10 hours for each reactor.

The rig has three typical leak points; the nut sealing the thermocouple sockets and the two nuts connecting the reactors to the rig. The two reactor nut leak points typically become a problem if the reactors are rotated while the nuts are closed. If rotation occurs while closing the lower nut, the 1/16 inch tube providing helium flows will be deflected and thus leakage is likely.

In addition, CO gas will in time destroy the rubber gaskets inside the valves. If any such valve leak should occur there is no other option but to replace the leaking valve. Because leaking valves can be very dangerous, additional closing nuts at any valve not leading directly to ventilation is installed.

Upon the presence of minor leaks, the pressure was lowered to approximately 15 bars and then rebuild with hydrogen. The leaks could then be detected with hydrogen detectors. Even part per billion leaks was detectable.

Detection of leaks required the operator to flush the system with helium before reconditioning the rig. Hydrogen detection at the reactor bottom valve should be performed before any mechanical work is started.

B.3.2 GC CALIBRATION

It is important to calibrate the different retention times corresponding to different compounds for the GC on a regular basis as these parameters typically change over time. Typically, the lightest molecules have the shortest retention times, but branched molecules and olefins deviate from this general rule. For example, propene has a longer retention time than propane in spite having lower mass. Figure B.3 presents a typical chromatogram for a GC FID analysis of the hydrocarbon product stream for a randomly chosen experiment. The calibrated retention times for different compounds detected by the GC FID for the same sample are presented in Table B.1. Calibration of retention times is performed during GC analysis. The peak identification program is started and peaks appear in the chromatogram. If the peaks correspond to the pre-calibrated retention times then the peaks will get ordered and identified as in Figure



B.3. If the peaks are not synchronized with the pre-calibrated retention times then some peaks will appear unidentified and the peak order will get displaced. Calibration of the retention times is performed manually by identifying the measured chromatogram peaks according to the sequence they appear in; the first peak is methane, the second is ethane and so forth (as presented in Table B.1) and then starting the identification program again.

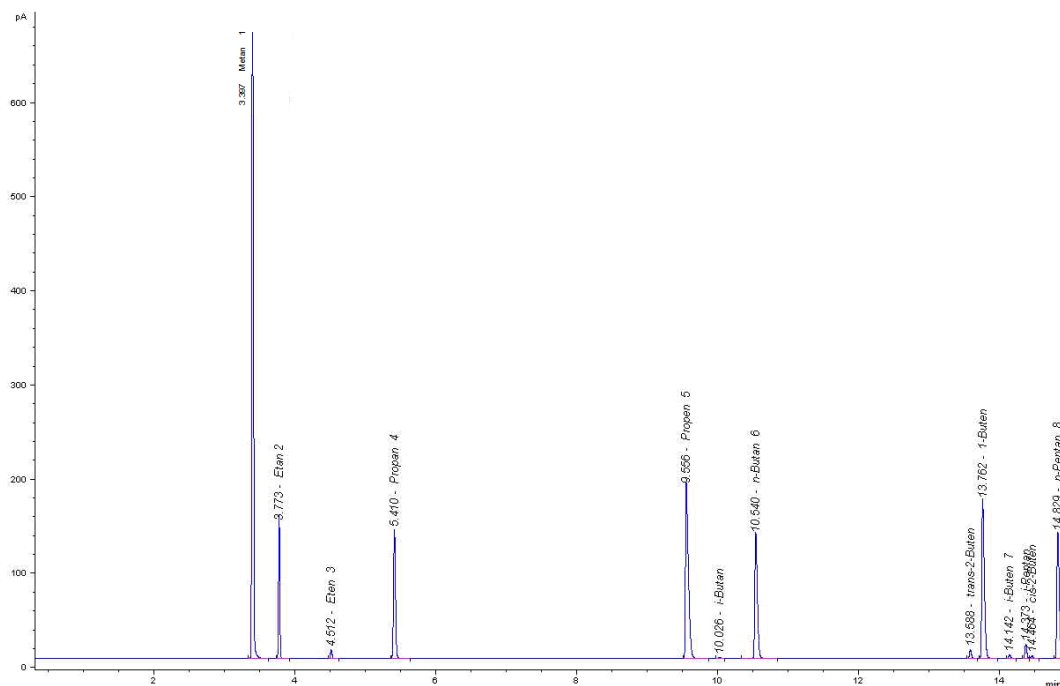


Figure B.3 GC FID analysis of the hydrocarbon product stream for a randomly chosen experiment. The peak order is constant, but the retention time for each compound (expressed by the abscissa) varies and must be calibrated.

Table B.1 Peak number and retention time corresponding to the different compounds detected by the GC FID.

Peak number	Compound	Retention time [min]
1	Methane	3,397
2	Ethane	3,773
3	Etene	4,512
4	Propane	5,410
5	Propene	9,556
6	i-butane	10,026
7	n-butane	10,540
8	Trans-2-butene	13,588
9	1-butene	13,762
10	i-butene	14,142
11	i-pentane	14,373
12	Cis-2-butene	14,464
13	n-pentane	14,829



Calibration requires passing exactly known amounts of different gases through the GC (in a pulsing manner) to find each response factor.

A problem with the GC used for this work is the lack of identification of alcohols in the GC column. Diffusivity differences predicts that alcohols with n carbon atoms will exit the GC column at almost the same time as paraffins with $n + 3$ carbon atoms. This means, for example, that the total C_4 selectivity includes the selectivity to CH_3OH and so on. However, FT synthesis over cobalt catalysts yield only small amounts of alcohols indicating that this error is only of minor importance.

C X-ray diffraction standards

The standards in this section were used to identify peaks in the measured X-ray diffractograms. They are collected from a database [40]. Figure C.1 presents the measured XRD pattern for a sample consisting of pure α -alumina.

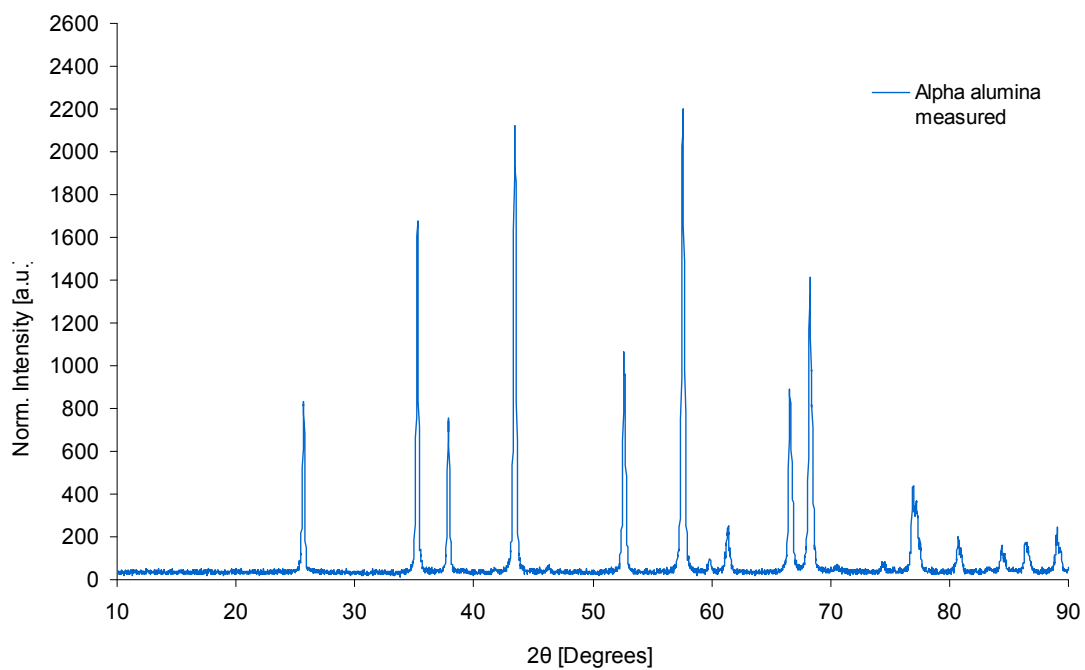


Figure C.1 The measured XRD pattern for pure α -alumina.



D Tables and data

D.1 CD-ROM CONTENTS

Folder name	Contents
FT-synthesis results	Results from the FT synthesis
H ₂ chemisorption results	H ₂ chemisorption results
HMS	Risk assessment tables
MFC calibration	Excel sheet for the MFC calibration
N ₂ adsorption/desorption results	N ₂ adsorption/desorption results
XRD results	XRD results and standards for phase identification





E Risk assessment



NTNU	Kartlegging av risikofylt aktivitet	Utarbeidet av	Nummer	Dato	
		HMS-avd.	HMSRV2601	01.12.2006	
HMS		Godkjent av	Side	Erstatter	
		Rektor	1 av 1	15.12.2003	

Enhet: IKP, NT-fakultet, NTNU

Dato: 10 june 2011



Deltakere ved kartleggingen (m/ funksjon):

Andreas Lillebø

Kort beskrivelse av hovedaktivitet/hovedprosess: Fischer-Tropsch synthesis rig Hall D

ID nr.	Aktivitet/prosess	Ansvarlig	Lov, forskrift o.l.	Eksisterende dokumentasjon	Eksisterende sikringstiltak	Kommentar
1	Heaters		AML	Manual, Datasheet	Gas-detection in Room	
2	Electrical components		AML	CE-Mark		
3	Flammable gases: carbon monoxide hydrogen		AML, kjemikalieforskriften	Datasheet	Gas-detection in Room	
4	High pressure		AML, kjemikalieforskriften	Datasheet	Gas-Detection in Room	
5	Setup of Gasbottles		AML, kjemikalieforskriften	Training-Certificate	Local procedures	Trained by department



NTNU	Risikovurdering	utarbeidet av	Nummer	Dato	
		HMS-avd.	HMSRV2603	04.02.2011	
HMS/KS		godkjent av	side	Erstatter	
		Rektor	1 av 3	9.2.2010	

Enhet: IKP, NT-fakultetet, NTNU

Dato: 10 juni 2011

Linjeleder:

Deltakere ved risikovurderingen (m/ funksjon):

Andreas Helland Lillebø

ID nr	Aktivitet fra kartleggings-skjemaet	Mulig uønsket hendelse/ belastning	Vurdering av sannsynlighet (1-5)	Vurdering av konsekvens:				Risiko-verdi	Kommentarer/status Forslag til tiltak
				Menneske (A-E)	Ytre miljø (A-E)	Øk/ materiell (A-E)	Om-dømme (A-E)		
1	Bytte gassflasker	Lekkasje av CO eller H2.	2	b	a	b	a	ppm gassalarm festet på operatør, ppb gassalarm for å sjekke at det ikke er noen lekkasje og stasjonær gassalarm.	
2	Kalibrering av massflow kontrollere	Lekkasje av CO eller H2	1	b	a	a	a	ppm gassalarm festet på operatør, ppb gassalarm for å sjekke at det ikke er noen lekkasje og stasjonær gassalarm.	
3	Ovner for oppvarming av reaktorer	Ukontrollert oppvarming grunnet defekt temperaturmåling eller elektrisk kortslutning	2	a	a	a	a	Nødknapp på sikringsskap for nedstengning.	
4	Fischer-Tropsch syntese	Lekkasje, avtrekk slutter å fungere eller samme som ID 3	2	b	a	a	a	Nødknapp på sikringsskap for nedstengning. ppm gassalarm festet på operatør, ppb gassalarm for å sjekke at det ikke er noen lekkasje og stasjonær gassalarm.	
5	Fischer-Tropsch gass analyse	Lekkasje	2	a	a	a	a	Nødknapp på sikringsskap for nedstengning. ppm gassalarm festet på operatør, ppb gassalarm for å sjekke at det ikke er noen lekkasje og stasjonær gassalarm.	



NTNU	Risikovurdering	utarbeidet av	Nummer	Dato	
		HMS-avd.	HMSRV2603	04.02.2011	
HMS/KS		godkjent av	side	Erstatter	
		Rektor	2 av 3	9.2.2010	

6	Tømming av produkt	Varm voks kan sprute ut under tømming eller lekkasje av syn-gas.	2	b	a	a	a	Nødknapp på sikringskap for nedstengning. Ppm gassalarm festet på operatør, ppb gassalarm for å sjekke at det ikke er noen lekkasje og stasjonær gassalarm. Visir og tykke arbeidshansker i tillegg til standard verneutstyr for å dekke all hud.
7	Generelt vedlikeholdsarbeid på riggen	Arbeid med lett verktøy innebærer fare for små kutt eller andre småskader.	4	a	a	a	a	Plaster er tilgjengelig i kjemihallen dersom man skulle være uheldig.

Sannsynlighet

1. Svært liten
2. Liten
3. Middels
4. Stor
5. Svært stor

Konsekvens

- A. Svært liten
- B. Liten
- C. Moderat
- D. Alvorlig
- E. Svært alvorlig

Risikoverdi (beregnes hver for seg):

- Menneske** = Sannsynlighet x Konsekvens **Menneske**
Ytre miljø = Sannsynlighet x Konsekvens **Ytre miljø**
Økonomi/materiell = Sannsynlighet x Konsekvens **Øk/materiell**
Omdømme = Sannsynlighet x Konsekvens **Omdømme**

Sannsynlighet vurderes etter følgende kriterier:

Svært liten 1	Liten 2	Middels 3	Stor 4	Svært stor 5
1 gang pr 50 år eller sjeldnere	1 gang pr 10 år eller sjeldnere	1 gang pr år eller sjeldnere	1 gang pr måned eller sjeldnere	Skjer ukentlig

Konsekvens vurderes etter følgende kriterier:

Gradering	Menneske	Ytre miljø Vann, jord og luft	Øk/materiell	Omdømme
E Svært Alvorlig	Død	Svært langvarig og ikke reversibel skade	Drifts- eller aktivitetsstans >1 år.	Troverdighet og respekt betydelig og varig svekket
D Alvorlig	Alvorlig personskade. Mulig uførhet.	Langvarig skade. Lang restitusjonstid	Driftsstans > ½ år Aktivitetsstans i opp til 1 år	Troverdighet og respekt betydelig svekket



NTNU	Risikovurdering	utarbeidet av	Nummer	Dato	
		HMS-avd.	HMSRV2603	04.02.2011	
HMS/KS		godkjent av	side	Erstatter	
		Rektor	3 av 3	9.2.2010	

C Moderat	Alvorlig personskade.	Mindre skade og lang restitusjonstid	Drifts- eller aktivitetsstans < 1 mnd	Troverdighet og respekt svekket
B Liten	Skade som krever medisinsk behandling	Mindre skade og kort restitusjonstid	Drifts- eller aktivitetsstans < 1 uke	Negativ påvirkning på troverdighet og respekt
A Svært liten	Skade som krever førstehjelp	Ubetydelig skade og kort restitusjonstid	Drifts- eller aktivitetsstans < 1 dag	Liten påvirkning på troverdighet og respekt

Risikoverdi = Sannsynlighet x Konsekvens

Beregn risikoverdi for Menneske. Enheten vurderer selv om de i tillegg vil beregne risikoverdi for Ytre miljø, Økonomi/materiell og Omdømme. I så fall beregnes disse hver for seg.

Til kolonnen "Kommentarer/status, forslag til forebyggende og korrigerende tiltak":

Tiltak kan påvirke både sannsynlighet og konsekvens. Prioriter tiltak som kan forhindre at hendelsen inntreffer, dvs. sannsynlighetsreducerende tiltak foran skjerpet beredskap, dvs. konsekvensreducerende tiltak.



NTNU	Kartlegging av risikofylt aktivitet	Utarbeidet av	Nummer	Dato	
		HMS-avd.	HMSRV2601	01.12.2006	
HMS		Godkjent av	Side	Erstatter	
		Rektor	1 av 1	15.12.2003	

Enhet: FT-rigg, Hall D

Dato: 12 june 2011

Deltakere ved kartleggingen (m/ funksjon):

Andreas Helland Lillebø

Kort beskrivelse av hovedaktivitet/hovedprosess:

Fischer-Tropsch syntese ved høyt trykk og relativt høy temperatur

ID nr.	Aktivitet/prosess	Ansvarlig	Lov, forskrift o.l.	Eksisterende dokumentasjon	Eksisterende sikringstiltak	Kommentar
1	Bytte gassflasker	Harry Brun	Ingen	HMS datablad	Stasjonær og håndholdt gassalarm og avtrekk	Trenings sertifikat fra institutt
2	Kalibrering av massflow kontrollere	Andreas Lillebø	Ingen	HMS datablad	Stasjonær og håndholdt gassalarm og avtrekk	
3	Ovner for oppvarming av reaktorer	Andreas Lillebø	ingen	Ingen	Sikringsskap med nødknapp påmontert riggen	
4	Fischer-Tropsch syntese	Andreas Lillebø	Ingen	HMS datablad	Stasjonære gassalamer + håndholdt gassalarm for de som jobber med riggen. Alt er montert i et kammer med undertrykk i tilfelle lekkasje..	
5	Fischer-Tropsch gass analyse	Andreas Lillebø	Ingen	HMS datablad	Avtrekk for utflow, Stasjonær og håndholdt gassalarm	
6	Tømming av produkt	Andreas Lillebø	ingen	HMS datablad	Visir og tykke hansker i tillegg til standard verne utstyr	
7	Generelt vedlikeholdsarbeid på riggen	Andreas Lillebø	ingen	HMS datablad	Ingen spesielle	